การสังเคราะห์สารประกอบเชิงซ้อนรูทิเนียมเพื่อเป็นสารไวแสงสำหรับเซลล์สุริยะชนิดสีย้อมไวแสง

นายศุภวิริยะ สรณารักษ์

วิทยานิพนธ์นี้เป็นส่วนหนึ่งของการศึกษาตามหลักสูตรปริญญาวิทยาศาสตรมหาบัณฑิต
สาขาวิชาเคมี   ภาควิชาเคมี
คณะวิทยาศาสตร์ จุฬาลงกรณ์มหาวิทยาลัย
ปีการศึกษา 2554
ลิขสิทธิ์ของจุฬาลงกรณ์มหาวิทยาลัย

SYNTHESIS OF RUTHENIUM COMPLEXES AS SENSITIZERS FOR DYE-
SENSITIZED SOLAR CELLS

Mr. Supawiriya Saranarak

A Thesis Submitted in Partial Fulfillment of the Requirements
for the Degree of Master of Science Program in Chemistry
Department of Chemistry
Faculty of Science
Chulalongkorn University
Academic Year 2011
Copyright of Chulalongkorn University

Thesis Title   SYNTHESIS OF RUTHENIUM COMPLEXES AS
SENSITIZERS FOR DYE-SENSITIZED SOLAR CELLS

By   Mr. Supawiriya Saranarak

Field of Study   Chemistry

Thesis Advisor   Assistant Professor Worawan Bhanthumnavin, Ph.D.

Thesis Co-Advisor   Associate Professor Buncha Pulpoka, Ph.D.

Accepted by the Faculty of Science, Chulalongkorn University in Partial Fulfillment of the Requirements for the Master's Degree

………………………………… Dean of the Faculty of Science

(Professor Supot Hannongbua, Dr.rer.nat.)

THESIS COMMITTEE

………………………………….. Chairman

(Assistant Professor Warinthorn Chawasiri, Ph.D.)

…………………………….……. Thesis Advisor

(Assistant Professor Worawan Bhanthumnavin, Ph.D.)

………………………………….. Thesis Co-Advisor

(Associate Professor Buncha Pulpoka, Ph.D.)

………………………………….. Examiner

(Assistant Professor Varawut Tangpasuthadol, Ph.D.)

………………………………….. External Examiner

(Assistant Professor Radchada Buntem, Ph.D.)

ศุภวิริยะ สรณารักษ์ : การสังเคราะห์สารประกอบเชิงซ้อนรูทิเนียมเพื่อเป็นสารไวแสง
สำหรับเซลล์สุริยะชนิดสีย้อมไวแสง. (SYNTHESIS OF RUTHENIUM
COMPLEXES AS SENSITIZERS FOR DYE-SENSITIZED SOLAR CELLS) อ. ที่
ปรึกษาวิทยานิพนธ์หลัก : ผศ. ดร.วรวรรณ พันธุมนาวิน,อ. ที่ปรึกษาวิทยานิพนธ์ร่วม
: รศ. ดร.บัญชา พูลโภคา, 89 หน้า.

ได้สังเคราะห์สารประกอบเชิงซ้อนของรูทิเนียมทั้งห้าชนิด **SS01-SS05** เพื่อศึกษา
สมบัติเชิงกายภาพและไฟฟ้า   เพื่อใช้เป็นส่วนสำคัญในเซลล์แสงอาทิตย์ชนิดสีย้อมไวแสง
สารประกอบในงานวิจัยฉบับนี้ ได้ทดลองเปรียบเทียบประสิทธิภาพของสารที่สังเคราะห์ได้กับ
สีย้อมมาตรฐาน N719 ซึ่งเป็นสารกลุ่มเดียวกับสารประกอบเชิงซ้อนที่สังเคราะห์ขึ้น งานวิจัย
ฉบับนี้ 2,3-ไดฟีนิลไพราซิโน[2,3-f][1,10]ฟีแนนโทรลิน ถูกใช้เป็นลิแกนด์ของสารเชิงซ้อนที่
สังเคราะห์ขึ้นเพื่อใช้เป็นหน่วยเก็บเกี่ยวแสงของสารประกอบ โดย **SS01-SS05** จะมีโครงสร้าง
ที่มีหมู่แทนที่ที่แตกต่างกันในตำแหน่งพาราบนวงเบนซีน ซึ่งจะเป็น หมู่ไฮโดรเจน หมู่เมทอก
ซี หมู่ไดเอทิลอะมิโน หมู่เมทิล และหมู่โบรโม ข้อมูลที่ได้จาก ^{1}H NMR และ ATR-IR สเปก
โตรสโกปี จะนำมาใช้ในการระบุโครงสร้างของสารประกอบ   ในการศึกษาสมบัติเชิงไฟฟ้า
ได้ใช้ไซคลิกโวลแทมเมทรีประกอบกับสเปกตรัมของการดูดกลืนแสง   เพื่อที่จะใช้ในการ
คำนวณหาระดับพลังงานของระดับพลังงาน HOMO และ LUMO ในการศึกษาเอกลักษณ์ทาง
ไฟฟ้าของเซลล์ที่ย้อมด้วย **SS01-SS05** พบว่าเซลล์ที่ได้ให้ประสิทธิภาพโดยรวมคิดเป็นร้อยละ
2.60, 3.04, 2.60, 2.50, และ 1.06 ตามลำดับ ซึ่งต่ำกว่าค่าร้อยละ 5.07 ซึ่งเป็นค่าประสิทธิภาพที่
ได้จากเซลล์ที่ย้อมด้วยสีย้อมมาตรฐานN719 ซึ่งเป็นผลมาจากค่าความหนาแน่นกระแสที่ต่ำ
ของเซลล์ที่ย้อมด้วย SS01-SS05 ที่เป็นเช่นนี้อาจเนื่องมาจาก สารไวแสงส่งผ่านอิเลคตรอนไป
ยังพื้นผิวของไททเนียมไดออกไซด์ได้น้อยกว่าเมื่อเทียบกับสีย้อมมาตรฐานN719

ภาควิชา: _____เคมี_____ ลายมือชื่อนิสิต..
สาขาวิชา: _____เคมี_____ ลายมือชื่อ อ.ที่ปรึกษาวิทยานิพนธ์หลัก.................
ปีการศึกษา: _____2554_____ ลายมือชื่อ อ.ที่ปรึกษาวิทยานิพนธ์ร่วม ....

5272658423 : MAJOR   CHEMISTRY
KEYWORDS :   DYE-SENSITIZED SOLAR CELL / PHOTOSENSITIZER / RUTHENIUM COMPLEX / LIGHT-HARVESTING UNIT / DYE

SUPAWIRIYA SARANARAK : SYNTHESIS OF RUTHENIUM COMPLEXES AS SENSITIZERS FOR DYE-SENSITIZED SOLAR CELLS. ADVISOR : ASST. PROF.WORAWAN BHANTHUMNAVIN, Ph.D., CO-ADVISOR : ASSOC. PROF.BUNCHA PULPOKA, Ph.D., 89 pp.

Five ruthenium complexes, **SS01-SS05**, were synthesized. The physical and electronic properties were studied and the compounds were used as a critical part of a dye-sensitized solar cell. The complexes, which are dyes or photosensitizers, are used as mediator to convert light to electric power. In this study, one of the bipyridine ligand of the synthesized complexes was a derivative of 2,3-diphenylpyrazino[2,3-*f*][1,10]phenanthroline, which was to serve as the light-harvesting unit of the complexes. The **SS01-SS05** bear different substituents at the *para*-position of the phenyl ring such as –H, –OMe, –NEt$_2$, –Me, and –Br. The data obtained from ^{1}H NMR and ATR-IR spectroscopy were used to identify the structure of the compounds. In studying electronic structure, cyclic voltammetry was used altogether with absorption spectra to calculate HOMO and LUMO electronic levels. Upon the study of photovoltaic characteristic of the cell staining with **SS01-SS05**, it was illustrated that the overall conversion efficiency of **SS01-SS05** were 2.60, 3.04, 2.60, 2.50, and 1.06%, respectively, which were lower than the efficiency (5.07%) obtained from the cell staining with standard N719. These were the results from the lower current density of the cells staining with **SS01-SS05**, possibly due to poorer electron injection from **SS01-SS05** onto the TiO$_2$ surface, when compared to the standard N719.

Department : Chemistry   Student's Signature

Field of Study : Chemistry Advisor's Signature

Academic Year : 2011   Co-advisor's Signature

ACKNOWLEDGEMENT

Finally, I would like to dedicate this thesis to my family who constantly present their understandings and encouragement to me during both of my pleasant and hard time. This thesis would not have been possible without their supports. Thank you!

CONTENTS

LIST OF TABLES

LIST OF FIGURES

LIST OF SCHEMES

LIST OF ABBREVIATIONS AND SIGNS

^{1}H NMR	proton nuclear magnetic resonance
^{13}C NMR	carbon-13 nuclear magnetic resonance
CDCl3	deuterated chloroform
DMSO- *d6*	deuterated dimethyl sulfoxide
DMSO	dimethylsulfoxide
DMF	*N,N´*-dimethylformamide
d	doublet (NMR)
dd	doublet of doublet (NMR)
m	multiplet (NMR)
t	triplet (NMR)
s	singlet (NMR)
ATR-IR	Attenuated total reflectant infrared spectroscopy
g	gram (s)
Hz	hertz
HRMS	high resolution mass spectrum
h	hour (s)
IR	infrared
J	coupling constant
mg	milligram (s)
mL	milliliter (s)
mmol	millimole (s)
m/z	mass per charge
M	molar
dcbp	4,4´-dicarboxy-2,2´-bipyridine
rt	room temperature
TLC	thin layer chromatography
UV	ultraviolet
δ	chemical shift
°c	degree celsius

μM	micromolar
% yield	percentage yield
DSSC	dye-sensitized solar cell
Jsc	Photocurrent Density
Voc	open circuit voltage
ff	fill factor
η	efficiency
IPCE	Incident photon to current conversion efficiency
AM	air mass
mA	milliampere
$AgNO_3$	silver nitrate
LiI	lithium iodide
I_2	iodine

CHAPTER I

INTRODUCTION

Nowadays, it cannot be avoided to mention that the energy have to be taken part in all of the human activities. Especially for economic growth, the development can be driven by the ability in providing the energy resources. Since the increasing of energy demands and the depleting of fossil fuel resources, the global will be faced the energy crisis for the next few decades. Moreover, the processes for the conversion of the fuel cell to the usable energy can generate the substances which affect to the environment directly. Hence, the renewable energies have become a mean for overcoming the exhaustion of fuel energy resources.

Among all of the renewable energy: solar, water, win, and bioenergy, solar energy is the most effective. A huge amount of an inexhaustible energy has been supplied from the sun to the earth's crust, about 3×10^{24} J per year or much higher than 1,000 times compared to the consumption of the whole world population. From these quantitative data, it can be implied that if human can collect all of such energy, we will never face all of energy crisis.[1]

In 1893, French scientist Edmond Beaquerel pioneered the photoelectric effect. Since then, many researchers and engineers have been attracted with the dream to converse sunlight to the usable energy such as electric power or chemical fuels. The common idea is to capture the light which can be harvested freely from the sun and converse into the valuable electric power or use to generate hydrogen as a fuel in fuel cells. Photovoltaic is the term for devices that can create the electron-hole pair upon the photons striking on the semiconductor. At the junction between the different materials, electric potential occurred here which was then created the electricity when applied to the external load.[2]

There are several types of photovoltaic cells have been developed. Among them, Dye-sensitized solar cells (DSSCs) are attracting widespread of interest for the

photovoltaic performance due to their low cost and high efficiency.[3-5] This type of cell was developed by Michael Grätzel and Brian O'regan in 1991 and this cell is also known as Grätzel cells.[6] Although it possesses the low efficiency than conventional silicon semiconductor, the ease to fabricate and application for flexible substrate is very attractive enough to take the efforts in the development of this type of cell.

1.1   Photovoltaic

The common character of all photovoltaic devices is the ability in conversion of solar energy into electric power. General condition for the action of photovoltaic equipment have been exploited the change of two electrodes with the difference in their work-function upon exposing to the light. The general process of energy conversion by photovoltaic principle can be simply divided into two steps.

a) The electronic excitation of the light absorber of the photovoltaic device by the light and

b) The separation of electronic charge.

The excitation pattern is different based on the type of photovoltaic devices. The excitation can be an electron-hole pair in semiconductor crystal network, an excited state in molecular sensitizer, or an exciton in organic conducting polymer.

To produce the electrical output, the excited electrons have to be transferred to the interfacial contact. This can be considered as the charge-separation step which can be succeeded by using the appropriate selective contact to the light absorber. The selectivity of the contacts to each electron or hole species is achieve by the potential barrier at the interface or the physical transparent to only one species.

Without aiming at an exact classification, the geometry of devices can be divided into two cases. One is a series configuration, where the carriers travel across the device with a single kind of path, for example a multilayer device. The other is a heterogeneous configuration, where the carriers are passing the device with different path such as dye-sensitized solar cell or organic (polymer blend) solar cell. The type

of photovoltaic devices can be simply categorized by using either kind of materials of the photocurrent generation which will be briefly discussed. [7]
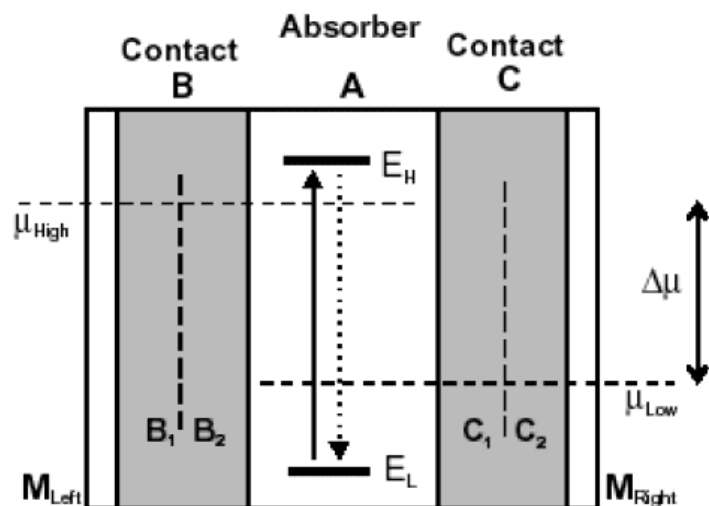
Figure 1.1 Idealized photovoltaic device, where A is an absorber, B and C are selective contacts for each electron or hole, and μ is electron potential.

1.1.1 Point-Contact Solar Cells.

The silicon solar cells developed at Stanford University are common in the series configuration with both negative and positive contact. These cells provided the efficiency at about 22% in 1988 and have been commercialized for rail operation under sunlight since then. The absorber is a thin layer made from silicon with excellent quality that makes the diffusion lengths are several times of the cell thickness. Upon the illumination, the excess carriers in the material can be induced and promoted the separation of electron and hole at the bulk material. Electron and hole are separated by the potential barrier of the point contact at the surface of electrodes where providing the selectivity to each charge species.

1.1.2 Photogalvanic Cells.

These cells are typically composed by two electrodes, immersed in electrolyte containing redox couple, with different selectivity to each redox species. The photogeneration was occurred here in solution by photoexcitation of the dye chromophore. The excited-dye reduces the oxidized form of redox couple in

electrolyte and both of electronic species, oxidized dye and reduced form of redox couple, would then transfer the charge to the appropriate electrode to generate the electric current. The efficiency and stability of this type of cell is very low. About 0.5% of 30 minutes are typical for the best outcome of the performance.
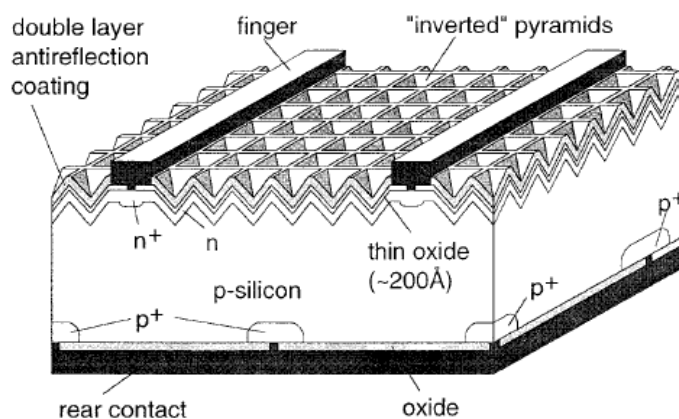
Figure 1.2 Cell structure of commercial silicon solar cell.[8]
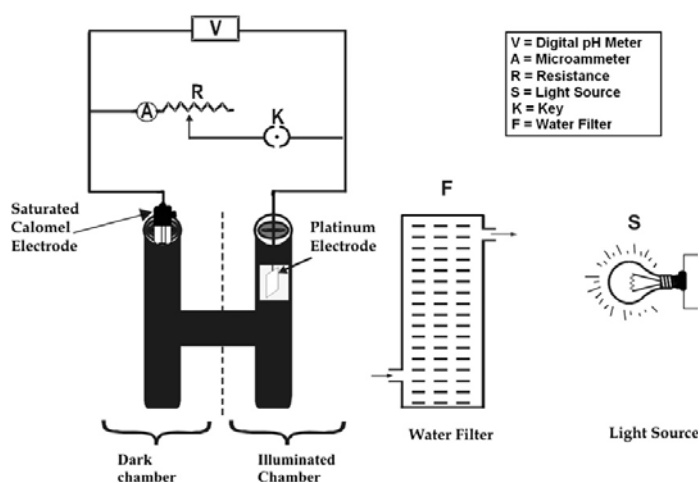
Figure 1.3 Experimental setup of photogalvanic cell.[9]

1.1.3 Photoelectrochemical Cell (PEC).

The core of this type of cell is the junction between semiconductor and liquid electrolyte which can be described by the same model of *p-n* junction device with some different. For some examples of nanoparticulated PEC, the absorber is the nanoporous semiconductor where the electron and hole were both generated here, where as the semiconductor of DSSC was a carrier of only one charge. The charge separation of the PEC cell depends on the kinetic difference in charge injection to the electrolyte. If one charge is more ready to inject to the electrolyte, the other will accumulate at the semiconductor and flow by the diffusion to the contact.
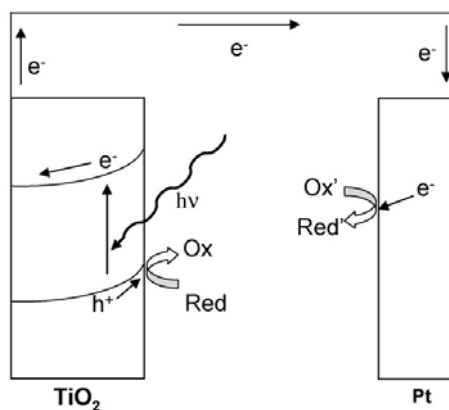
Figure 1.4 Photoelectrochemical cell.[10]

1.1.4 Organic Cell.

Several configurations of these cells have been studied by using conjugated polymer (CP) as the absorbers of the device. One of the simple configuration composes of three layers of material: $n-TiO_2/CP/p-CuI$. Where the polymer contacts to $n-TiO_2$, which is selective to electron, and p-CuI, which is selective to hole. Nonetheless this configuration provides quite low conversion efficiency. Another on type was composed by the conjugated polymer contacted between the two asymmetric metal electrodes with different work-function. This type also achieves the similar efficiency. From many efforts, heterogeneous configuration has been achieved by blending two phases, donor and acceptor, as interdispersed network. This configuration provides the promising result. The conjugated polymer is

employed as donor. Upon the illumination, electron would transfer from donor to acceptor which usually is a small molecule compound such as functionalized fullerene. In addition, the cell requires the arrangement of organic layer between the electrodes with different work function.

The mechanism of electronic process was started with the electron acceptation and hole rejection of fullerene from conjugated polymer when exposed to the light. The Fermi level of cathode, i.e. indium-doped tinoxide (ITO), should appropriate with Fermi level of fullerene, hence, reduced fullerene could inject electron to the cathode. On the other hand, the polymer blend, contacted to ITO as well, should not inject hole at the ITO interface. The corresponding task was achieve by using a layer of poly-(3,4-ethylenedioxythiophene) (PEDOT) which is poor electron conductor and also improve the selectivity to the holes.
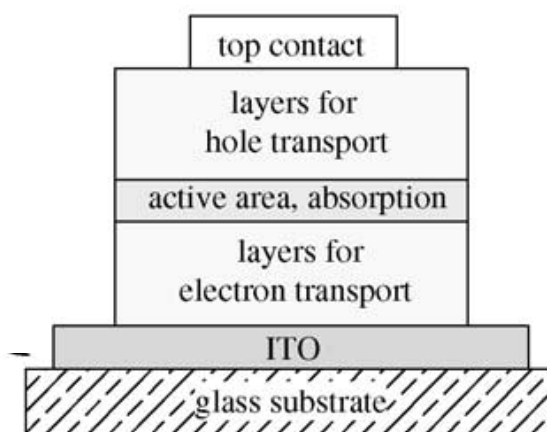
Figure 1.5 Basis structure of organic solar cell.[11]

1.1.5 Solar cell with a single phase contact to the molecular absorber.

The configuration of this cell is a serial layer of dye/Au/TiO_2. Photon incident on molecular absorber causes the separation of Fermi level of TiO_2 and Au. It is interesting that TiO_2 is not contacted directly to the molecular absorber. The contact at the electronic ground state of molecular absorber is Au layer. Meanwhile the selective contact at the high-energy state of molecular absorber is TiO_2 by virtue of the very thin layer that electron can be ballistically transferred to TiO_2. The initial efficiency of this device has been reported as 10%.
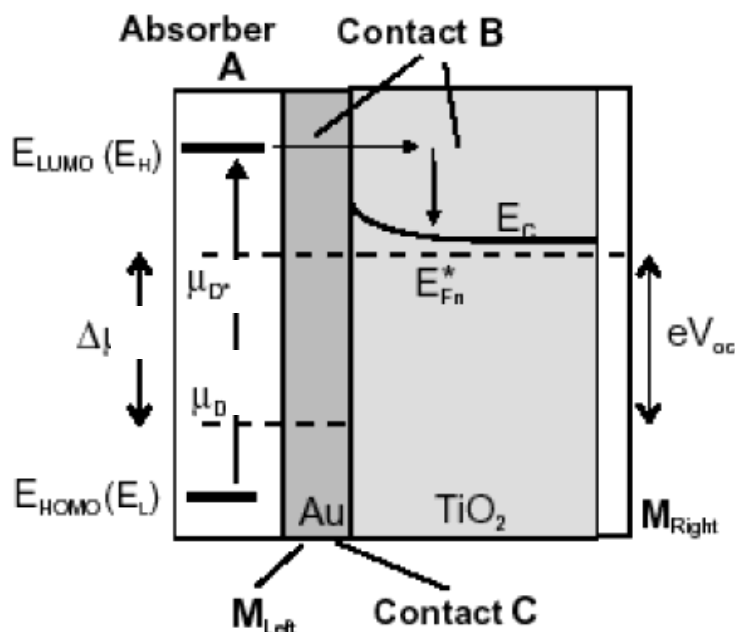
Figure 1.6 Solar cell with a single phase contact to the molecular absorber.[7]

1.2   Principle of Dye-sensitized solar cells (DSSCs)

Dye-sensitized solar cell is just a type of photovoltaic device. Figure 1.7 illustrates the principle operation of DSSC. The key components of the system are monolayer of dye, also called sensitizer or photosensitizer, which is deposited onto the mesoporous metal oxide film electrode. The oxide electrode is electrically contacted to the counter electrode by electrolyte or hole conductor.

The material of metal oxide electrode can be TiO_2 or other alternatives such as ZnO, SnO_2 etc. Photoexcitation occurred upon illumination results in electron injection of photosensitizer into the Fermi level of metal oxide electrode. The photosensitizer is then regenerated by electron donation from redox system in electrolyte, such as iodide/triiodide in organic solvent. The regeneration of photosensitizer intercepts the electron recapture of electron in TiO_2 electrode by oxidized form of photosensitizer. Finally, the redox system is regenerated, in turn, by the reduction at the counter electrode, and the electric circuit is completed via the migration of electron through the external load. The voltage of the device corresponds to the potential difference between the Fermi level of metal oxide electrode and redox

potential of the electrolyte. Overall performance generates electric power upon the illumination without losing any permanent chemical transformation.[1]
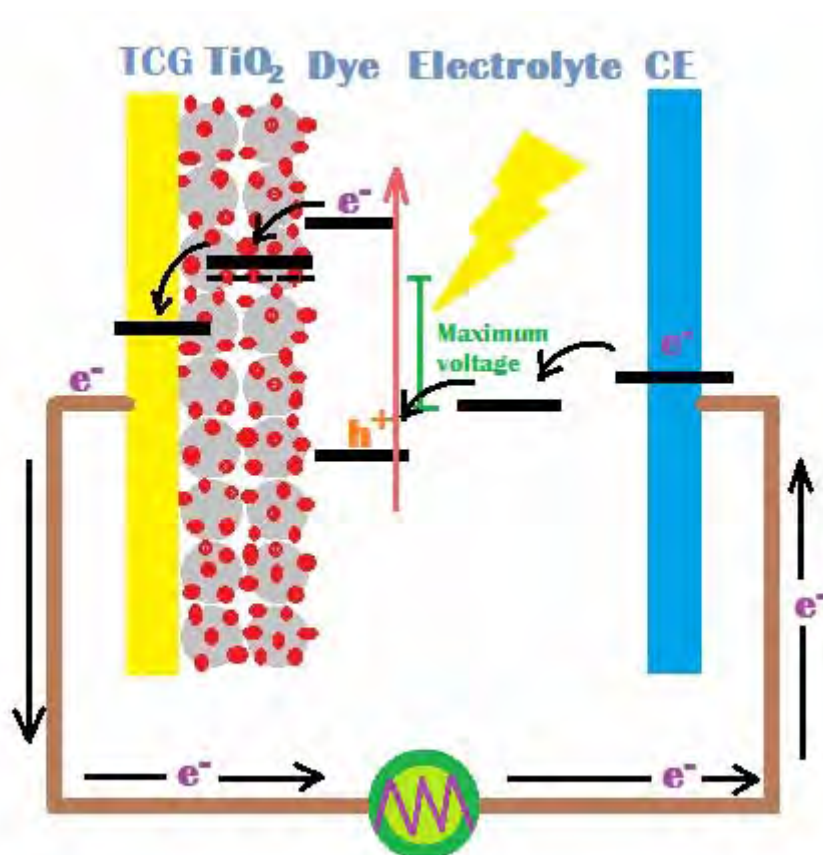
Figure 1.7 Principle operations of Dye-sensitized solar cells (DSSCs)

1.3   Electron-Transfer Process[12]

1.3.1   Reaction 1 and 2: Electron injection and Excited state decay

One of the most surprises is the ultrafast electron injection from excited state of ruthenium sensitizer to TiO_2 electrode. Even though, the mechanism of this process is still under argument, it is generally accepted that the fast femto-second injection process is observed for the attachment of this type of sensitizer absorbed onto the oxide surface. For the performance of DSSC device, the electron injection process has to consider altogether with the decay of excited state of dye, **Reaction 1**. The life time of excited state of ruthenium dye is 20-60 ns. For kinetic competition,

this would then be slow enough for electron injection that can compete with excited state decay process.

1.3.2 Reaction 3: Regeneration of oxidized photosensitizer

For 20-years lifetime of DSSC device in outdoor conditions, the turnover number, the cyclic life of the dye in a device, should be above 10^8. The lifetime of oxidized sensitizer must be over 100 s if the regeneration time is 1μs in the case of iodide used as electron donor in redox couple.

1.3.3 Reaction 4: Transportation of electron through the oxide film

This TiO_2 electrode film is composed by ensembly packing of individual particle where electrons can transport by hopping from one to the next particle. The transport mechanisms are still under debate today.

1.3.4 Reaction 5 and 6: Electron recombination from semiconductor to oxidized dye or redox couple in electrolyte

The kinetics of back-electron transfer reaction from electrode to the oxidized dye occur on a micro to milli second time scale relying on density of electron collected in semiconductor and the light intensity. Whereas the electron recombination occurred from TiO_2 to redox species in electrolyte is depended on the electron life time of redox couple.

1.4 Materials[12]

1.4.1 Mesoporous metal oxide electrode

The breakthrough efficiency of DSSCs in 1991 was achieved by the use of mesoporous TiO_2 electrode coated onto transparent conducting glass (TCG) which possesses the high internal surface area to support the sensitizer molecule.[6] Since then, TiO_2 still provides the highest efficiency, but many candidates have been arise by other oxide materials such as ZnO, SnO_2, and $SrTiO_3$ etc.

1.4.1.1 TiO$_2$

A stable and nontoxic oxide is extensively used as white pigment in several kind of industrial product such as paint, toothpaste, self-cleaning materials and sunscreen etc. Naturally, TiO$_2$ can be formed in several crystal structures: rutile, anatase, and brookite. Although rutile is a most stable form but anatase is preferable in DSSCs application because it has higher conduction band edge energy, E$_c$. This leads to the higher Fermi level and also higher open-circuit voltage in DSSCs application
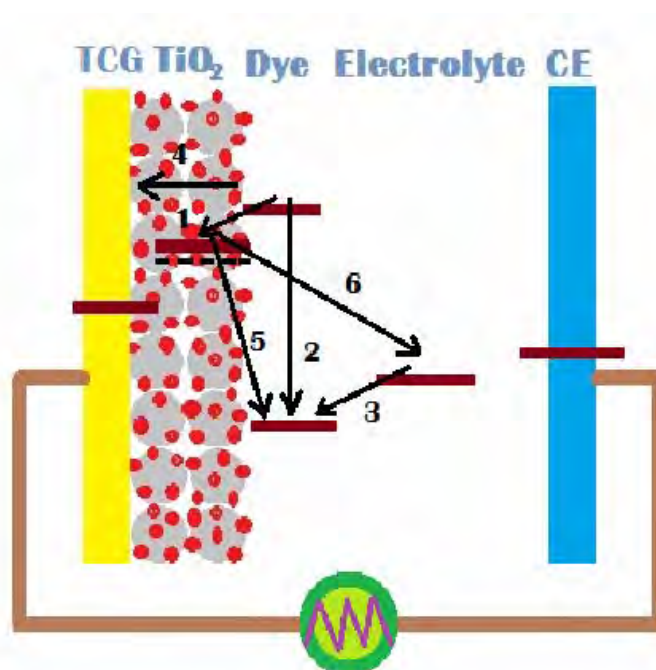
Figure 1.8 Electron-Transfer Processes of DSSCs

The most common method to prepare TiO$_2$ nanoparticle is the hydrolysis of titanium (IV) alkoxide with excess water by using acid or base as a catalyst followed by hydrothermal growth and crystallization. To deposit anatase particle onto conducting glass, the corresponding TiO$_2$ particle is formulated in paste with polymer additive. Deposition techniques can be doctor blading or screen printing. Finally, the coated conducting glass is sintered at about 450°C in air to

eliminate all organic species and to make the electrical connection between the anatase particles.

1.4.1.2 Other metal oxide.

One of the first generation of semiconductor used in DSSCs is ZnO. When compared to anatase, the conduction band edge and energy gap are quite similar. Even if, ZnO possesses the higher electron mobility than TiO_2, but the chemical stability of ZnO is quite poor because it can be dissolved under both basic and acidic conditions.

One of the chemically stable oxide, SnO_2, provides the lower conduction band edge than anatase about 0.5 eV. Hence, this material can be used as an alternative for dyes with low LUMO energy which inject electron insufficiently into anatase such as perylene sensitizer.[13]

1.4.2 Dyes

Dye, a photosensitizer or sensitizer, is one of crucial parts that should be achieved with some essential characteristics:

1) The photosensitizer should absorb the whole range of visible region of spectrum.

2) For strongly binding onto electrode surface, anchoring group, such as carboxyl (-COOH), phosphonyl (-PO_3H_2), and sulfonyl (-SO_3H) etc., are required.

3) The excited state level of dye should be higher than the conduction band edge of semiconductor (for *n*-type DSSCs) to achieve the sufficient electron transfer process of electron from excited state of photosensitizer to the conduction band of semiconductor. Whereas, for *p*-type DSSCs, the HOMO energy of dye should be lower than valent band of a semiconductor.

4) For regeneration of dye, the HOMO of the oxidized state level of the dye should be lower than the HOMO level of electrolyte.

5) The aggregation on the semiconductor surface of the dye should be avoided by structure optimization or by use of coabsorber.

6) Stability of the dye is required for long-term application.

Since, the requirements have been published, several photosensitizers including metal and metal-free compounds have been designed and applied to DSSCs.

1.4.2.1 Metal complexes

Several metal complexes, i.e. Ru, Os, Re, Fe, Pt, and Cu, have been investigated intensively as a photosensitizer for DSSCs application due to their broad absorption at visible region of spectrum. Normally, the structure of a complex consists of central metal ion with ancillary ligand containing at least one anchoring group. The absorption at the visible region is a result from metal to ligand charge transfer (MLCT) process. Ancillary ligand normally is bipyridine or terpyridine which can be structurally or electronically tuned by the substituent such as electron-withdrawing or electron donating group.

Among many metal complexes, ruthenium complexes have shown the best photovoltaic performance. Due to their broad absorption of visible spectrum, proper energy level, long-excited state lifetime, and good stability, several ruthenium sensitizers can reach more than 10% conversion efficiency under standard conditions. *cis*-Bis(2,2´-bipyridyl-4,4´-dicarboxylic acid)(NCS)$_2$ruthenium (II), coded as N$_3$, was revealed by Grätzel and coworkers in 1993.[14] This dye showed the outstanding properties at that time with conversion efficiency of 10%. A derivative of N3 dye has been developed by Nazeeruddin and coworkers called N719.[15] This compound derivatizes by replacing of two proton of N3 with two tetrabutylammonium ion. The N3 and N719 have been used as reference and basis for design of other ruthenium complexes by changing an ancillary ligand to improve the ability in light absorption of the complex.

The effect of thiocyanate ligand was used to facilitate good separation between the injected electron and oxidized dye which leaded to reduce the recombination of charge from the electrode to the dye molecule. This is the result of the electron donating property of thiocynate ligand by shift the distribution of HOMO level of dye cation away from TiO_2 surface and reducing the charge recombination process.[16]
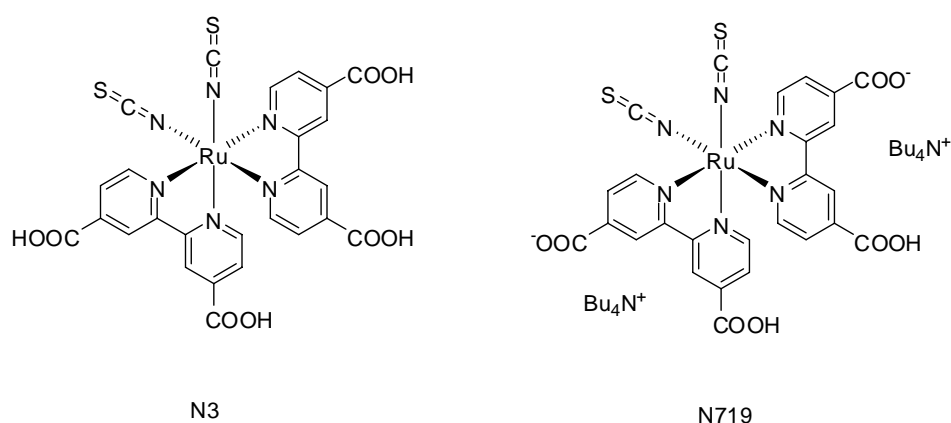
Figure 1.9 Structures of N3 and N719

1.4.2.2 Metal-free sensitizer or organic dye.

Organic dyes have been developed as alternatives for many advantages:

1) The diversity of organic photosensitizer provides the several molecular and electronic structures.

2) For environmental issue and the cost of manufacturing, organic dyes are superior to rare transition metal complexes.

3) Organic dyes possess the higher molar extinction coefficient than metal complexes which make the organic dye are attractive to thin-film DSSC application.

Several compounds, including coumarin,[17,18] indoline,[19] tetrahydroquinoline,[20] triarylamin,[21] heteroanthrocene,[22] *N,N´*-dialkylaniline,[23] and natural dyes[24,25] etc., have been applied to DSSCs performance.

1.4.3 Electrolyte

Nowadays, there are three kinds of electrolytes have been applied to DSSCs with different characteristic:

1) The most common electrolyte is iodide/triiodide in organic solvent. Sometimes lithium ion could be added to facilitate the transportation of electron. This electrolyte is good for ion diffusion and it can interpenetrate well to a mesoporous TiO_2 film. Moreover, this electrolyte still keeps the highest efficiency for all DSSCs. Nonetheless, it is limited by long-term stability due to the volatilization of organic solvent.

2) Inorganic ionic liquid is made from salts or salt mixture. It looks like solid, but it possesses the properties of liquid and performs well in conductivity. Unfortunately, the efficiency declines after the long period of time.

3) For solid, electrolyte due to their morphology that makes it hard to fill into the porous of TiO_2 film.

1.4.4 Counter electrode

For counter electrode, the opposite of TiO_2 electrode, it is commonly used platinised conducting glass for efficient generation of I^-. Platinum is technically the best material to construct the efficient devices. Due to the cost of Pt, many counter electrodes have been developed, including carbon cathode. Carbon cathodes have been a considerable candidates which can be used in many forms such as carbon black, carbon nanotube etc.

1.5   Efficiency measurement

1.5.1   Conversion efficiency[12]

The current-voltage (I-V) characteristics of solar cells under illumination are used in determination of conversion efficiency, η. From the I-V curve, the intercept of V = 0 indicates the short-circuit current, I_{SC} (or short-circuit current density, J_{SC}). Whereas the intercept of I = 0 indicates the open-circuit voltage, V_{OC}. Fill factor, *ff*, is defined by a ratio of maximum power point, P_{max} (obtained from the maximum value from the plot of power, I×V, and voltage, V), divided by I_{SC} and V_{OC}.

$$ff = \frac{Pmax}{Isc \times Voc} = \frac{Vmp \times Imp}{Isc \times Voc} \qquad \text{eq1.1}$$

$$\eta = \frac{Pmax}{Pin} = \frac{Isc \times Voc \times ff}{Pin} \qquad \text{eq1.2}$$

Where, the P_{in} is the power density of incident light.

a)   b)
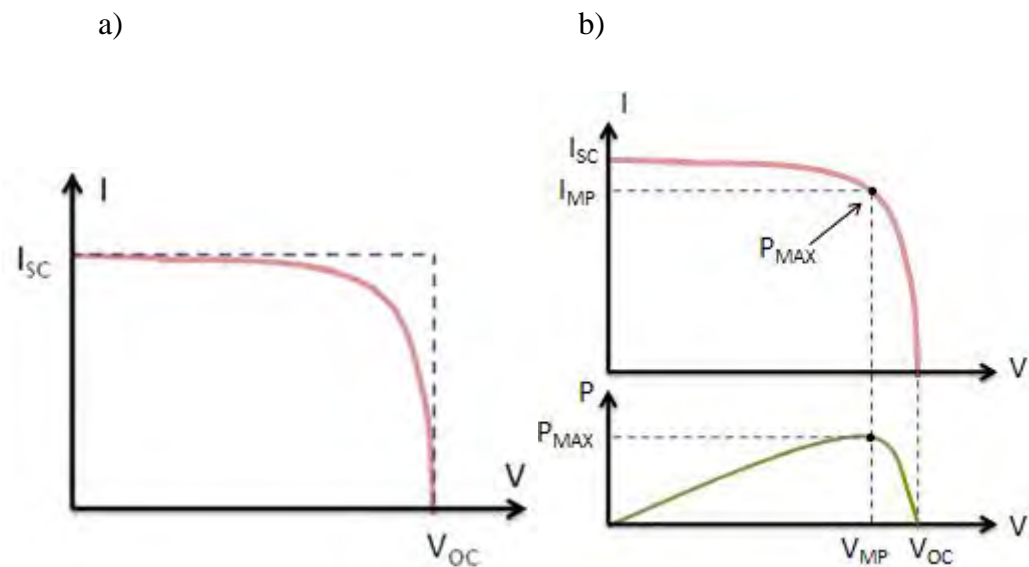
Figure 1.10 I-V curve obtained from the measurement: a) I-Vcharacteristic, b) determination of Pmax

From the experiment, I_{SC} value depends directly on the light intensity. The maximum radiation of the sun, directly overhead, has the shortest path length through the earth's atmosphere. The path length is called air mass, AM, which can be estimated by AM = 1/cosθ. Where, the θ is the angle of elevation of the sun. For the standard measurement for global experiment, AM = 1.5 G (global), derived from θ = 42°, is preferred.

1.5.2 Incident photon to current conversion efficiency (IPCE)[1]

The incident photon to current conversion efficiency corresponds to the number of electron occurred from photogeneration divided by the monochromatic photon flux striking the cell.

$$IPCE(\lambda) = LHE(\lambda)\ \Phi_{inj}\ \eta_{coll} \qquad eq1.3$$

Where, LHE(λ) is the light-harvesting efficiency for photons of wavelength λ, Φ_{inj} is the quantum yield for electron injection from the excited sensitizer, and η_{coll} is the electron collection efficiency.

1.6 Quinoxaline synthesis
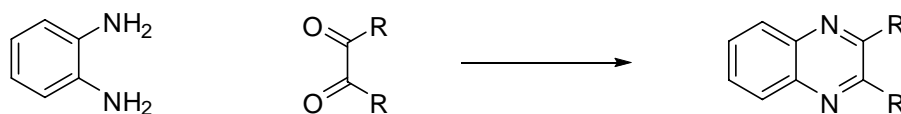
Scheme 1.1 Quinoxaline synthesis

A key to improve photoproperties, such as an absorption at long wavelength or in visible region, an increment of the extinction coefficient etc., is an extension of π-conjugation system of a compound. Several experiments have been performed to achieve the goal including Wittig synthesis,[26] cross-coupling reaction by using transition metals as catalysts,[27] and aromatic including with heteroaromatic cyclization.[28] In this study, quinoxaline synthesis, which is a type of a synthesis of

heterocyclic compound, has been employed to modify the sensitizer for DSSCs applications.

Chemistries of quinoxaline have attracted the large extension to many kinds of applications, due to their bioactivities, such as anti-viral, anti-bacterial, anti-protozoal, anti-cancer and anti-HIV etc. Moreover, quinoxaline derivatives have also been appeared in application of dye, light-harvesting device, organic semiconductor, photonic nanowire etc.[29]

Several methods are available for the synthesis experiment. Several methodology has been developed such as the condensation of aryl-1,2-diamine with α-diketone, 1,4-addition of 1,2-diamine to diazenylbutane, cyclization - oxidation of phenacyl bromide (2-bromoacetophenone), and oxidative coupling of epoxides with ene-1,2-diamine. The most common method, used in this study, is the condensation of aryl-1,2-diamine with α-diketone by heating in solvent with or without catalyst. Many catalysts have been reported as alternatives for synthetic application, for instance, MnO_2, $POCl_3$, zeolite, iodine, $CuSO_4.5H_2O$ etc.
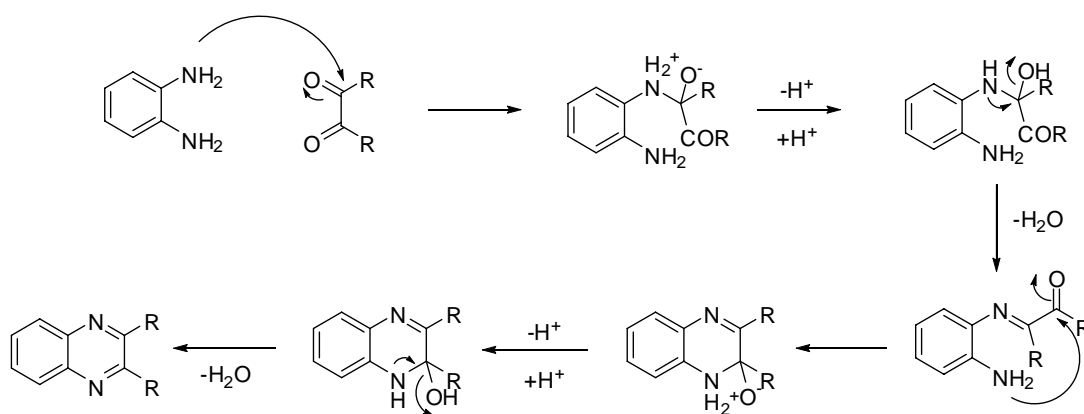
Scheme 1.2 Mechanism for quinoxaline synthesis reaction without using any catalysts

In this study, 1,10-phenanthroline-5,6-diamine is was used as aryl-1,2-diamine compound and benzil derivatives are used as α-diketone compounds. The nomenclature fixes 2,3-phenylpyrazino[2,3-*f*][1,10]phenanthroline as a core structure and varies the substituent at *para*-position of phenyl moiety for the derivatives.
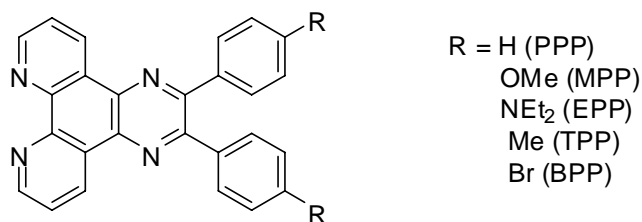
Figure 1.11 Structure of 2,3- phenylpyrazino[2,3-*f*][1,10]phenanthroline derivatives

1.7 Literature reviews

In 2004, Wang and coworkers developed a new heteroleptic pyridyl polypyridyl ruthenium sensitizer with high molar extinction coefficient, named as Z910.[30] A new sensitizer showed a highly efficient and stable sensitizer for DSSCs. All parameters: short-circuit current density (J_{sc}), open-circuit voltage (V_{oc}), fill factor (ff), and conversion efficiency, of this sensitizer are 1.72 mA/cm^2, 777 mV, 0.764 and 10.2%, respectively. For the stability test, 3-methoxypropionitrile-based electrolyte was used under moderate thermal stress and visible-light soaking at 100 mW/cm^2 at 55°C. All photovoltaic characteristics are stable during the accelerating test of 1000 hr.
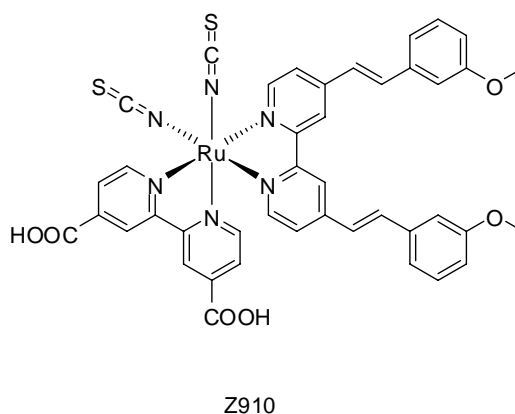
Z910

Figure 1.12 Structure of Z910

In 2004, Wang and coworkers synthesized a new amphiphilic ruthenium sensitizer, coded as Z955.[31] The dye was replaced carbonyl groups by phosphonyl groups to facilitate as anchoring groups. The photovoltaic characteristics illustrated

short-circuit current density (J_{sc}), open-circuit voltage (V_{oc}), fill factor (ff), and conversion efficiency as 16.37 mA/cm^2, 707 mV, 0.693 and 8.0%, respectively.
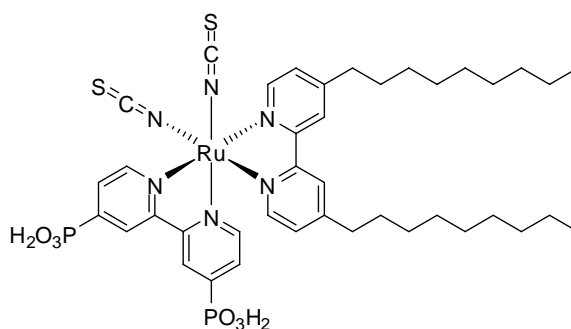
Z955

Figure 1.13 Structure of Z955

In 2005, K8 developed by Klein and coworkers[32] was synthesized by using of 4,4´-bis(carboxyvinyl)-2,2´-bipyridine as ligands for ruthenium complex instead of 2,2´-bipyridine-4,4´-dicarboxylic acid used in synthesis of N3 and N719. The absorption at metal to ligand charge transfer (MLCT) band of this complex is bathochromically shifted 20 nm and the molar extinction coefficient is higher than N3. Short-circuit current density (J_{sc}), open-circuit voltage (V_{oc}), fill factor (ff), and conversion efficiency characteristics are 18.0 mA/cm^2, 640 mV, 0.75 and 8.64%, respectively. This sensitizer provides the good efficiency because of its strong light absorption results from the long π-conjugation.

In 2007, N945 was synthesized by Nazeeruddin and coworkers.[33] The new sensitizer complex employed 4,4´-di-(2-(3,6-dimethoxyphenyl)ethenyl)-2,2´-bipyridine as a light-harvesting unit. This sensitizer exhibits the excellent photovoltaic performance with short-circuit currentdensity of18.84 mA.cm-2, open-circuit voltage of 0.78 V, fill factor of 0.73, and overall conversion efficiency of 10.82% under standard measurement (AM = 1.5 G). This high conversion efficiency is the result from the extended-π-conjugation including with the electron donating group for enhancing the molar extinction coefficient.
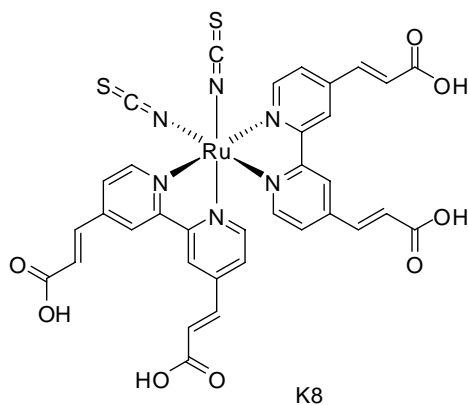
Figure 1.14 Structure of K8
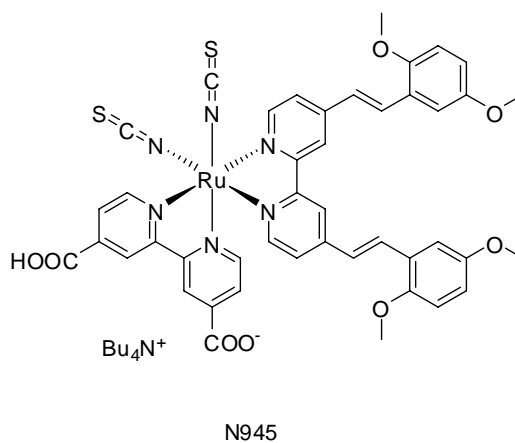
Figure 1.15 Structure of N945

In 2007, Kuang and coworkers synthesized a high efficiency and stable sensitizer, denoted K77.[34] This sensitizer exhibits the efficiency more than 10.5% by using a volatile electrolyte. Moreover, this sensitizer shows the long-term stability over 1000 h under light soaking and thermal stress when use in combination with non-volatile electrolyte (with conversion efficiency up to 9.5%).
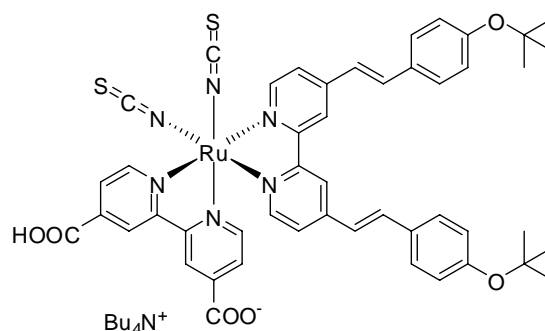
K77

Figure 1.16 Structure of K77

In 2009, Cao and coworkers synthesized the new sensitizer by extending (hexylthio)thiophene moiety onto the 4,4´-position of light-harvesting pyridine unit of heteroleptic ruthenium complex.[35] The new sensitizer showed the overall conversion efficiency of 10.57% comparing to Z907 and C101. The photovoltaic performance shown in **Table 1.1**.

Table 1.1 Photovoltaic parameters of Z907, C101, and C106

Dye	J_{sc}(mA.cm^{-2})	V_{oc}(V)	*ff*	η(%)
Z907	17.13	0.73	0.72	9.05
C101	17.75	0.75	0.78	10.33
C106	18.28	0.75	0.77	10.57
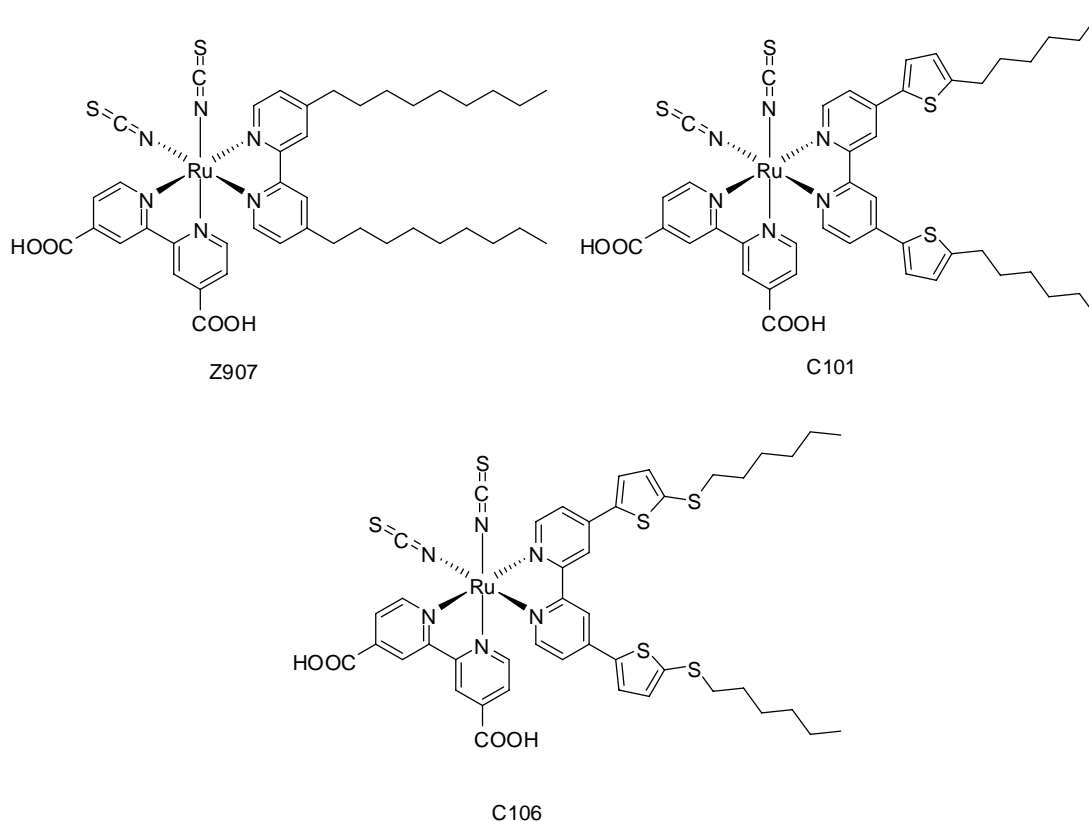
Figure 1.17 Structures of Z907, C101, and C106

1.8   Objectives

According to the idea obtained from the literature reviews, the ruthenium complexes with higher conjugated bipyridine ligand provide the higher conversion efficiency due to the improvement of light absorption of the complexes. The ruthenium complexes containing 2,3-diphenylpyrazino[2,3-*f*][1,10]phenanthroline derivatives have been synthesized and studied as photosensitizers for dye-sensitized solar cells. The experiment was used N719 as standard sensitizer to compare the results obtained from synthesized-dye complexes.

1.9   Statement of propose

Due to the energy crisis that human will be faced inevitably. Many efforts have been taken to alleviate this problem for a past few decades. Photovoltaic devices such as solar cell have been explored to convert light into electricity by the photoelectric principle. Although silicon solar cell provides a ahigh conversion

efficiency, but their requirement of high processes in fabrication and non-flexibility make the cell inherits the high cost and low application.

Dye-sensitized solar cell is just a one type of photovoltaic device which has been developed to compensate the drawbacks of silicon cell. Due to the performance of dye-sensitized solar cell is still low, many attempts have been tried to develop this type of cell. One issue has been discussed for a past few years that dye is the critical component of a device. Many studies, especially from Grätzel group, revealed that ruthenium sensitizers provided the high efficiency. Nonetheless the molar extinction coefficient of the ruthenium complexes is quite low, this limited their performance as photosensitizers of the device. To enhance the molar extinction coefficient, light-harvesting unit such as organic ligand with high-π-conjugation should be applied to the ruthenium complexes.

In this study, the researchers have developed the five new heteroleptic ruthenium complexes. For the structure of these complexes, the bipyridine ligand containing carboxy group as the anchoring part of the molecule and thiocyanate ligand were still remained. 2,3-Diphenylpyrazino[2,3-*f*][1,10]phenanthroline ligands have been used to exploit the light-harvesting property of the molecule including with the study of electron-donating effect by introducing the electron-rich functional group such as OMe, NEt$_2$, Me, and Br. Finally the new heteroleptic ruthenium complexes were expected to become the effective sensitizer for dye-sensitized solar cell application.

CHAPTER II

EXPERIMENT

2.1   General

The weight of all chemicals was determined on a Mettler Toledo AB204-S electrical balance. Evaporation of solvents was carried out on a Büchi Rotavapor R-114 rotary evaporator equipped with a Büchi B-480 Waterbath. The progress of the reactions was followed by thin layer chromatography (TLC) performed on Merck D.C. silica gel 60 F_{254} 0.2 mm precoated aluminium plates and visualized using UV light (254, 365 nm). Column chromatography was performed on activated aluminium oxide 90 (Activity I), and Sephadex LH-20.

Proton (^{1}H) and carbon (^{13}C) nuclear magnetic resonance (NMR) spectra were recorded on a Varain Mercury-400 plus spectrometer operating at 400 MHz and Bruker Avance 300 spectrometer (^{1}H: 300 MHz, ^{13}C: 75 MHz). Unless stated otherwise, the spectra were taken in $CDCl_3$ or DMSO-d_6. Chemical shifts (δ) are reported in parts per million (ppm) relative to tetramethylsilane (TMS) or using the residual protonated solvent signal as a reference. Coupling constants (J) are proton-proton coupling unless otherwise noted and are reported in hertz (Hz). Multiplicities were designated as followed: s = singlet, d = doublet, dd = doublet of doublet, t = triplet, q = quartet, m = multiplet.

Infared spectra were recorded on Thermo Scientific-Nicolet S10 ATR-FTIR spectrometer. Elemental analyses were performed by Scientific and Technological Research Equipment Centre, Chulalongkorn University. Bruker micrOTOF-Q II High resolution mass spectrometry (HRMS) was performed at the Department of Chemistry, Faculty of Science, Chulalongkorn University. Absorption spectra were recorded on a Varian Cary 50 Probe UV-Visible spectrometer. Cyclic voltammetry was performed on a μ-AUTOLAB TYPE III potentiostat with scan rate of 50 mV.s^{-1}

using Pt wire, glassy carbon and Ag/AgNO$_3$ as counter electrode, working electrode and reference electrode, respectively.

2.2   Materials

Commercial grade solvents for column chromatography were distilled before use. Solvents for reactions were AR grade. All chemicals were purchased and used as received without further purification. The chemicals were purchased from the following vendors:

- Across Organics (New Jersey, USA): trifluoroacetic acid

- Advanced Scientific Technology; dichloromethane, ethyl acetate

-Aldrich Chemical Co., Inc. (Steinheim, Germany); dichloro-(*p*-cymene)-ruthenium(II) dimer

- BDH Chemicals Ltd. (Poole, England); sulfuric acid, 10% Pd/C, sodium cyanide, anisole

- Carlo Erba Reagenti (Milan, Italy); nitric acid, potassium dichromate, potassium bromide

- Fluka Chemical Corp. (Buchs, Switzerland); 1,10-phenanthroline monohydrate, Celite, fluorobenzaldehyde, bromobenzaldehyde, tolualdehyde, diethylamine, oxalyl chloride, 4,4´-dimethyl-2,2´-bipyridine, tetrabutylammonium hexafluorophosphate

- Merck Co.,Ltd. (Darmstadt, Germany); hydrazine monohydrate, hydroxylamine hydrochloride, toluene, diethyl ether, silver nitrate, ethanol, deuterated chloroform, hexadeuterated dimethylsulfoxide

- RCI Labscan Ltd. ; anhydrous *N,N´*-dimethylformamide

- Riedel-de Haën AG (Seelze, Germany); dimethylsulfoxide

- Sigma-Aldrich, Co., (St. Louise, Missouri, USA); ammonium thiocyanate, barium carbonate

- Suksapan Panit (Bangkok, Thailand); sodium chloride, sodium sulfate, sodium bicarbonate, sodium carbonate

- Thai Industrail Gas Public Co., Ltd. (Bangkok, Thailand); nitrogen gas,

2.3 Synthesis

2.3.1 Synthesis of ligands

2.3.1.1 Synthesis of 1,10-phenanthroline-5,6-dione[36] (1)

(1)
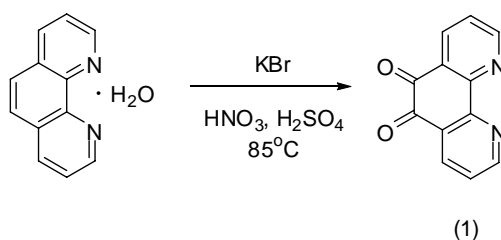
Phenanthroline monohydrate (1.00 g, 5.04 mmol) was dissolved in concentrated sulfuric acid (20 mL) in a round-bottom flask. Potassium bromide (5.95 g, 50 mmol) was added to the cold acidic mixture in small portions and the cold concentrated nitric acid (10 mL) was then added dropwise to the mixture. The reaction setup was equipped with a condenser and the reaction mixture was refluxed at 85°C for 3 hours. The residue bromine gas was eliminated by flowing nitrogen gas through the mixture and the mixture was then poured into 400 mL of cold water. $NaHCO_3$ was used for neutralization. The precipitate was collected by extracting with DCM. The organic layer was collected, washed with water (2×200 mL) and brine (2×200 mL), dried with Na_2SO_4, and evaporated under reduced pressure to obtain the corresponding product as a yellow solid (1.04 g, 4.93 mmol, yield 98%). ^{1}H NMR (CDCl$_3$, 400 MHz) δ: 7.60 (dd, 2H, J = 5 Hz, J = 8 Hz, Ar), 8.51 (d, 2H, J = 8 Hz, Ar), 9.13 (d, 2H, J = 5 Hz, Ar). IR (ATR-IR) ν = 3058 (m) (C-H), 1678 (s) (C=O), 1574 (s) (C=C), 1454 (m) (C=C); UV-Visible (EtOH, nm): λ_{max} (ε × 10^4) 252 (1.96).

2.3.1.2 Synthesis of 1,10-phenanthroline-5,6-dioxime[38] (2)
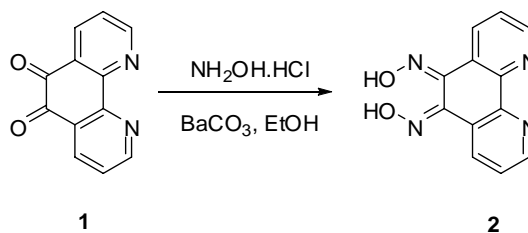
A mixture of 1,10-phenanthroline-5,6-dione (**1**) (1.00 g, 4.76 mmol), hydroxylamine hydrochloride (1.16 g, 16.65 mmol), and barium carbonate (1.41 g, 7.14 mmol) was dissolved in ethanol and refluxed for 12 hours. The white precipitate was filtered and treated with 0.2 M hydrochloric acid for half an hour. The solid residue was filtered, washed with successive amount of water, ethanol and ether, respectively, and dried in air. The white powder product was collected as an non-dissolved product (0.64 g, 2.66 mmol, yield 60%).

2.3.1.3 Synthesis of 5,6-diamino-1,10-phenanthroline[38] (3)
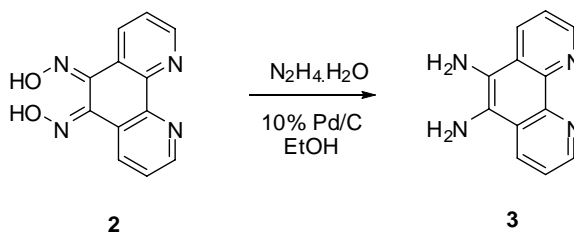
A suspension of 1,10-phenanthroline-5,6-dioxime (**2**) (0.64 g, 2.66 mmol) and 10% Pd/C (0.4 g) and 100 mL of dried ethanol was stirred and refluxed under nitrogen atmosphere. A solution of 7 mL of hydrazine monohydrate in 15 mL of dried ethanol was then added dropwise to the reaction over a period of 1 hour and the mixture was stirred for another 12 hours. The hot mixture was filtered through a bed of Celite and washed with hot ethanol until the eluent became colorless. The filtrate was concentrated with rotary evaporator to give a slurry residue. The residue was triturated with water and left at 4°C overnight. A tan solid was separated by filtration to obtain the corresponding amine product in 74% yield (0.42 g, 1.97 mmol). ^{1}H NMR (DMSO-d_6, 400 MHz) δ: 5.42 (exchange, 2H, NH), 7.64 (dd, 2H, $J = 4$ Hz, $J = 8$ Hz, Ar), 8.52 (d, 2H, $J = 8$ Hz, Ar), 8.79 (d, 2H, $J = 4$ Hz, Ar). IR (ATR-IR) ν =

3260 (m,b)(N-H), 3187 (m,b)(N-H), 1651 (m)(N-H bending), 1604 (m)(C=C), 1583 (m)(C=C), 1479 (m)(C=C), 796 (s)(C-H bending); UV-Visible (EtOH, nm): λ_{max} ($\varepsilon \times 10^4$) 268 (2.31).

2.3.1.4 General procedure in synthesis of some benzil derivatives[37] (4a-c)

A solution of benzaldehyde derivatives (2 mL) in 5 mL of ethanol and a solution of sodium cyanide (0.2 g) in 5 mL of water were mixed together and refluxed for 4 hours. After cooling down to room temperature, the mixture was extracted with dichloromethane. The organic phase was washed with water (2×20 mL) and brine (2×20 mL), dried and solvent was evaporated. The resulting benzoin oil (~2 mL) was further refluxed in concentrated nitric acid for an additional 3 hours. The acidic solution was allowed to cool to room temperature and poured into cold water to obtain the light-yellow solid which was then extracted with dichloromethane. The organic layer was washed with successive amount of saturated sodium bicarbonate solution, water, and brine to give the corresponding product

Synthesis of 4,4´-difluorobenzil (4a)
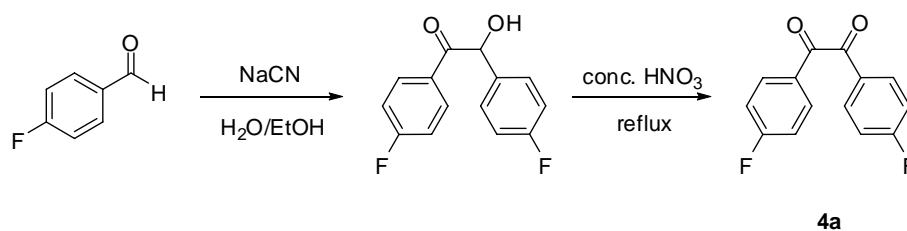
(1.40 g, 5.69 mmol, yield 61%). ^{1}H NMR (CDCl$_3$, 400 MHz) δ: 7.20 (dd, 4H, $J = 9$ Hz, $J = 9$ Hz, Ar), 8.02 (dd, 4H, $J = 5$ Hz, $J = 9$ Hz, Ar). IR (ATR-IR) ν = 3075 (m) (C-H), 1660 (s) (C=O), 1596 (m) (C=C), 1407 (m) (C=C), 839 (m) (C-H bending), 882 (m) (C-H bending); UV-Visible (CH$_2$Cl$_2$, nm): λ_{max} ($\varepsilon \times 10^4$) 263 (1.87).

Synthesis of 4,4´-dibromobenzil (4b)

4b
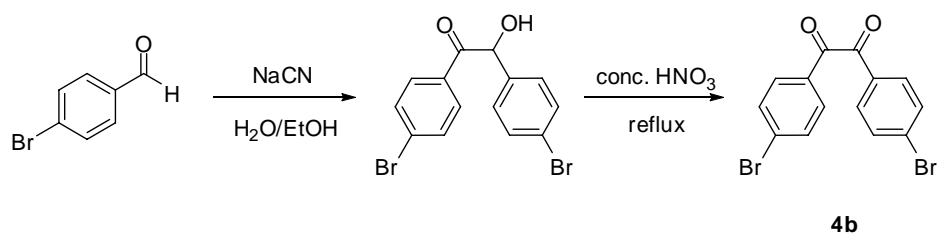
(0.83 g, 2.27 mmol, yield 42%). ^{1}H NMR (CDCl$_3$, 400 MHz) δ: 7.65 (d, 4H, J = 9 Hz, Ar), 7.81 (d, 4H, J = 9 Hz, Ar). IR (ATR) ν = 3093(m) (C-H), 1660 (s) (C=O), 1583 (m) (C=C), 1479 (m) (C=C), 830 (m) (C-H bending); UV-Visible (CH$_2$Cl$_2$, nm): λ$_{max}$ (ε × 10^4) 279 (3.17).

Synthesis of 4,4´-dimethylbenzil (4c)

4c
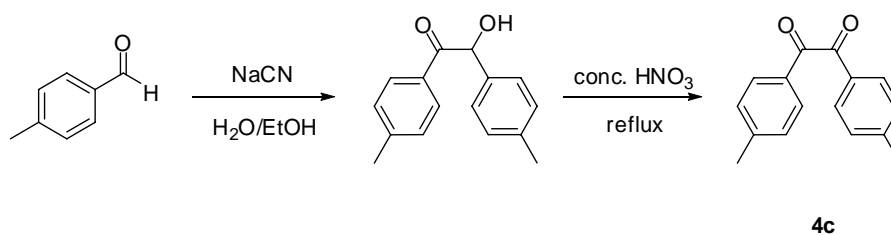
(0.62 g, 2.62 mmol, yield 31%). ^{1}H NMR (CDCl$_3$, 400 MHz) δ: 2.43 (s, 6H, Me), 7.29 (d, 4H, J = 8 Hz, Ar) , 7.85 (d, 4H, J = 8 Hz, Ar). IR (ATR) ν = 1656 (s) (C=O), 1600 (s) (C=C), 1541 (m) (C=C), 834 (m) (C-H bending); UV-Visible (CH$_2$Cl$_2$, nm): λ$_{max}$ (ε × 10^4) 270 (1.95).

2.3.1.5 Synthesis of 4,4´-bisdiethylaminobenzil (4d)

4a **4d**
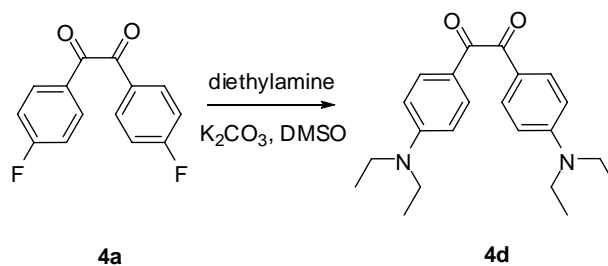
The reaction was carried out following the method by Jiwu et al. with a slight modification.[39] First, a slurry of 4,4´-difluorobenzil (4a) (0.30 g, 1.2 mmol),

potassium carbonate (660 mg, 4.8 mmol) and diethylamine (2 g, 27.3 mmol) in DMSO was heated at 90°C in a screw-capped tube for 1 day. When the reaction completed, water was added to the reaction mixture that caused the formation of the solid product. The crude product was further purified by column chromatograghy using silica gel with dichloromethane as an eluent to obtain the corresponding product (0.34g, 0.97 mmol, 80%).^{1}H NMR (CDCl$_3$, 400 MHz) δ: 1.19 (t, 12H, J = 7 Hz, Me), 3.41 (q, 8H, J = 7 Hz, CH$_2$), 6.61 (d, 4H, J = 4 Hz, Ar), 7.83 (d, 4H, J = 9 Hz, Ar). IR (ATR-IR) ν = 2868 (m) (C-H), 1648 (s) (C=O), 1578 (m) (C=C), 1522 (m) (C=C), 1243 (m) (C-N), 1140 (m) (C-N), 826 (m)(C-H bending); UV-Visible (EtOH, nm): λ$_{max}$ (ε × 10^4) 371 (4.93).

2.3.1.6 Synthesis of anisil[40] (4e)

4e
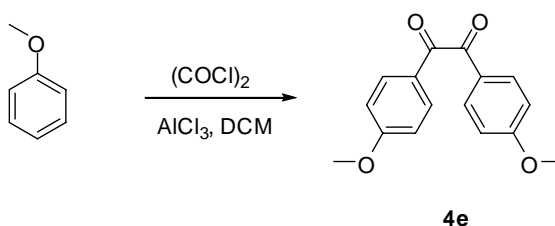
The procedure was a modified Friedel-Craft acylation reaction. First, a solution of oxalyl chloride (2.1 g) in dichloromethane was added to a suspension of aluminium (III) chloride (5 g) in dichloromethane at 0°C under a nitrogen atmosphere. After standing for half an hour, a solution of anisole (10 mL) in dichloromethane was added dropwise and the mixture left for 2 hours at the same temperature. The reaction was allowed to cooled to room temperature and was then refluxed for 1 hour. The dichloromethane solvent removed by rotary evaporation to give a deep red slurry. The large amount of chip ice was added to the slurry. The resulting suspension was extracted with dichloromethane and basicified by using NaHCO$_3$. The organic phase was collected, dried and evaporated to obtain the light-green anisil product (1.34 g, 4.96 mmol, 30%).^{1}H NMR (CDCl$_3$, 400 MHz) δ: 3.89 (s, 6H, Me), 6.97 (d, 4H, J = 8 Hz, Ar), 7.95 (d, 4H, J = 8 Hz, Ar). IR (ATR-IR) ν = 1651 (s) (C=O), 1592 (s) (C=C), 1505 (s) (C=C), 1260 (s) (C-O), 1110 (m) (C-O), 826 (m) (C-H bending); UV-Visible (CH$_2$Cl$_2$, nm): λ$_{max}$ (ε × 10^4) 299 (2.83).

2.3.1.7 Synthesis of 2,2′-pyridine-4,4′-dicarboxylic acid[41] (5)

5
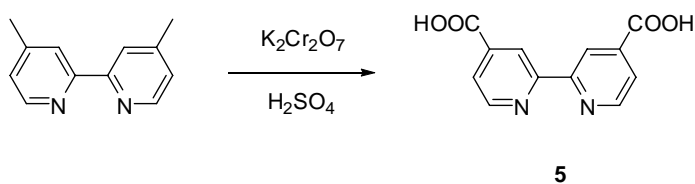
A solution of 4,4′-dimethyl-2,2′-pyridine (1 g, 5.4 mmol) was dissolved in 30 mL of concentrated sulfuric acid and heated up to 70-80°C. Potassium dichromate (5 g, 17 mmol) was added slowly to the hot acid solution over a period of 2 hours by controlling the temperature not over 80°C. The deep green acid solution was poured into 150 mL of ice/water to give a greenish precipitate which was then isolated from the mixture by vacuum filtration. The solid was further refluxed in a half concentrated nitric acid for 2 hours. The acid mixture was cooled to room temperature and was then poured into 200 mL of ice/water. The white precipitate was washed with water to obtain the corresponding product (0.93 g, 3.80 mmol, 70%). ^{1}H NMR (DMSO-d_6, 400 MHz) δ: 7.92 (d, 2H, J = 5 Hz, Ar), 8.84 (s, 2H, Ar), 8.92 (d, 2H, J = 5 Hz, Ar). IR (ATR-IR) ν = 3110 (m) (C-H), 1699 (s) (C=O), 1605 (m) (C=C), 1458 (m) (C=C), 762 (m) (C-H bending); UV-Visible (DMF, nm): λ_{max} ($\varepsilon \times 10^4$) 295 (1.32).

2.3.1.8 General procedure for the synthesis of pyrazino[2,3-f][1,10]phenanthroline derivatives[42] (6a-e)

A slurry of 5,6-amino-1,10-phananthroline (100 mg, 0.5 mmol) and benzil derivatives (**4a-e**) (1.3 eq.) in toluene was equipped in a screw-capped tube. The reaction was heated at 90°C with trifluoroacetic acid as a catalyst under a dark condition by wraping with aluminum foil. After the reaction was competed, the liquid was removed by vacuum evaporation to give the crude product. The crude product was dissolved and passed through the neutral alumina column with dichloromethane as an eluent to obtain the corresponding product (6a-e)

Synthesis of 2,3-diphenylpyrazino[2,3-f][1,10]phenanthroline (PPP ligand, 6a)
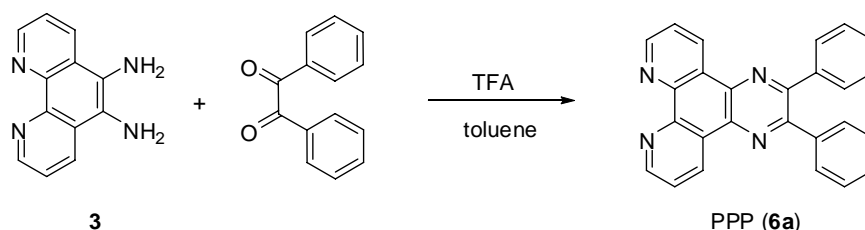
White solid, (122.52 mg, 0.32 mmol, yield 67%).^{1}H NMR (CDCl$_3$, 400 MHz) δ: 7.45 (m, 6H, Ar), 7.68 (d, 4H, J = 7 Hz, Ar), 7.76 (dd, 2H, J = 4 Hz, J = 8 Hz, Ar), 9.27 (d, 2H, J = 4 Hz, Ar), 9.54 (d, 2H, J = 8 Hz, Ar); ^{13}C NMR δ: 123.8, 127.0, 128.3, 129.1, 130.1, 133.2, 137.8, 138.8, 147.6, 152.0, 152.6; IR (ATR-IR) ν = 3019 (m) (C-H), 1570 (m) (C=C), 1492 (m) (C=C), 770 (s) (C-H bending), 736 (m) (C-H bending); UV-Visible (CH$_2$Cl$_2$, nm): λ$_{max}$ (ε × 10^4) 270 (5.54), 309 (2.27), 363 (2.18); HRMS (ES$^+$) m/z 385.1452, calcd for C$_{26}$H$_{17}$N$_4$ [M+H]$^+$ 385.1453; Anal. Calcd for C$_{26}$H$_{16}$N$_4$: C, 81.23; H, 4.20; N, 14.57. Found: C, 81.42; H, 4.21; N, 14.53.

Synthesis of 2,3-bis(4-methoxyphenyl)pyrazino[2,3-f][1,10]phenanthroline (MPP ligand, 6b)
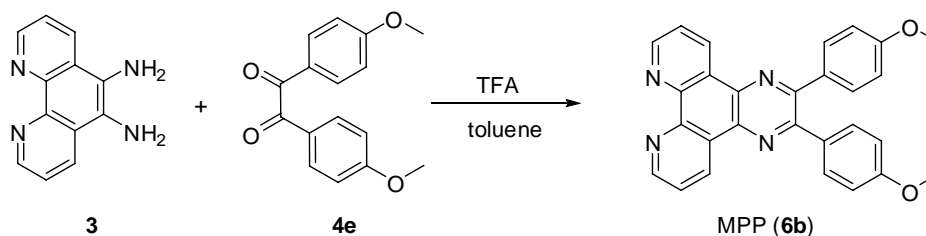
Yellow solid, (150.11 mg, 0.34 mmol, yield 71%).^{1}H NMR (CDCl$_3$, 400 MHz) δ: 3.87 (s, 6H, Me), 6.93 (d, 4H, J = 8 Hz, Ar), 7.67 (d, 4H, J = 8 Hz, Ar), 7.77 (dd, 2H, J = 4 Hz, J = 8 Hz, Ar), 9.26 (d, 2H, J = 4 Hz, Ar), 9.53 (d, 2H, J = 8 Hz, Ar); ^{13}C NMR δ: 55.3, 113.9, 123.8, 127.1, 131.4, 133.1, 137.3, 147.5, 151.8, 160.4; IR (ATR-IR) ν = 1605 (s) (C=C), 1510 (s) (C=C), 1239(m) (C-O), 1127 (m) (C-O), 830 (m) (C-H bending), 800 (m) (C-H bending), 735 (m) (C-H bending); UV-Visible (CH$_2$Cl$_2$, nm): λ$_{max}$ (ε × 10^4) 273 (4.15), 328 (2.08), 380 (1.82); HRMS (ES$^+$) m/z 445.1714, calcd for C$_{28}$H$_{21}$N$_4$O$_2$ [M+H]$^+$ 445.1665; Anal. Calcd for C$_{28}$H$_{20}$N$_4$O$_2$: C, 75.66; H, 4.54; N, 12.60. Found: C, 75.60; H, 4.53; N, 12.59.

Synthesis of 4,4´-(pyrazino[2,3-f][1,10]phenanthroline-2,3-diyl)bis(*N,N´*-diethylaniline) (EPP ligand, 6c)
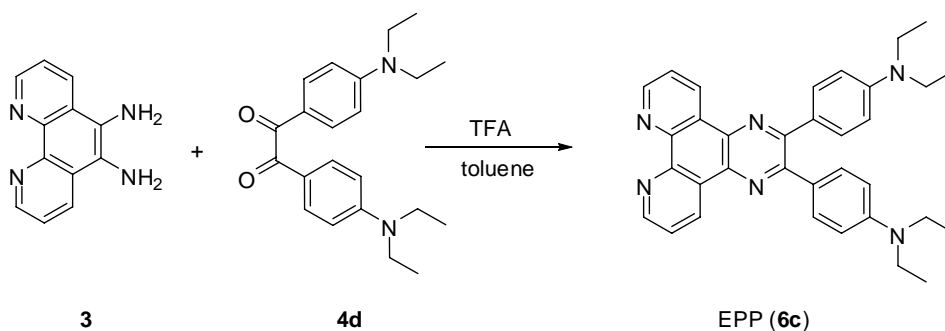
Orange solid, (187.89 mg, 0.36 mmol, yield 75%).^{1}H NMR (CDCl$_3$, 400 MHz) δ: 1.20 (t, 12H, *J* = 7 Hz, Me), 3.41 (q, 8H, *J* = 7 Hz, CH$_2$), 6.69 (d, 4H, *J* = 8 Hz, Ar), 7.71 (d, 6H, *J* = 8 Hz, Ar), 9.20 (d, 2H, *J* = 2 Hz, Ar), 9.51 (d, 2H, *J* = 8 Hz, Ar); ^{13}C NMR δ: 12.6, 44.5, 111.2, 111.3, 123.5, 127.5, 131.2, 132.9, 136.4, 147.2, 148.2, 151.1, 152.3; IR (ATR) ν = 2968 (m) (C-H), 1600 (s) (C=C), 1519 (m) (C=C), 1368 (m) (C-N), 1191 (m) (C-N), 809 (m) (C-H bending), 740 (m) (CH bending); UV-Visible (CH$_2$Cl$_2$, nm): λ$_{max}$ (ε × 10^4) 256 (5.18), 287 (3.05), 330 (2.58), 394 (2.58), 430 (2.38); HRMS (ES$^+$) *m/z* 549.2754, calcd for C$_{34}$H$_{35}$N$_6$ [M+Na]$^+$ 549.2743; Anal. Calcd for C$_{34}$H$_{34}$N$_6$: C, 77.54; H, 6.51; N, 15.96. Found: C, 77.07; H, 6.51; N, 15.92.

Synthesis of 2,3-dip-tolylpyrazino[2,3-f][1,10]phenanthroline (TPP ligand, 6d)
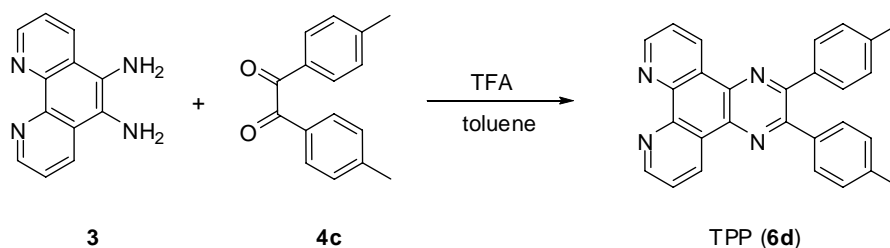
Yellow solid, (153.04 mg, 0.37 mmol, yield 78%).^{1}H NMR (CDCl$_3$, 400 MHz) δ: 2.43 (s, 6H, Me), 7.23 (d, 4H, *J* = 8 Hz, Ar) 7.60 (d, 4H, *J* = 8 Hz, Ar), 7.99 (dd, 2H, *J* = 4 Hz, *J* = 8 Hz, Ar), 9.51 (d, 2H, *J* = 4 Hz, Ar), 9.72 (d, 2H, *J* = 8 Hz, Ar); ^{13}C NMR δ: 152.5, 151.8, 147.5, 139.2, 137.5, 136.1, 133.2, 129.9, 129.1, 127.1, 123.8, 21.4; IR (ATR) ν = 2916 (m) (C-H), 1609 (m) (C=C), 1522 (m) (C=C), 813 (s)

(C-H bending), 723 (m) (C-H bending); UV-Visible (CH$_2$Cl$_2$, nm): λ_{max} ($\varepsilon \times 10^4$) 269 (6.40), 369 (3.00); HRMS (ES$^+$) m/z 413.1788, calcd for C$_{28}$H$_{21}$N$_4$ [M+H]$^+$ 413.1766; Anal. Calcd for C$_{28}$H$_{20}$N$_4$: C, 81.53; H, 4.89; N, 13.58. Found: C, 81.62; H, 4.85; N, 13.78.

Synthesis of 2,3-bis(4-bromophenyl)pyrazino[2,3-f][1,10]phenanthroline (BPP ligand) 6e
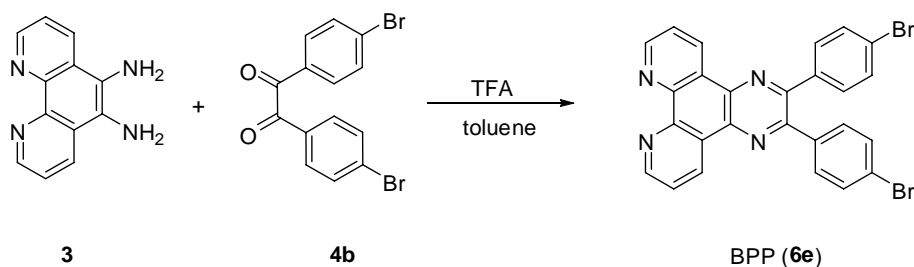
White solid, (180.54 mg, 0.33 mmol, yield 70%). ^{1}H NMR (CDCl$_3$, 400 MHz) δ: 7.52 (d, 4H, $J = 8$ Hz, Ar), 7.55 (d, 4H, J = 8 Hz, Ar), 7.76 (dd, 2H, $J = 4$ Hz, $J = 8$ Hz, Ar), 9.27 (d, 2H, $J = 4$ Hz, Ar), 9.44 (d,2H, $J = 8$ Hz, Ar) ; ^{13}C NMR δ: 123.9, 124.0, 126.7, 131.5, 131.8, 133.2, 137.2, 138.0, 147.5, 151.1, 152.2; IR (ATR) ν = 3023 (m) (C-H), 1583(m) (C=C), 1501 (m) (C=C), 800 (m) (C-H bending), 735 (m) (C-H bending); UV-Visible (CH$_2$Cl$_2$, nm): λ_{max} ($\varepsilon \times 10^4$) 271 (4.92), 313 (2.16), 367 (1.95); HRMS (ES$^+$) m/z 542.9623, calcd for C$_{26}$H$_{15}$Br$_2$N$_4$ [M+H]$^+$ 542.9643; Anal. Calcd for C$_{26}$H$_{14}$ Br$_2$N$_4$: C, 57.59; H, 2.60; N, 10.33. Found: C, 57.66; H, 3.04; N, 10.04.

2.3.2 General procedure for synthesis of ruthenium complexes (7a-e)

The procedure was modified from the general synthesis procedure of heteroleptic ruthenium complexes.[43] Dichloro(*p*-cymene)ruthenium(II) dimer (1 eq.) and pyrazino[2,3-f][1,10]phenanthroline derivatives (**6a-e**) (2 eq.) were dissolved in anhydrous DMF. The mixture was heated at 85°C under a nitrogen atmosphere in the dark for 4 hours. The 2,2´-pyridine-4,4´-dicarboxylic acid (2 eq.) was added to the mixture and the mixture was heated up to the temperature in range between 135-140°C for 4 hours. The 20-fold mole equivalent of ammonium thiocyanate was then added and the mixture was further heated for an additional 4 hours under the same

condition. After the reaction was completed, the mixture was cooled to room temperature and water was added to the DMF solution dropwise to precipitate the product. The resulting dark purple solid was filtered and washed with successive amount of water to give the crude product. The solid was purified by passing through the Sephadex LH20 by using mixed dichloromethane and methanol (ratio 1:1) as an eluent. The main red band was collected and evaporated to obtain the corresponding product complex.

Synthesis of Ru(PPP)(H$_2$bpdc)(NCS)$_2$ (SS01) (7a)

PPP, 6a   SS01, 7a
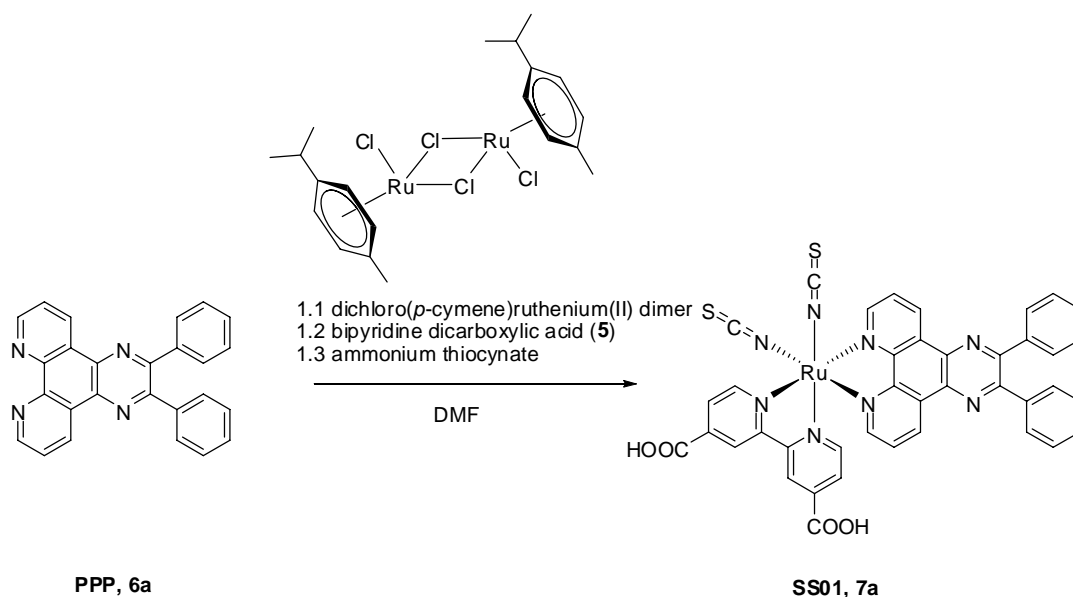
The dichloro(*p*-cymene)ruthenium(II) dimer (**SS01, 7a**) (76.2 mg, 0.125 mmol) was reacted with 2,3-diphenylpyrazino[2,3-f][1,10]phenanthroline (6a) (95.6 mg, 0.25 mmol), 2,2´-pyridine-4,4´-dicarboxylic acid (5) (60.7 mg, 0.25 mmol) and 20-folded mole of ammonium thiocyanate to obtain the corresponding product complex (176.69 mg, 0.21 mmol, yield 84%).^{1}H NMR (DMSO-d_6, 400 MHz) δ: 7.49 (m, 7H, Ar), 7.57 (b, 2H, Ar), 7.66 (m, 3H, Ar), 7.80 (b, 1H, Ar), 8.06 (b, 1H, Ar), 8.43 (m, 2H, Ar), 9.00 (s, 1H, Ar), 9.22 (m, 2H, Ar), 9.55 (b, 1H, Ar), 9.62 (b, 1H, Ar), 9.68 (b, 1H, Ar); ^{13}C NMR (DMSO-d_6, 400 MHz) δ: 165.4, 164.9, 159.1, 157.8, 154.1, 153.9, 153.6, 153.4, 153.3, 153.1, 150.3, 149.1, 138.6, 137.9, 137.9, 137.8,

136.8, 136.7, 134.6, 134.2, 132.4, 131.6, 129.9, 129.8, 129.6, 129.5, 128.6, 128.4, 128.4, 127.1, 126.2, 125.0, 123.0, 122.5; IR (ATR) ν = 3424 (b)(O-H), 3050 (m)(C-H), 2095 (s)(C≡N), 1716 (m)(C=O), 1605(m)(C=C), 1450 (m)(C=C), 766 (m)(C-H bending), 727 (m)(C-H bending), 697 (m)(C-H bending); UV-Visible (DMF, nm): λ_{max} ($\varepsilon \times 10^4$) 283 (4.93), 362 (2.34), 520 (1.19); HRMS (ES⁻) *m/z* 845.0332, calcd for $C_{40}H_{23}N_8O_4RuS_2$ [M-H]⁻ 845.0327; Anal. Calcd for $C_{40}H_{24}N_8O_4RuS_2$: C, 56.80; H, 2.86; N, 13.25. Found: C, 56.76; H, 2.87; N, 13.36.

Synthesis of Ru(MPP)(H₂bpdc)(NCS)₂ (SS02) (7b)

MPP, 6b   **SS02, 7b**
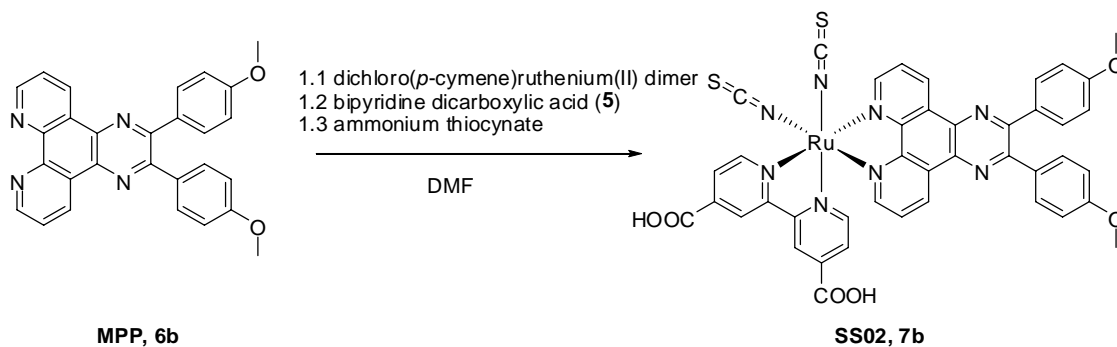
The dichloro(*p*-cymene)ruthenium(II) dimer (**SS02, 7b**) (69 mg, 0.11 mmol) was reacted with 2,3-bis(4-methoxyphenyl)pyrazino[2,3-f][1,10]phenanthroline (6b) (100 mg, 0.22 mmol), 2,2′-pyridine-4,4′-dicarboxylic acid (5) (54.9 mg, 0.22 mmol) and 20-folded of ammonium thiocyanate to obtain the corresponding product complex (181.39 mg, 0.20 mmol, yield 89%). ¹H NMR (DMSO-d_6, 400 MHz) δ: 3.80 (s, 3H, Me), 3.83 (s, 3H, Me), 6.95 (b, 2H, Ar), 6.99 (d, 2H, Ar), 7.55 (m, 6H, Ar), 7.74 (b, 1H, Ar), 8.00 (b, 1H, Ar), 8.37 (m, 2H, Ar), 8.98 (s, 1H, Ar), 9.02 (b, 1H, Ar), 9.12 (s, 1H, Ar), 9.42 (b, 1H, Ar), 9.63 (m, 2H, Ar); ¹³C NMR (DMSO-d_6, 400 MHz) δ: 165.5, 165.0, 160.4, 160.4, 159.1, 157.9, 153.7, 153.6, 153.0, 152.3, 152.2, 149.9, 148.7, 138.6, 137.8, 135.9, 135.7, 134.7, 134.1, 132.1, 131.3, 131.2, 130.1, 130.1, 129.6, 128.5, 128.3, 126.8, 126.2, 125.9, 125.0, 123.0, 122.5, 113.9, 113.9, 55.3; IR (ATR) ν = 3402 (b)(O-H), 2099 (s)(C≡N), 1716 (m)(C=O), 1600 (m)(C=C), 1514 (m)(C=C), 1243 (m)(C-O), 1020 (m)(C-O), 809 (m)(C-H bending), 766 (m)(C-H bending), 727 (m)(C-H bending); UV-Visible (DMF, nm): λ_{max} ($\varepsilon \times 10^4$) 303 (5.77), 381 (2.99), 519 (1.41); HRMS (ES⁻) *m/z* 905.0541, calcd for $C_{42}H_{27}N_8O_6RuS_2$ [M-H]⁻

905.0538;Anal. Calcd for $C_{42}H_{28}N_8O_6RuS_2$: C, 55.68; H, 3.12; N, 12.37. Found: C, 55.73; H, 3.20; N, 12.34.

Synthesis of Ru(EPP)(H₂bpdc)(NCS)₂ (SS03) (7c)

EPP, 6c   **SS03, 7c**

The dichloro(*p*-cymene)ruthenium(II) dimer (**SS03, 7c**) (58.1 mg, 0.09 mmol) was reacted with 4,4′-(pyrazino[2,3-f][1,10]phenanthroline-2,3-diyl)bis(N,N-diethylaniline) (6c) (100 mg, 0.19 mmol), 2,2′-pyridine-4,4′-dicarboxylic acid (5) (46.3 mg, 0.19 mmol) and 20-folded of ammonium thiocyanate to obtain the corresponding product complex (146.34 mg, 0.15 mmol, yield 78%).^{1}H NMR (DMSO-*d₆*, 400 MHz) δ: 1.13 (t, 12H, Me), 3.40 (m, 8H, CH₂), 6.62 (b, 2H, Ar), 6.65 (b, 2H, Ar), 7.50 (m, 6H, Ar), 7.75 (b, 1H, Ar), 7.90 (b, 1H, Ar), 8.23 (m, 1H, Ar), 8.41 (b, 1H, Ar), 8.90 (b, 1H, Ar), 8.99 (s, 1H, Ar), 9.18 (s, 1H, Ar), 9.26 (b, 1H, Ar), 9.55 (b, 1H, Ar), 9.64 (b, 1H, Ar); ^{13}C NMR (DMSO-*d₆*, 400 MHz) δ: 165.3, 164.8, 159.1, 157.8, 153.5, 152.8, 152.7, 152.3, 152.2, 152.2, 150.1, 150.1, 149.2, 148.4, 148.3, 148.1, 138.1, 137.3, 134.7, 134.6, 134.6, 134.4, 134.0, 131.6, 130.8, 130.8, 128.6, 128.5, 128.3, 126.3, 126.1, 125.5, 125.1, 124.9, 124.2, 122.9, 122.5, 111.2, 111.2, 110.5, 110.5, 43.6, 12.5, 12.4; IR (ATR) ν = 3351 (b)(O-H), 2972 (m)(C-H), 2103 (s)(C≡N), 1726 (m)(C=O), 1600 (m)(C=C), 1514 (m)(C=C), 1368(m)(C-N), 1191 (m)(C-N), 804 (m)(C-H bending), 723 (m)(C-H bending); UV-Visible (DMF, nm): λ_{max} (ε × 10⁴) 299 (4.01), 456 (2.77); HRMS (ES⁻) *m/z* 987.1792, calcd for $C_{48}H_{41}N_{10}O_4RuS_2$ [M-H]⁻ 987.1797; Anal. Calcd for $C_{48}H_{42}N_{10}O_4RuS_2$: C, 58.34; H, 4.28; N, 14.18. Found: C, 58.02; H, 4.33; N, 14.21.

Synthesis of Ru(TPP)(H₂bpdc)(NCS)₂ (SS04) (7d)

TPP, 6d   **SS04, 7d**

1.1 dichloro(*p*-cymene)ruthenium(II) dimer
1.2 bipyridine dicarboxylic acid (**5**)
1.3 ammonium thiocynate

DMF

The dichloro(*p*-cymene)ruthenium(II) dimer (**SS04, 7d**) (74.2 mg, 0.12 mmol) was reacted with 2,3-dip-tolylpyrazino[2,3-f][1,10]phenanthroline (6d) (100 mg, 0.24 mmol), 2,2´-pyridine-4,4´-dicarboxylic acid (5) (59.2 mg, 0.24 mmol) and 20-folded of ammonium thiocyanate to obtain the corresponding product complex (152.24 g, 0.17 mmol, yield 72%). ^{1}H NMR (DMSO-d_6, 400 MHz) δ: 2.34 (s, 3H, Me), 2.37 (s, 3H, Me), 7.20 (b, 2H, Ar), 7.23 (b, 2H, Ar), 7.47 (m, 5H, Ar), 7.60 (b, 1H, Ar), 7.75 (b, 1H, Ar), 8.03 (b, 1H, Ar), 8.31 (m, 2H, Ar), 9.00 (s, 1H, Ar), 9.06 (b, 1H, Ar), 9.18 (s, 1H, Ar), 9.45 (b, 1H, Ar), 9.64 (m, 2H, Ar); ^{13}C NMR (DMSO-d_6, 400 MHz) δ: 165.3, 164.8, 159.0, 157.7, 153.8, 153.6, 153.5, 152.9, 152.8, 152.7, 149.9, 148.7, 139.2, 139.2, 138.3, 137.4, 136.2, 136.2, 136.0, 134.9, 134.7, 134.1, 132.0, 131.2, 129.6, 129.5, 128.9, 128.9, 128.4, 128.2, 126.9, 126.8, 126.1, 125.9, 125.9, 124.9, 122.9, 122.5, 120.7, 20.8, 20.8; IR (ATR) ν = 3484 (b)(O-H), 2099 (s)(C=N), 1716 (m)(C=O), 1604 (m)(C=C), 1527 (m)(C=C), 813 (m)(C-H bending), 719 (m)(C-H bending); UV-Visible (DMF, nm): λ_{max} (ε × 10^4) 290 (4.24), 368 (2.26), 520 (1.05); HRMS (ES⁻) *m/z* 873.0647, calcd for $C_{42}H_{27}N_8O_4RuS_2$ [M-H]⁻ 873.0640; Anal. Calcd for $C_{42}H_{28}N_8O_4RuS_2$: C, 57.72; H, 3.23; N, 12.82. Found: C, 57.37; H, 3.24; N, 12.87.

Synthesis of Ru(BPP)(H₂bpdc)(NCS)₂ (SS05) (7e)
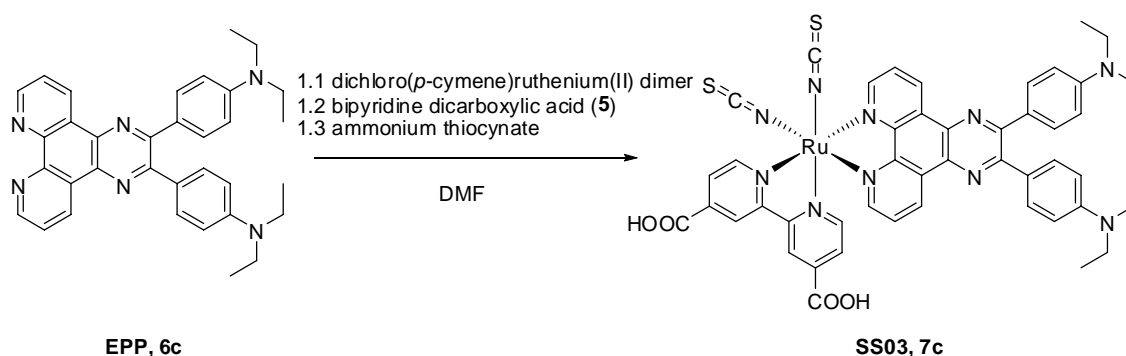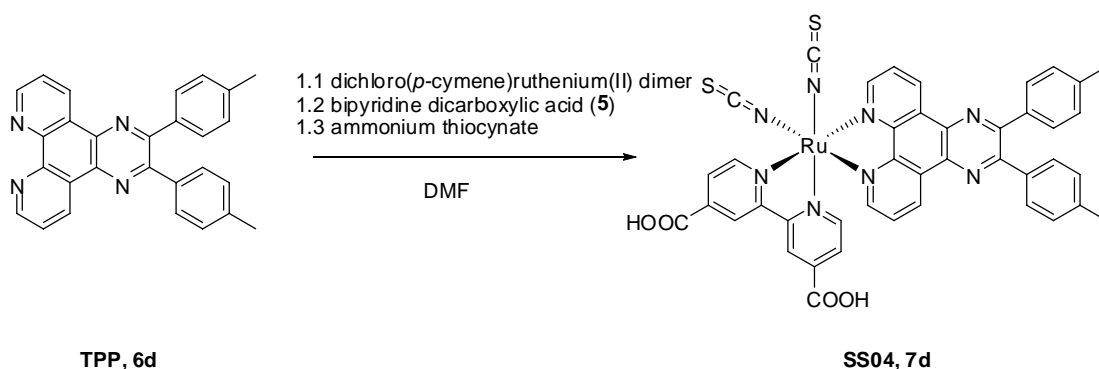

BPP, 6e   SS05, 7e
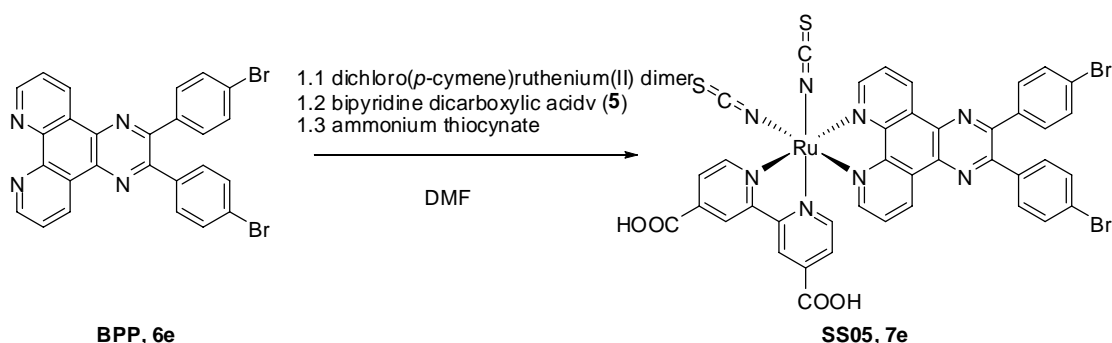
The dichloro(*p*-cymene)ruthenium(II) dimer (**SS05, 7e**) (56.5 mg, 0.09 mmol) was reacted with 2,3-bis(4-bromophenyl)pyrazino[2,3-f][1,10]phenanthroline (6e) (100 mg, 0.18 mmol), 2,2´-pyridine-4,4´-dicarboxylic acid (5) (45 mg, 0.18 mmol) and 20-folded of ammonium thiocyanate to obtain the corresponding product complex (159.18 mg, 0.16 mmol, yield 86%).^{1}H NMR (DMSO-d_6, 400 MHz) δ: 7.58 (m, 10H, Ar), 7.76 (b, 1H, Ar), 8.05 (b, 1H, Ar), 8.38 (m, 2H, Ar), 8.98 (s, 1H, Ar), 9.13 (b, 1H, Ar), 9.17 (s, 1H, Ar), 9.52 (b, 1H, Ar), 9.61 (b, 1H, Ar), 9.69 (b, 1H, Ar); ^{13}C NMR (DMSO-d_6, 400 MHz) δ: 165.5, 164.9, 159.0, 157.8, 154.2, 154.2, 154.0, 153.6, 153.0, 151.7, 151.6, 150.2, 149.1, 138.7, 137.9, 136.7, 136.5, 134.7, 134.2, 132.3, 131.9, 131.8, 131.5, 131.5, 129.5, 128.3, 128.1, 127.1, 126.2, 125.2, 125.0, 123.6, 123.6, 123.0, 122.5, 122.5; IR (ATR) ν = 3479 (b)(O-H), 2099 (s)(C=N), 1712 (m)(C=O), 1583 (m)(C=C), 809 (m)(C-H bending), 714 (m)(C-H bending); UV-Visible (DMF, nm): λ_{max} (ε × 10⁴) 287 (5.53), 363 (2.69), 520 (1.29); HRMS (ES⁻) *m/z* 1002.8526, calcd for $C_{40}H_{21}Br_2N_8O_4RuS_2$ [M-H]⁻ 1002.8517; Anal. Calcd for $C_{40}H_{22}Br_2N_8O_4RuS_2$: C, 47.87; H, 2.21; N, 11.16. Found: C, 47.61; H, 2.32; N, 11.19.

2.4   UV-Visible spectroscopy

The characterization of absorption properties was performed on a Varian Cary 50 Probe UV-Visible spectrometer. For pyrazino[2,3-f][1,10]phenanthroline derivatives (**6a-e**), the spectrum were collected in dried dichloromethane at room temperature at concentration between 10^{-6}-10^{-5} M. For ruthenium complexes (**SS01-05**), the spectra were collected in anhydrous DMF at room temperature.

2.5   Cyclic voltammetry

Cyclic voltammetry was performed on a μ-AUTOLAB TYPE III potentiostat with scan rate of 50 mV.s^{-1} using Pt wire, glassy carbon and Ag/AgNO$_3$ as counter electrode, working electrode and reference electrode, respectively. The experiment was performed in anhydrous DMF solution with 0.1 M tetrabutylammonium hexafluorophosphate as an electrolyte at dye concentration of 10^{-3} M.

2.6   Computational Study

For the theoretical insight into the electronic states of **SS01-05** at the HOMO and LUMO level. *Guassian03* package provided by the facility of Department of Chemistry, Faculty of Science, Chulalongkorn University was employed for this study by using Density Functional Theory (DFT) calculation with B3LYP model at LanL2DZ as basis set.

2.7   Fabrication of dye-sensitized solar cell[44,45]

Transparent conducting glass coated with F-doped SnO$_2$ (FTO, purchased from Dyesol Industries Pty Ltd) was used to prepare working and counter electrodes. The conducting glasses, 2×1.3 cm^2, were dipped into 40 mM TiCl$_4$ in aqueous solution at 75°C for 30 minutes which was then washed with water and ethanol, respectively. 20 nm-sized TiO$_2$ paste (Ti-Nanoxide D/SP, purchased from Solaronix) was triply cast onto corresponding FTO-glasses by screen-printing technique. >100 nm-sized TiO$_2$ paste (Ti-Nanoxide R/SA, purchased from Solaronix) was then coated for a light scattering layer. The TiO$_2$-coated electrode was then sintered stepwise to 500°C in air. The TiO$_2$ electrodes were dipped again in 40 mM TiCl$_4$ solution and sintered at the same condition. The hot electrodes were cooled to 80°C for 30 minutes and each electrode was then soaked into a solution of 20% methanol in dichloromethane containing 0.3 mM of each dye (**SS01-05**). The dye bath containing titania electrode was kept in a dark condition for 24 hours. Platinised counter electrodes were prepared by coating of 70 mM of H$_2$PtCl$_6$ in isopropanol onto the conducting glasses and then sintered at 500°C for 30 minutes. The sensitized titania electrode and the platinised counter electrode were assembled by using hot-melt

ionomer film (Surlyn) as electrodes separator. The electrolyte containing 0.5 M of LiI, 0.05 M of I_2, and 0.4 M of pyridine in mixed γ-butyrolactone and 1-methyl-2-pyrrolidone with ratio of 3:7 was filled by vacuum back filling system. The hole for electrolyte injection was sealed using sealant and cover glass.

2.8   DSSC performance

The photovoltaic performance characteristics: short-circuit current density, J_{sc}, open-circuit voltage, V_{oc}, fill factor, ff, and conversion efficiency, η, were obtained under illumination with a 1000 W xenon lamp using a Keithley Model 2400. The light intensity comfirmed to be homogeneous over 0.16 cm^2 area was calibrated by a Si solar cell at standard measurement (AM = 1.5 G, 100 $mW.cm^{-2}$). For Incident photon to current efficiency, the data were recorded as a function from 350 to 700 nm using monochromater (Newport Corp.) as the light separator.

CHAPTER III

RESULTS AND DISCUSSIONS

3.1   Molecular design

It has been noted that, for the DSSC application, molecule has to provide the light-harvesting property combined with the anchoring moiety for depositing on the TiO_2 electrode. For the rational design, we exploited the nature of ruthenium metal which possesses the long-lived charge transfer property[46,47] which can make most of ruthenium dyes achieve the high efficiency when compared with other organic dyes. Unfortunately, metal complexes have the low molar extinction coefficient which limits the performance of dye and also the cell. Basic π-conjugated organic compounds possess higher molar extinction coefficient but their absorptions lack in the visible range of the electromagnetic spectrum, these compounds have to be bonded altogether with ruthenium metal to improve the absorption properties of the dye. Among the various poly-π-conjugated compounds, polypyridine derivatives have been chosen for this application, because they are strong π-acceptors resulting in strong Ru-N bond that can make the complex quite stable. This polypyridine ruthenium complex shown in **Figure 3.1** possessess the higher extinction coefficient than the complex without the organic ligands and inherits the absorption in the visible range of spectrum the ruthenium core. Moreover, when the dye injects its electron to the Femi-level of the electrode upon being exposed to the light, it is necessary for the dye to regain an electron which can be transferred from the counter electrode by an electrolyte to prevent the permanent transformation of the dye molecule. Due to octahedron structure of ruthenium(II) ion, 4 or 3 coordination sites will be used for absorption and anchoring moieties, therefore, 2 or 3 empty sites will be filled by isothiocyanato ligand to promote the electron reinjection from the electrolye. The type of these composited ruthenium complexes have been achieved by Grätzel laboratory known as N3, N719 and Black dye which were mentioned in previous chapter.
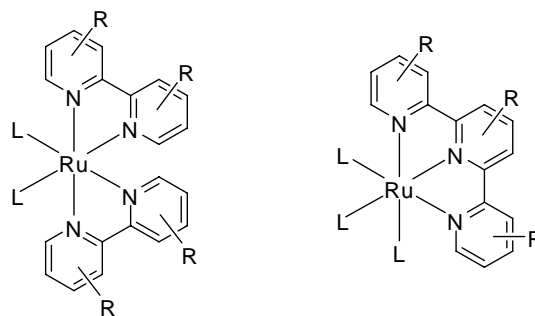
Figure 3.1 Polypyridine ruthenium complexes

The aim of this study is to improve the photovoltaic efficiency of the ruthenium dye by extending the π conjugation in the organic part for increasing the molar extinction coefficient to expand the absorption to cover the wider range of wavelengths. The quinoxaline cyclization[48] has been employed for the synthesis of the target compounds by condensation of diamino- and diketo-compound. 1,10-phenanthroline-5,6-diamine **3** has been used as diamino-compound with the coordinating region, and benzil derivatives has been used as diketo-compound **4a-e** in extension for longer π-conjugation. The ligand obtained from the design was called pyrazino[2,3-f][1,10]phenanthroline derivatives **6a-e**. Upon the complexation performance, a ruthenium(II) complex precursor will be reacted with the corresponding ligand altogether with bipyridine dicarboxylic acid **5** and ammonium thiocyanate to obtain the desired ruthenium complex as shown in **Figure 3.2**.
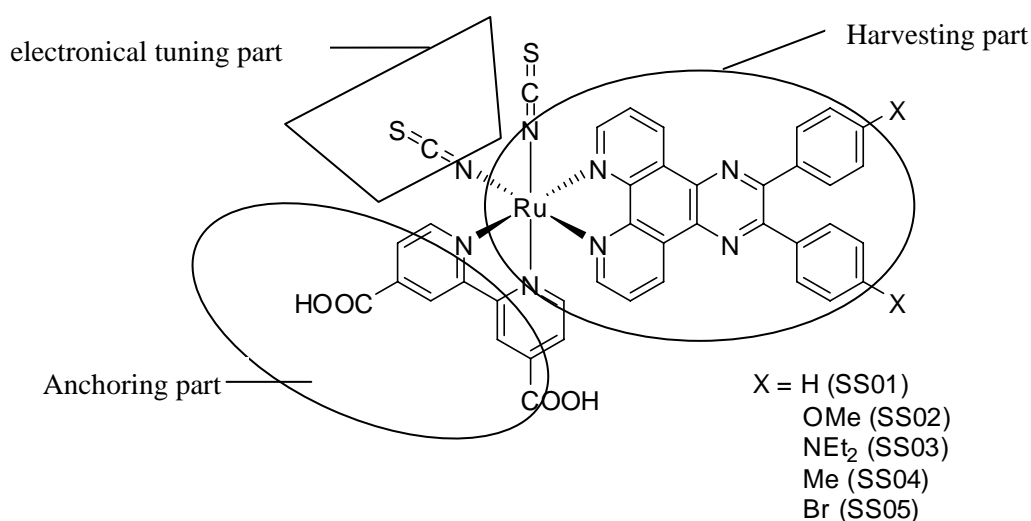
Figure 3.2 Resulting designed ruthenium complexes

3.2   Synthesis of the ruthenium complexes

The synthesis of the ruthenium complexes have been divided into 2 parts. The first part is the synthesis of pyrazino[2,3-f][1,10]phenanthroline ligand **derivatives 6a-e** and the second part covers the complexation of the ruthenium metal ion with the ligand **SS01-05**.

3.2.1   Synthesis of Pyranzino[2,3-f][1,10]phenanthroline derivatives

The core structure of these ligands was a derivative of quinoxaline, so the condensation reaction of diamino and diketo compound has been employed to obtain the corresponding quinoxalinic conpound with slight modification from the procedure[42] of Szydlo et al. In addition, for the important property of ligand, the molecules have to contain the coordinating moieties. Hence, 5,6-diamino-1,10-phenanthroline serving as diamino compound with chelating properties has been synthesized and used in this study. The 1,10-phenanthroline-5,6-diamine was synthesized first by oxidation of 1,10-phenanthroline monohydrate using concentrated nitric acid in concentrated sulfuric acid solution containing bromide ion to obtain 1,10-phenanthroline-5,6-dione **1** in 98% yield. The 1,10-phenanthroline-5,6-dione **1** was then reacted with hydroxylamine hydrochloride using barium carbonate as the catalyst of the reaction to obtain the corresponding dioxime product. The dioxime compound **2** was then reduced with hydrazine monohydrate by using 10%Pd/C as a catalyst to gain 1,10-phenanthroline-5,6-diamine **3** in 74% yield. The synthesis scheme is illustrated below in Scheme 3.1.
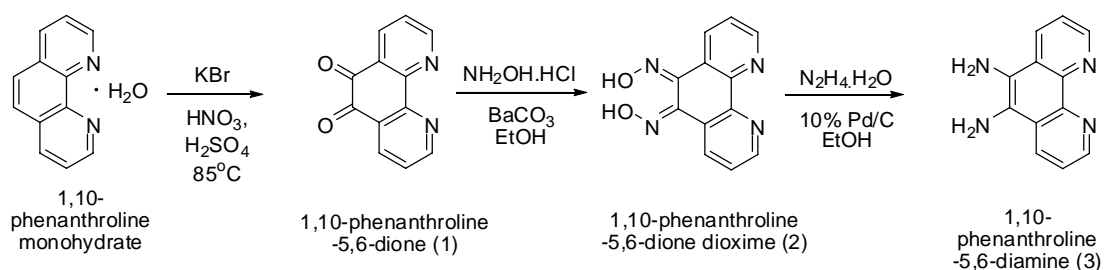
Scheme 3.1 Synthesis of 1,10-phenanthroline-5,6-diamine

For diketo compound, benzil and their derivatives **4b-e** have been employed in this study. Unfortunately, all benzil compounds cannot be obtained by using the same route of the synthesis reaction due to their electronic properties of the substrate. So the experiment in this study has to be performed using the different reaction. For the synthesis of 4,4´-dibromobenzil **4b** and 4,4´-dimethylbenzil **4c** exploited the reaction of benzoin synthesis[37] with further oxidation in concentrated nitric acid with 42% and 31% yield, respectively. The common benzoin synthesis reaction is the reaction of benzaldehyde compound itself by using cyanide ion as a catalyst. The mechanism of which is illustrated in **Scheme 3.2**. This is why the electron rich carbonyl carbon center such as 4-alkoxybenzaldehyde and 4-dialkylamino benzaldehyde cannot proceed as expected to give the corresponding benzoin derivatives. To obtain the anisil **4e** and 4,4´-bis(diethylamino)benzil **4d**, different procedures have to be employed. For the synthesis of anisil, double acylation of aromatic compound has been used to obtain the expected product in 30% yield.

For benzaldehyde with electron-rich substituent

EDG = electron donating group
  OR (4-alkoxybenzaldehyde)
  NR$_2$ (4-dialkylaminobenzaldehyde
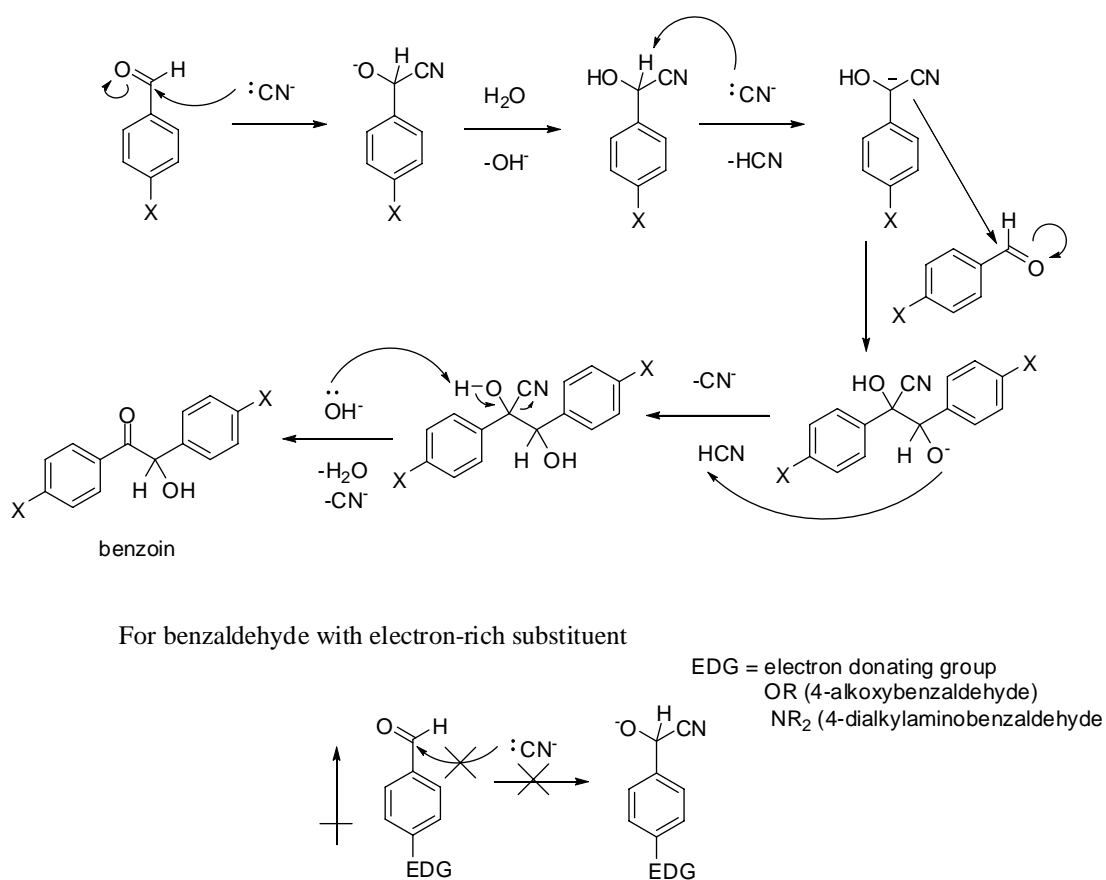
Scheme 3.2 Mechanism of benzoin synthesis reaction
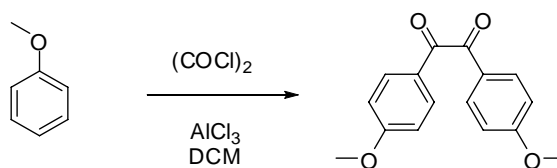
Scheme 3.3 Synthesis of anisil

Unfortunately for dialkylaminobenzil, the complex of the catalyst, AlCl₃, with such benzil is very strong complex even in basic condition, so this derivative cannot be obtained easily. Hence the 4,4´-bis(diethylamino)benzil would be synthesized by an alternative route. First, 4,4´-difluorobenzil **4a** was synthesized employing the benzoin synthesis with further oxidizing in concentrated nitric acid to obtain the corresponding product. And the 4,4´-difluorobenzil **4a** was reacted with diethylamine as the nucleophilic aromatic substitution reaction to obtain 4,4´-bis(diethylamino)benzil **4d** in 80% yield.
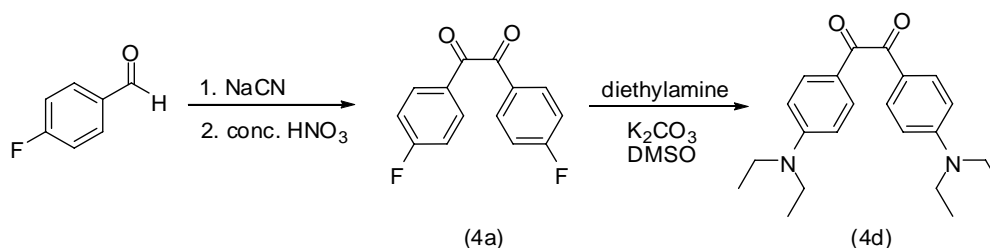
Scheme 3.4 Synthesis of 4,4´-bis(diethylamino)benzil

For the diamino and diketo compounds, the condensation step had to be performed. Since the electron demand of each component is different, hence the conventional procedures, for example, heating in acetic acid or ethanol could not drive the reaction to get to expected product. Generally, the quinoxaline cyclization was performed by the condensation of diketo-compound and diamino-compound with the same mechanism of double imination[b]. Thus, the reaction will take place rapidly, if diketo-compound is electron deficient and diamino-compound is an electron rich. Unfortunately in some experiments of quinoxaline cyclization in this study, the electron demand is reversed. For example, the synthesis of 4,4´-(pyrazino[2,3-f][1,10]phenanthroline-2,3-diyl)bis(N,N´-diethylaniline) (EPP), the substrate is diketo-compound with dialkylamino as substituent. The effect of the electron of

amino group makes such keto-derivatives possess too much electron by donating the electron from nitrogen atom. Whereas the electron of nitrogen amine of 5,6-amino-1,10-phananthroline normally is electron poor because of its aniline-liked properties including with the EN effect of nitrogen atom in pyridine ring. In this study amino compound have no enough potential to attack at the carbon center at carbonyl moiety with too much electron density that makes this reaction cannot drive spontaneously. Upon the cyclization, there are two factors have to be done, first, the kinetic energy must be high enough to overcome the activation energy of the reaction, second, the by-product of the equilibrium has to be removed out of the reaction. In this study, trifluoroacetic acid in toluene had been employed which was modified from the experiment developed by Florence *et al.*[42] Because of acidity of trifluroacetic acid used as catalyst is high enough to reduce the activation energy of the reaction. In addition, the azeotropic property of toluene had been exploited to remove water generated as by-product of the reaction which could achieve the reaction to the right hand side of the equation to obtain the product with good yield (67-78% yield). The reaction equation was illustrated in scheme 3.5.

Scheme 3.5 Synthesis of pyranzino[2,3-f][1,10]phenanthroline derivatives

3.2.2 Synthesis of ruthenium complexes

The complexation was fellow the general standard one-pot synthesis of heteroleptic ruthenium complex.[49] First, pyrazino[2,3-f][1,10]phenanthroline ligand **6a-e** was reacted with dichloro(*p*-cymene)ruthenium(II) dimer, commercial availble. The reaction was stood at low temperature (about 80-85°C) under a nitrogen atmosphere for about 4 hours. The progress of the reaction was monitored by TLC.

The bipyridine dicarboxylic acid **5** was further added. This step was performed at higher temperature about 140°C and stood for another 4 hours. At the end of this step, the complex with two bipyridinyl and dichloro ligands was obtained. It was then reacted with excess amount of thiocyanate ion to gain the corresponding isothiocyanato ruthenium complex. In addition, it should be noted that, the intermediate complexes (complex without the isothiocyanato ligand) has to be avoided to be exposed to the light because the light can cause the *cis-trans* isomerization of such ruthenium complexes.[49]
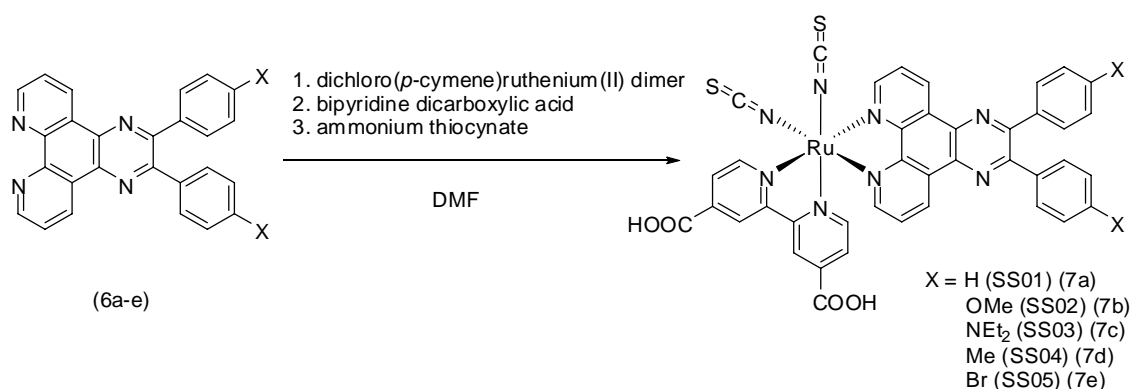
Scheme 3.6 Synthesis of ruthenium complexes

Due to the high hydrophobicity of ligand, that makes the ruthenium complex be easily separated by only adding water into the DMF reaction mixture without preconcentration by evaporation of residue DMF. We have to mention that before this procedure was found, many efforts had made tried to remove DMF solvent before adding water. Among many efforts, one was taken by using high temperature cooperating with methanol in reduced pressure evaporation to preconcentrate the DMF mixture.

In the investigation of the structure of ruthenium complexes, ^{1}H NMR, IR spectra had been determined. All of ^{1}H NMR spectra of the ruthenium complexes in this study illustrated that all proton signals of each complex show the non-equivalent pattern of the protons which could be implied that the complexes developed in this study belong to C_1 point group of symmetry. Because the ruthenium dye possesses the two different bipyridinyl ligand and two isocyanato group which arranged in *cis*-configuration. The evidence confirms this hypothesis is illustrated by

IR spectra which showed signal at about 2,100 cm^{-1} assigned as the characteristic of C=N bond with *cis*-configuration.

For the proton assignment, COSY is a technique to illustrate the correlation of proton and the proton of carbon next to itself. From the Figure 3.3 shows the correlation spectrum of **SS01**. Proton at the *a* and *a´* positions are not connected to any neighbor, so each of them should correlate with themselves. Whereas the only one signal which does not relate with the other except itself appears at chemical shift about 8.95 ppm. This means that there is another signal hidden somewhere. When consider at 9.15 ppm, the distorted doublet signal with proton integration ratio of 2 protons shows 2 types of correlation. One is a correlation of signal at 9.15 ppm with a multiplet at about 7.65 ppm and the other is correlated with itself. This means that another *a´* position was revealed. To eliminate some complication, protons at *e* and *e´* positions have to be found. At these positions, the correlation of each protons has to be related with 2 other protons. The signals at 8.40 ppm and 7.65 ppm belong to *e* and *e´* positions. The *e* position at 8.40 ppm correlates with the doublet at 9.65 ppm and 9.50 ppm. The *e´* position at 7.65 ppm correlates with doublets at 9.15 ppm and 8.05 ppm. The assignment of the *d* and *f* protons was based on the electron density at the aromatic positions. The *d* positions are proton on carbon adjacent to N of the pyridine ring which are more deshielded than *f* because of the electronegativity of nitrogen atom. Hence, the signals at 9.55 and 9.67 were assigned as *f* and *d*, respectively. For protons at the *b* and *c* positions would correlate together. The signals at 8.40 ppm and 9.60 ppm belong to protons at the *b* and *c* positions, respectively. The signals at 7.40 ppm and 7.75 ppm belong to *b´* and *c´* positions, respectively. To differentiate the normal (a-h) and prime (a´-h´) proton series, the very strong field ligand, pyridine ligand for this complex, effect the internal electron density. *Trans*-effect has dominated in this type of complex. The strong-field ligand withdraws electron from metal resulting in the depletion of electron at the ligand which are *trans* to the more powerful strong-field ligand. From this effect, it make the normal series deshields than prime series due to the normal series is *trans* to pyridine ligand.[50]

Figure 3.3 The COSY spectrum of **SS01**
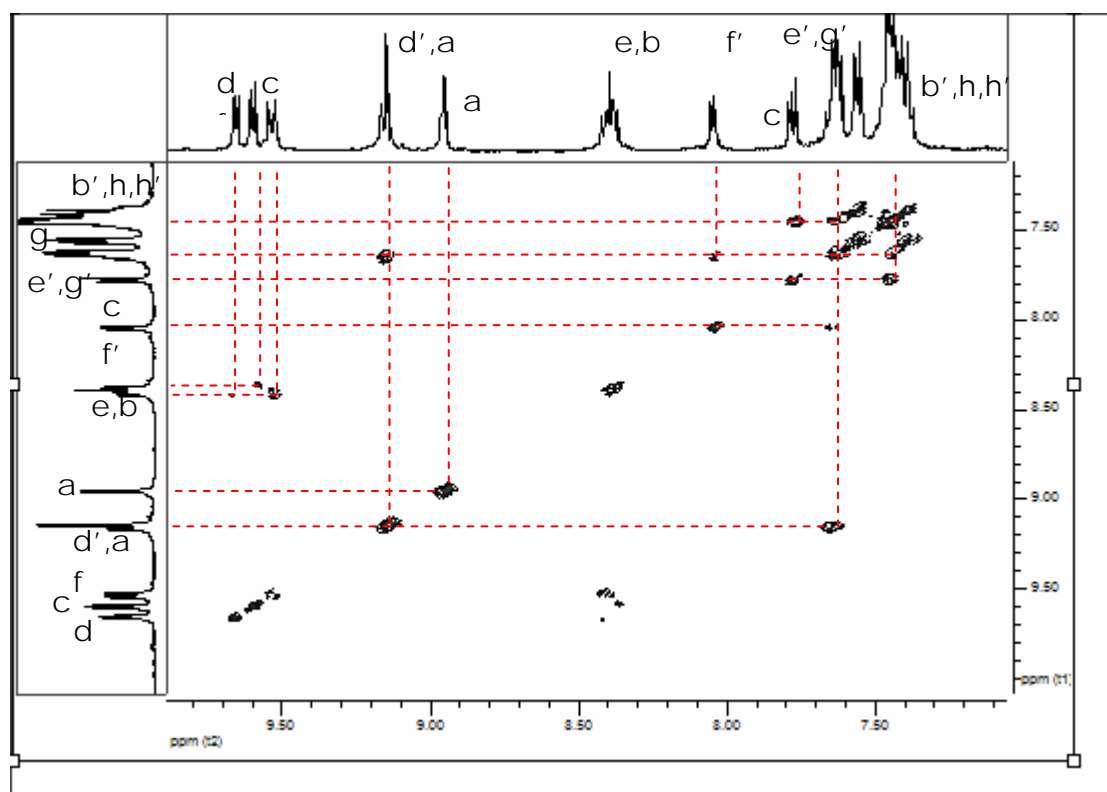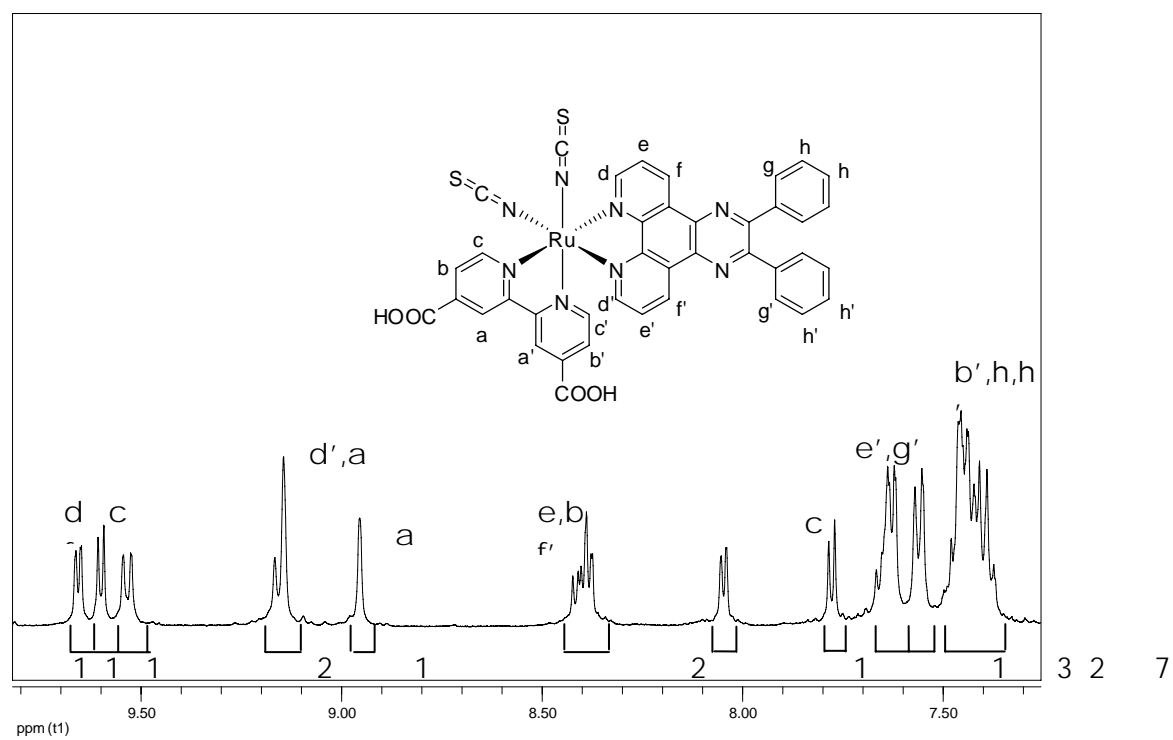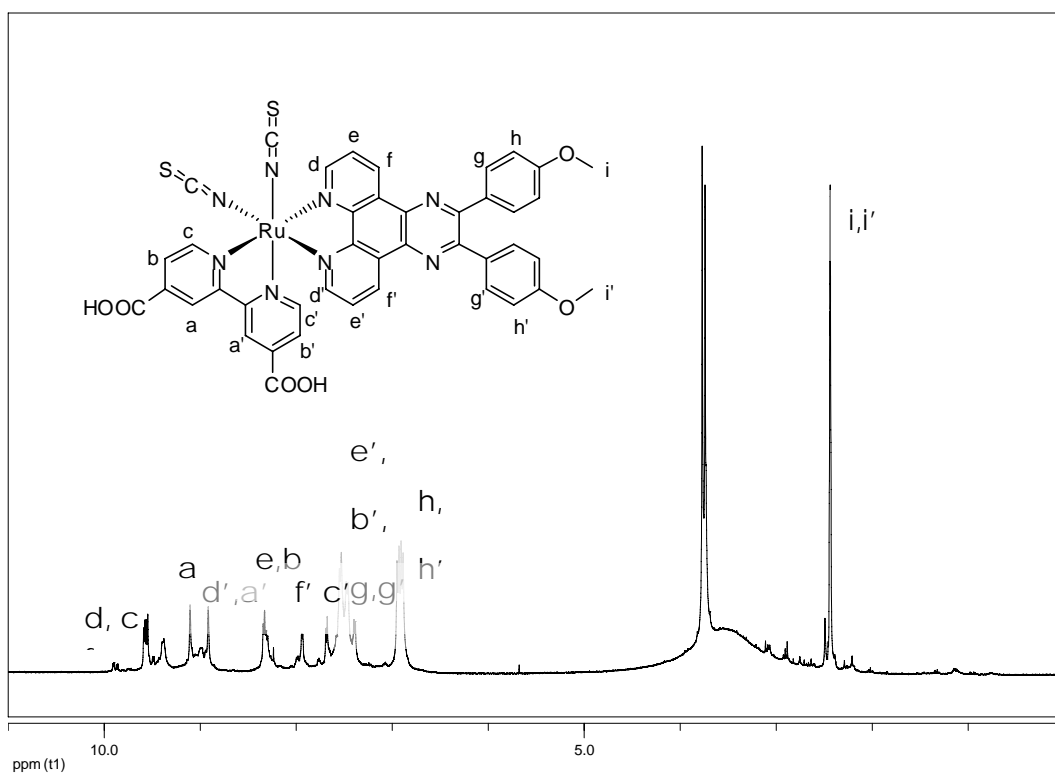

Figure 3.4 ^{1}H assignment of **SS01**

Figure 3.5 ^{1}H NMR spectrum of **SS02**
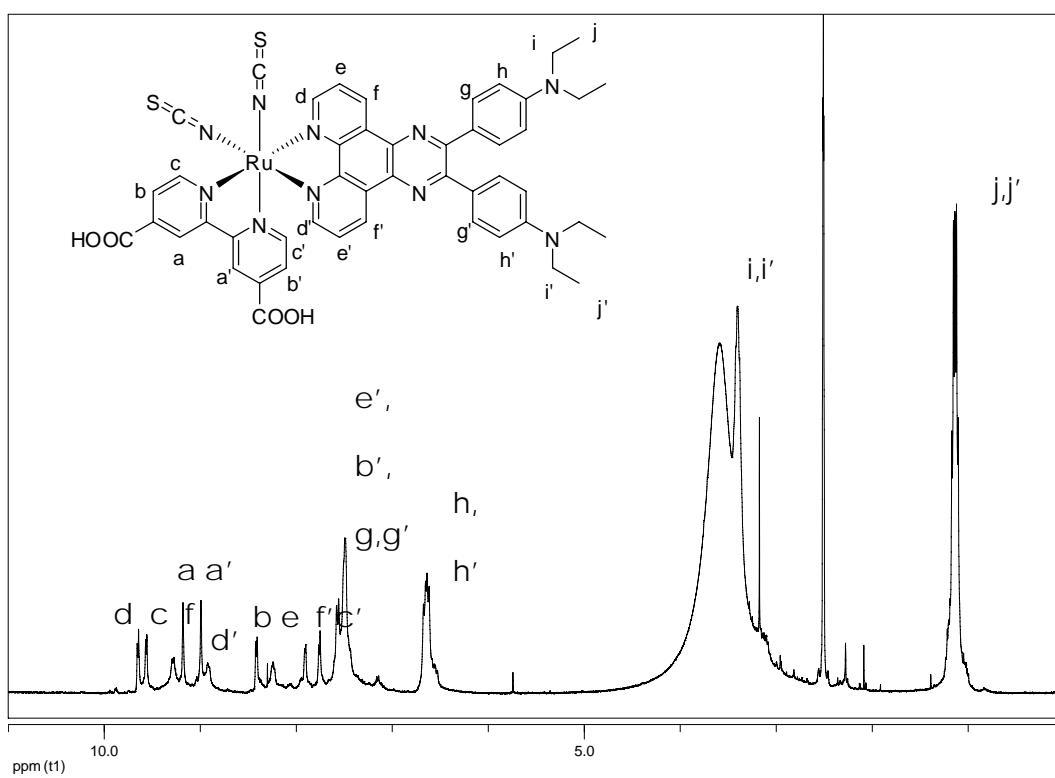
Figure 3.6 ^{1}H NMR spectrum of **SS03**
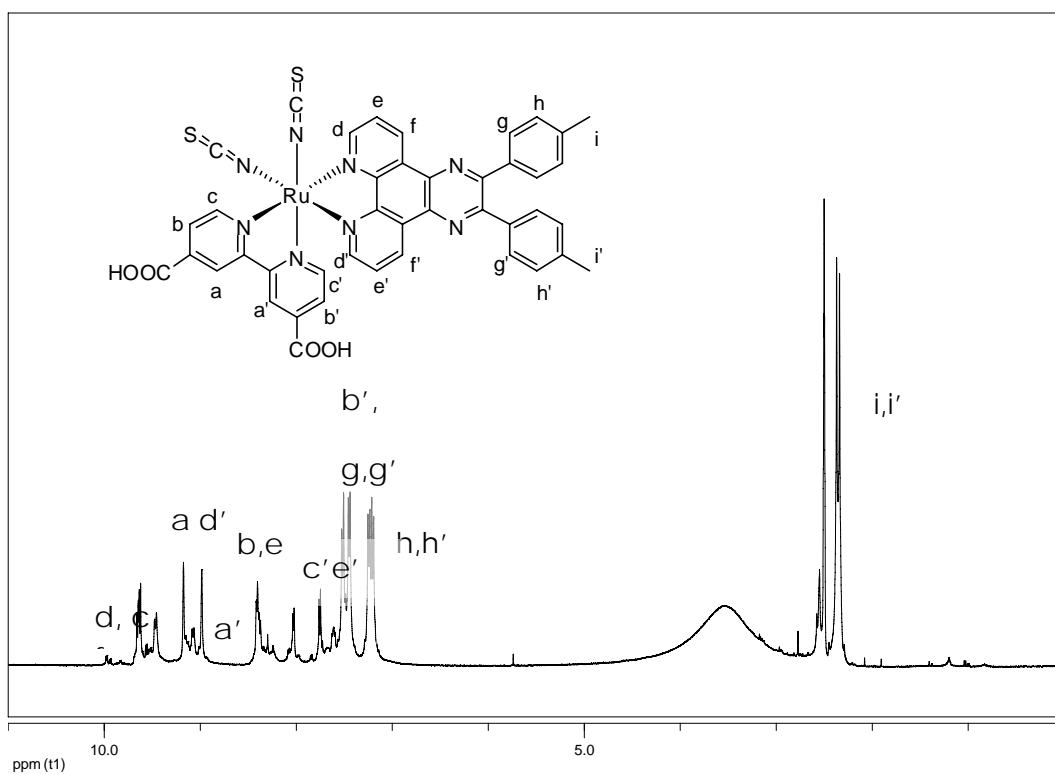
Figure 3.7 ^{1}H NMR spectrum of **SS04**
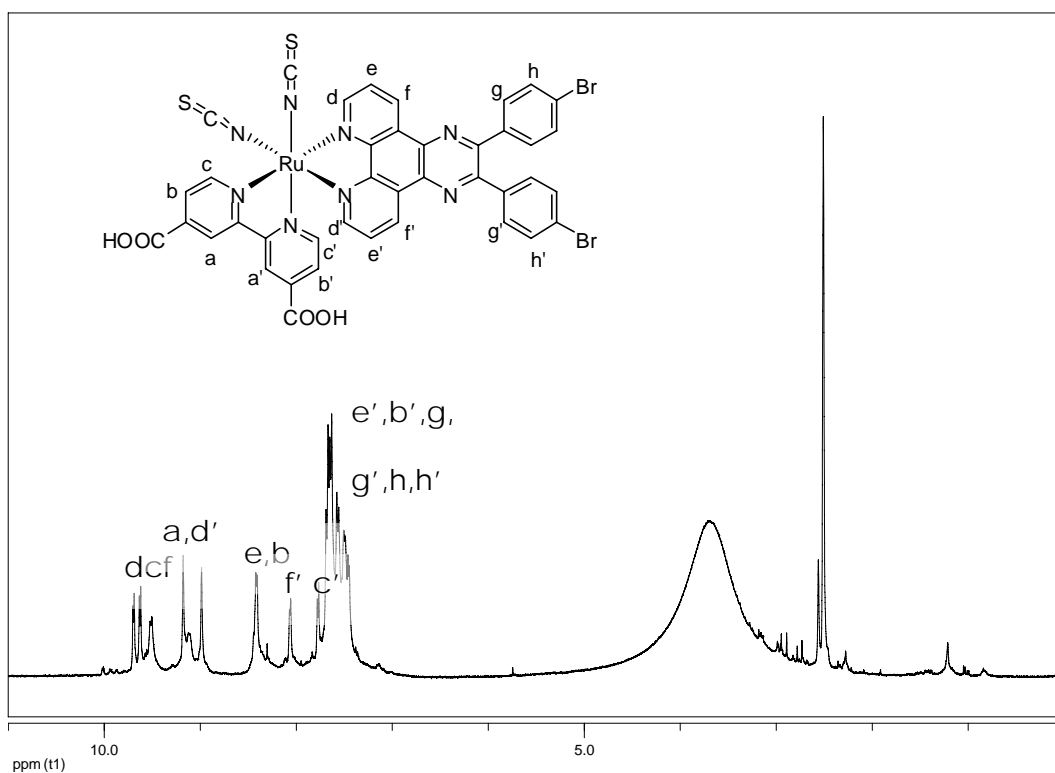
Figure 3.8 ^{1}H NMR spectrum of **SS05**

3.3 Elemental analyses

For elemental analysis, the data shown in Table 3.1 were obtained by the facility of Scientific and Technological Research Equipment Centre (STREC) of Chulalongkorn University.

Table 3.1 Elemental analysis data

Compound	Cald.			Found		
	%C	%H	%N	%C	%H	%N
SS01 (H)	56.86	2.74	13.26	56.76	2.87	13.36
SS02 (OMe)	55.68	3.12	12.37	55.73	3.2	12.34
SS03 (Net$_2$)	58.34	4.28	14.18	58.02	4.33	14.21
SS04 (Me)	57.72	3.23	12.82	57.37	3.24	12.87
SS05 (Br)	47.87	2.21	11.16	47.61	2.32	11.19

3.4 High resolution mass spectroscopy

The molecular weights of **SS01-05** dyes were determined by using Bruker micrOTOF-Q II High resolution mass spectrometry, which was the property of Department of Chemistry, Faculty of Science, Chulalongkorn University. Mode of operation was ESI-Negative. The results of the experiments were illustrated in **Table 3.2**.

3.5   ATR-FTIR spectroscopy

The ATR-IR spectra illustrated in Figure 3.9 were provided by using Thermo Scientific-NICOLET;S10 ATR-FTIR spectrometer with solid sample. All compounds show the significant signal at about 3400 (broad), 2100 and 1710 cm^{-1} which belonged to O-H stretching of carboxyl moieties, C=N stretching of thiocyanate ligand with *cis*-configuration[44] and C=O stretching of carboxyl moieties, respectively. For the rest of the signals depend on the nature of such compounds. For **SS01** and **SS04**, no significant peak is observed except the peak at aromatic region. For **SS02** the C-O-C stretching at 1243 and 1020 cm^{-1} are detected. The signals at 1368 and 1191 cm^{-1} of **SS03** belong to C-N stretching of aryl and alkyl amine, respectively. The signals at 1071 cm^{-1} belongs to C-Br stretching of aryl halide of **SS05**.

Table 3.2 High resolution spectroscopic data

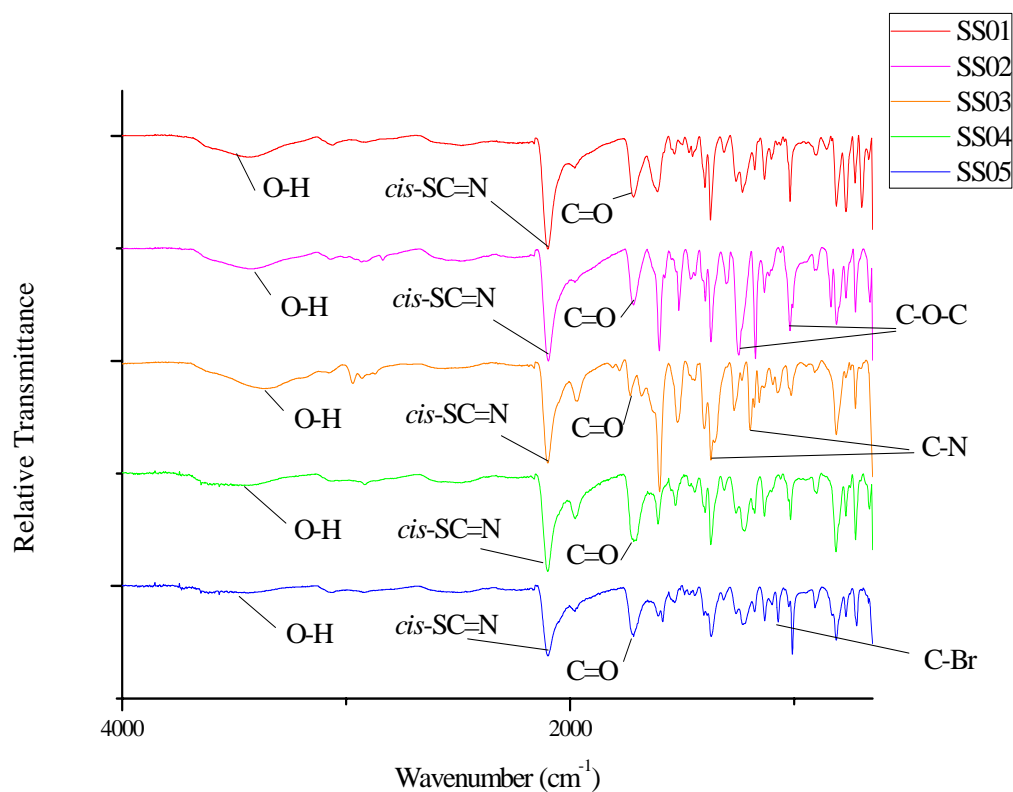| Compound	Cald. Mass	Obs. Mass	Mode
SS01 (H)	845.0327	845.0332	ESI-Negative
SS02 (OMe)	905.0538	905.0541	ESI-Negative
SS03 (Net_2)	987.1797	987.1792	ESI-Negative
SS04 (Me)	873.064	873.0647	ESI-Negative
SS05 (Br)	1002.8517	1002.8526	ESI-Negative

Figure 3.9 Relative ATR-IR spectra

3.6 Absorption spectroscopy

Figure 3.10 shows the normalized absorption spectra of **SS01-05** and N719 at concentration about 10^{-4} M. Polypyridinyl ruthenium dye complexes normally provide 3 absorption maxima, in this study, at the range of 283-309, 363-384 and 519-535 nm. At the range between 283-309 nm is corresponded to π-π* transition, referred as ligand-based charge transfer (LC) transition, of π-overlaped orbitals of two bipyridine ligands, bipyridine dicarboxylic acid and pyrazino[2,3-f][1,10]phenanthroline with molar extinction coefficient between about early 4×10^4 to late 5×10^4 M^{-1}cm^{-1}. The second group of absorption spectra, refered as MLCT I, at range of 363-384 nm are belonged to metal to ligand charge transfer (MLCT) transition with molar extinction coefficient about 2×10^4 M^{-1}cm^{-1}. The last group in range between 519-535 nm, referred as MLCT II, with molar extinction coefficient about 1×10^4 M^{-1}cm^{-1} belongs to MLCT transition, but the higher-energy transition relates to the transition from metal to organic ligands whereas the lower-energy transition relates to the transition

from metal to the thiocyanate ligands. Among the **SS01-05**, we have found the exotic absorption behavior of **SS03**. The absorption of two MLCT transition are broad and merged together at the region of blue spectrum that make the solution of **SS03** becomes dark red instead of dark purple. This is the result caused by the origin absorption of the EPP ligand **6e** which is broader than the others shown in **Figure 3.11**. Therefore, that broadens the MLCT I transition of **SS03** and consequently overlapped with MLCT II transition to obtain the corresponding exotic experience. This becomes the promising photoproperty, which is not only a bathochromic shift of absorption but new pattern or character also, that dye can absorb the light in wider range of spectrum compared to other ruthenium dyes.[45,51,52,53]
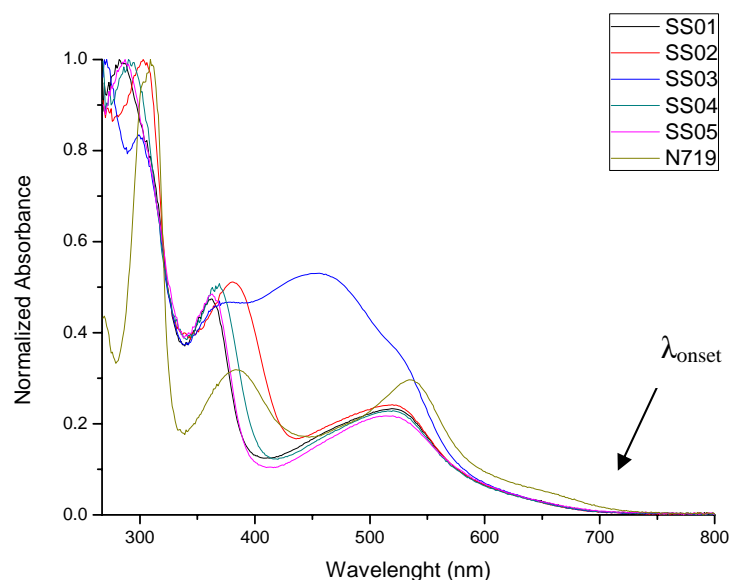

Figure 3.10 Normalized absorption spectra of **SS01-05** and N719

For the λ_{onset}, also called edge of absorption, it can be used for calculation of energy gap (E_g) of a compound. By using the following equations (**eq1-2**), the λ_{onset} can be converted to E_g (eV) which can further be used to define the electronic properties of a compound[54].
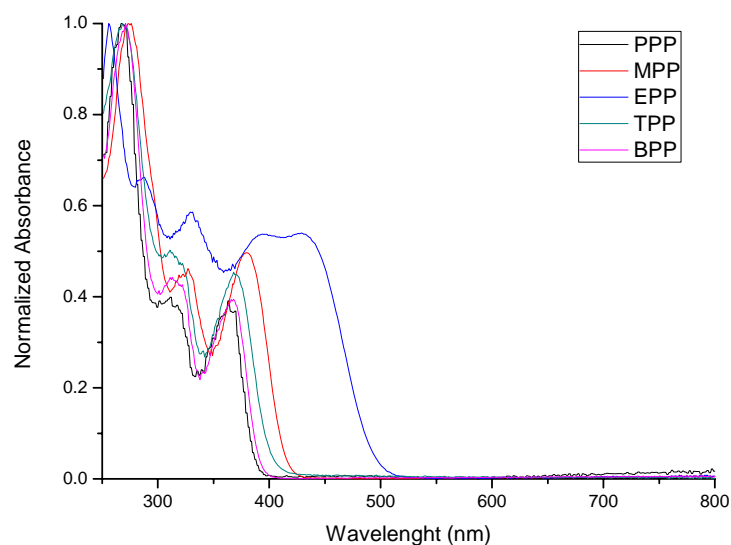
Figure 3.11 Normalized absorption spectra of pyrazino[2,3-f][1,10]phenantroline **6a-e**

$$Eg\ (eV) = \frac{hc}{\lambda_{onset}\ (nm)} \qquad \textbf{eq3.1}$$

or
$$Eg\ (eV) = \frac{1240}{\lambda_{onset}\ (nm)} \qquad \textbf{eq3.2}$$

From **Table 3.3**, the E_g obtained by the calculation were illustrated. The data indicate that The E_g is increasing when varied the substituent from electron withdrawing group to electron donating group. This is the cause of destabilization of the substituent which containing electron donating property such as alkoxy and amiono group.

Table 3.3 The electronic absorption of the **SS01-05** and N719 altogether with E_g of corresponding compounds

Ru complex	λ_{max}(nm) / ε [$\times 10^4$ M^{-1}cm^{-1}]			λ_{onset}(nm)	E_g(eV)
	LC	MLCT I	MLCT II		
SS01 (H)	283/4.93	362/2.34	520/1.19	695	1.78
SS02 (OMe)	303/5.77	381/2.99	519/1.41	679	1.83
SS03 (Net$_2$)	299/4.01	456/2.77		672	1.85
SS04 (Me)	290/4.24	368/2.26	520/1.05	701	1.77
SS05 (Br)	287/5.53	363/2.69	520/1.29	718	1.72
N719	309/3.69	384/1.23	535/1.08	780	1.59

3.7 Electrochemical study

All electrochemical data of **SS01-05** and N719 were collected by using cyclic voltammetric method. The experiment was performed by using glassy carbon as working electrode, Ag/AgNO$_3$ as referent electrode, and platinum wire as counter electrode. To obtain cyclic voltammogram of each compound, a ruthenium dye was dissolved in DMF solution with 0.1 M tetrabutylammonium pentafluorophosphate to get the final concentration of dye at 10^{-3} M. the resulting dye solution was degassed by nitrogen bubbling. A measurement was performed at scan rate at 50 mVs^{-1}. For the cyclic voltammogram shown in Figure 3.12, the first oxidation potential belongs to Ru^{II}/Ru^{III} couple at E$_{onset}$ of 0.303, 0.298, 0.275, 0.300, 0.309, and 0.235 V corresponding to **SS01**, **SS02**, **SS03**, **SS04**, **SS05**, and N719 as shown in **Table 3.4**. For **SS01-05**, the trend illustrates that the oxidation potential is cathodically shift when varies from electron withdrawing group (Br group for **SS05** at 0.309 V) to electron donating group (NEt$_2$ group for **SS03** at 0.275).
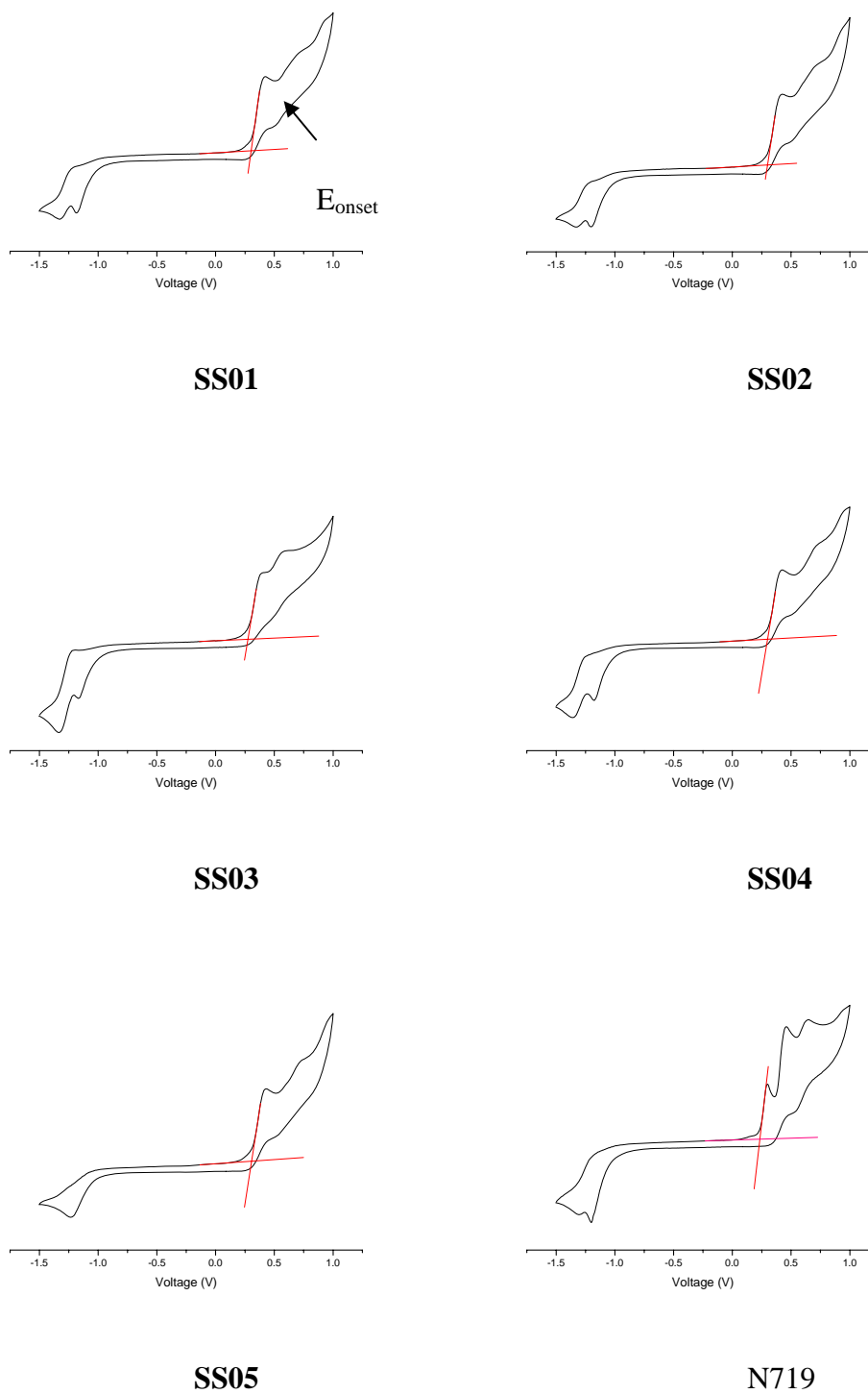
E_{onset}

SS01

SS02

SS03

SS04

SS05

N719

Figure 3.12 Cyclic voltammograms of **SS01-05** and N719

The highest occupied molecular orbital (HOMO) energy level can be calculated by using data provided by a cyclic voltammogram as a parameter in **eq 3**. By using ferrocene as reference, first oxidation potential at E_{onset} can be used directly in this equation[54]. Altogether with E_g (eV) obtained from **eq 2**, the lowest unoccupied molecular orbital (LUMO) energy level can be calculated from the **eq 4**. All electronic properties obtained from the experimental calculation of **SS01-05** and N719 are illustrated in **Table 3.4.**

$$E_{HOMO}(eV) = -(E_{onset} - E_{Fc/Fc}^{+} + 4.8) \qquad \text{...............eq 3}$$

$$E_{LUMO}(eV) = E_{HOMO} + E_g \qquad \text{...............eq 4}$$

Where $E_{Fc/Fc}^{+}$ is -0.048 eV obtained from E_{onset} of referent ferrocene couple.[44]

Table 3.4 Electronic properties of **SS01-05** and N719

Ru complex	$^{ox}E_{onset}$(eV)	HOMO(eV)	E_g(eV)	LUMO(eV)
SS01 (H)	0.303	-5.15	1.78	-3.37
SS02 (OMe)	0.298	-5.15	1.83	-3.32
SS03 (Net$_2$)	0.275	-5.12	1.85	-3.27
SS04 (Me)	0.300	-5.15	1.77	-3.38
SS05 (Br)	0.309	-5.16	1.72	-3.44
N719	0.235	-5.08(-5.05)[54]	1.59	-3.49(-3.25)[54]

For the use as photosensitizer, the HOMO level have to lower than redox couple (I_2/I_3^-) to accept the electron from electrolyte in the regeneration of oxidized dye molecule, and the LUMO lever have to higher than the conduction band of titanium dioxide with the purpose of the electron injection to the electrode upon the illumination. The results indicated that **SS01**-**SS05** could be used as photosensitizer for dye-sensitized solar cell application, due to the LUMO and HOMO levels of all

complexes are higher than the conduction band of TiO_2, -4.2 eV, and lower than HOMO level of redox couple (I_2/I_3^-), -4.8 eV, in electrolyte system, respectively.[54,55,56]
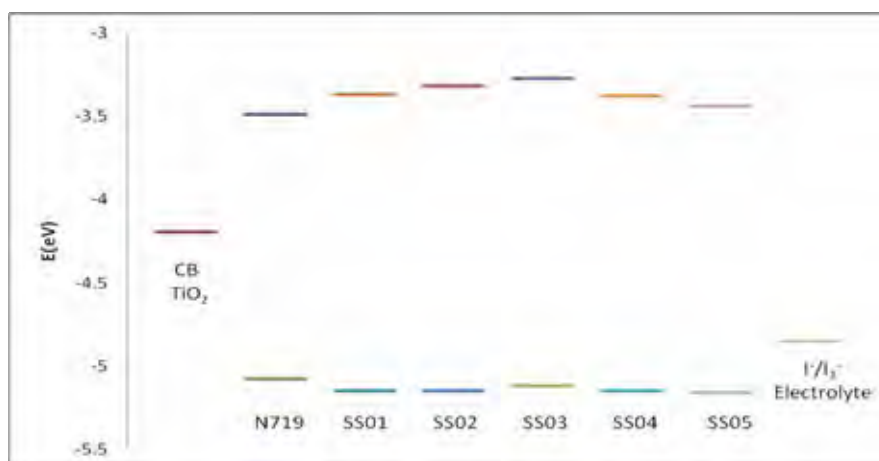

Figure 3.13 Energy diagram obtained from experiment

3.8 Computational Study

For electronic insight, Density Functional Theory (DFT) calculation was performed by using B3LYP with LanL2DZ as basis set. The calculation was provided by *Gaussion03* from the facility of Department of Chemistry, Faculty of Science, Chulalongkorn University.

Table 5 and Figure 3.14 illustrate the summary results. The trends of HOMO and LUMO increase when vary the substituent from electron withdrawing group (Br) to electron donating group (NEt$_2$). This means that the HOMO and LUMO of the complexes can be both tuned from the remote substituent. This result correlates well with the experiment obtained from cyclic voltammetry. In addition, when compared with absorption spectra, the calculated E_g relate well with the E_g obtained from absorption that increase upon varying of substituent from electron withdrawing group to electron donating group.
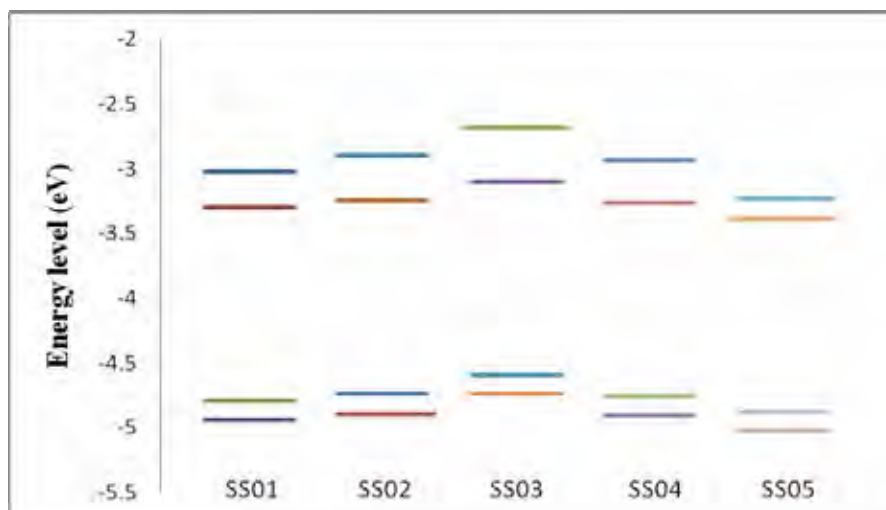
Figure 3.14 Energy diagram (HOMO-1, HOMO, LUMO, LUMO+1) of **SS01-05** obtained from DFT calculation using B3LYP/LanL2DZ as a basis set

Figure 3.15 illustrates the orbital population densities of LUMO+1, LUMO, HOMO, HOMO-1 of **SS01-05** complexes. For HOMO and HOMO-1, the electron population in these states was normally located on $Ru-(NCS)_2$. For LUMO, electron of all complexes was populated on the bipyridine-dicarboxylic-acid moiety. Nonetheless, for LUMO+1, all complexes show the electron populated on pyrazino[2,3-f][1,10]phenanthroline ligand except **SS03** which electron populates on bipyridine-dicarboxylic-acid ligand.[44]

Table 3.5 Electronic energy level of **SS01-05** obtained from DFT calculation using B3LYP/LanL2DZ as a basis set

(eV)	**SS01** (H)	**SS02** (OMe)	**SS03** (NEt_2)	**SS04** (Me)	**SS05** (Br)
LUMO+1	-3.02216	-2.89889	-2.68773	-2.93563	-3.22762
LUMO	-3.29755	-3.24911	-3.09836	-3.26217	-3.38245
HOMO	-4.78822	-4.74224	-4.59203	-4.7523	-4.87721
HOMO-1	-4.93871	-4.89217	-4.74142	-4.90469	-5.02551

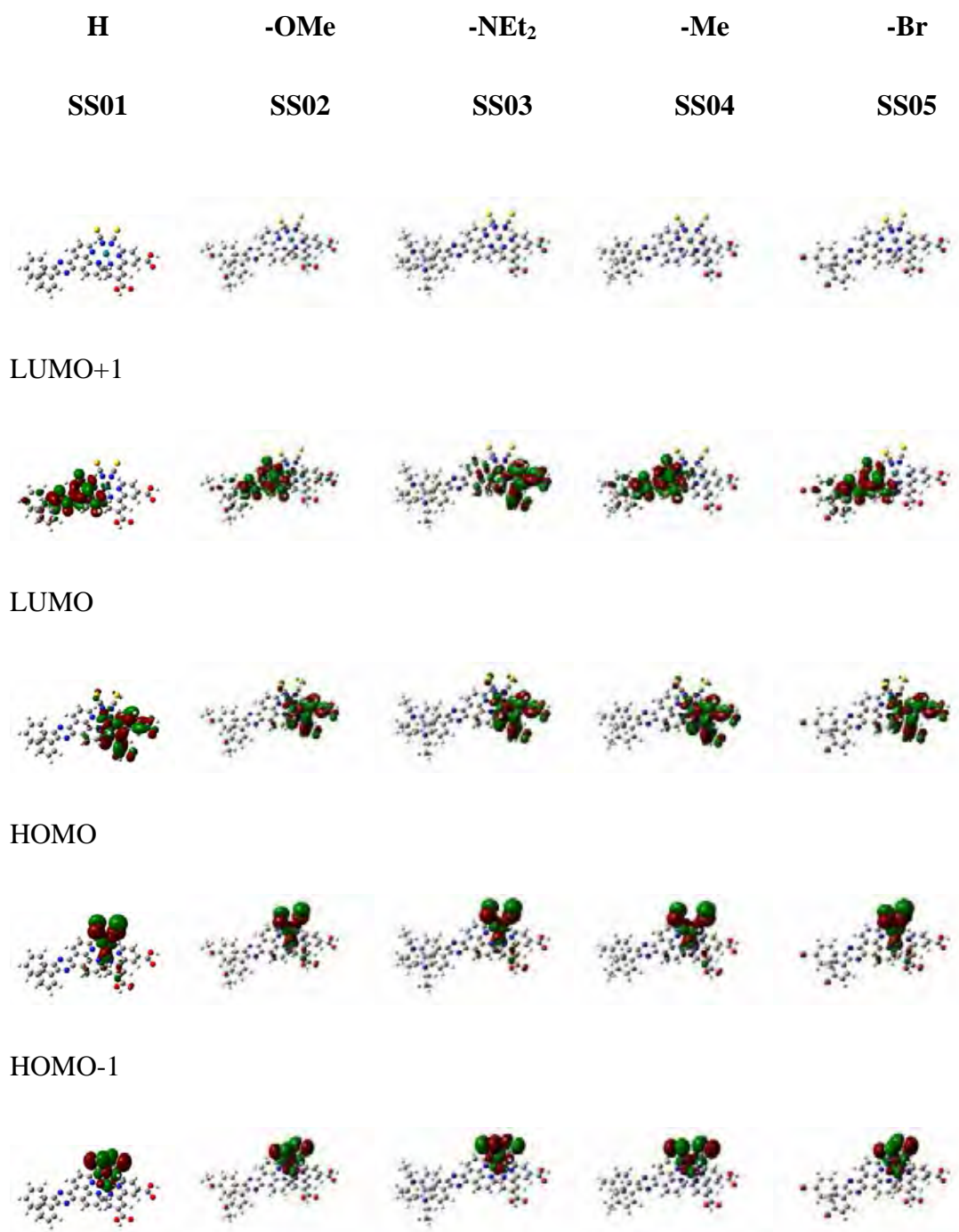| H	-OMe	-NEt$_2$	-Me	-Br
SS01	**SS02**	**SS03**	**SS04**	**SS05**

LUMO+1

LUMO

HOMO

HOMO-1

Figure 3.15 The orbital population densities of LUMO+1, LUMO, HOMO, HOMO-1 of **SS01-05** obtained from DFT calculation using B3LYP/LanL2DZ as a basis set

3.9 Fabrication

Transparent conducting glass coated with F-doped SnO_2 (FTO, purchased from Dyesol Industries Pty Ltd) was cut into 2×1.3 cm^2 size, which were then washed stepwise with detergent, water, aqua rigia, ethanol and isopropanol, respectively. The surface of cleaned glasses was prepared by immerging in 40 mM $TiCl_4$ in aqueous solution at 75°C for 30 minutes which was then washed with water and ethanol, respectively. The area of contact of $TiCl_4$ solution was restricted by using copper tape. The $TiCl_4$-dipped glasses were washed with water and ethanol, respectively.
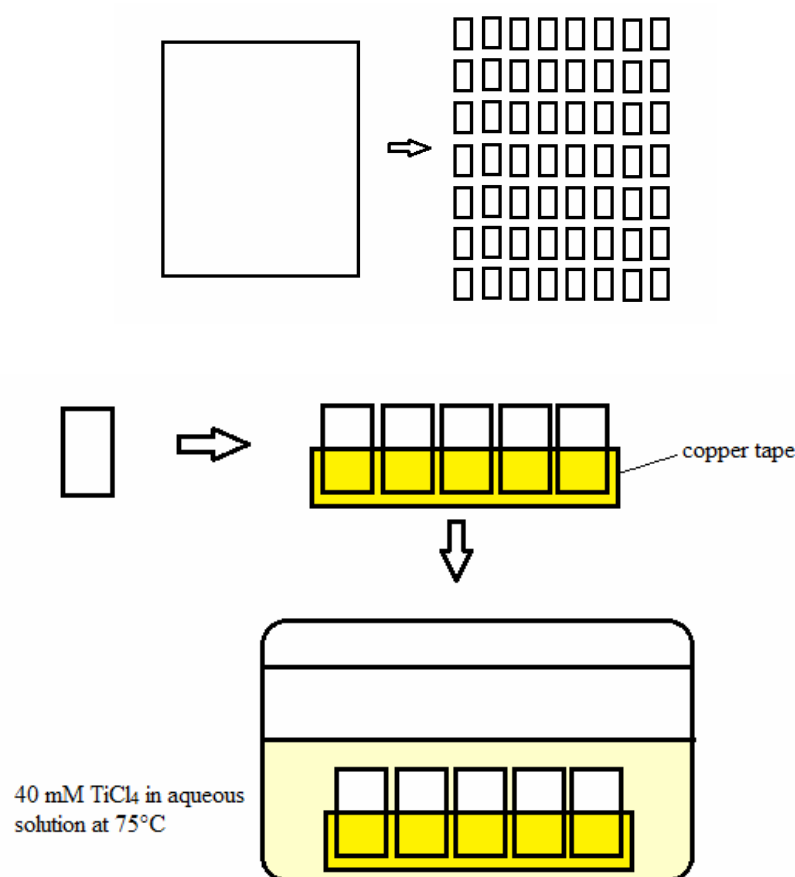

Figure 3.16 Surface preparation of glass electrode

TiO_2-nanoparticle layers were coated on corresponding glass electrode by using screen-printing technique. 20 nm-sized TiO2 paste (Ti-Nanoxide D/SP, purchased from Solaronix) was triply cast onto glass electrode and followed by the monolayer of >100 nm-sized TiO_2 paste (Ti-Nanoxide R/SA, purchased from

Solaronix). The smaller particle layer was used as the electron extractor from photosensitizer and the larger particle layer was used as light scattering layer. The TiO_2-coated electrode was sintered stepwise at temperature gradient of 325, 375, 450, and 500°C to eliminate the all of organic substances. The sintered electrodes were dipped in 40 mM $TiCl_4$ in aqueous solution at 75°C for 30 minutes and sintered again at the same condition.
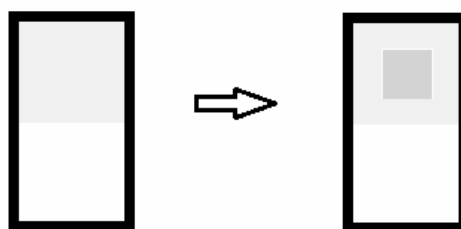

Figure 3.17 Titania electrode prepared by screen-printing technique

For counter electrodes, the same size of conducting glasses were drill to obtain a hole for electrolyte injection. The drilled electrodes were washed stepwise with detergent, water, aqua rigia, ethanol and isopropanol, respectively. The platinised counter electrodes were prepared by coating of 70 mM of H_2PtCl_6 in isopropanol onto the conducting glasses and then sintered at 500°C for 30 minutes.
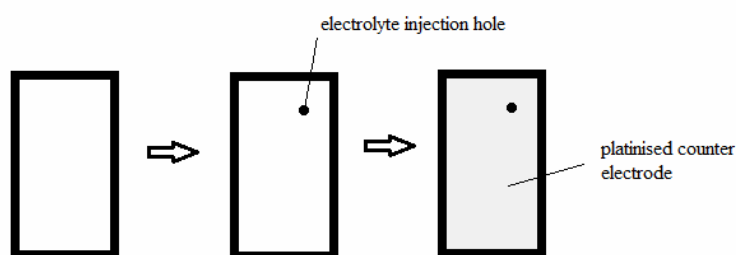

Figure 3.18 Preparation of platinized counter electrode.

For preparation of dye-electrode, the titania electrode was heated up to 80°C for 30 minutes and each electrode was then soaked into a solution of 20% methanol in

dichloromethane containing 0.3 mM of each dye (**SS01-05** and N719). The dye bath containing titania electrode was kept in a dark condition for 24 hours. After dye soaking, the electrodes were washed with 20% methanol in dichloromethane until the eluent became colorless.
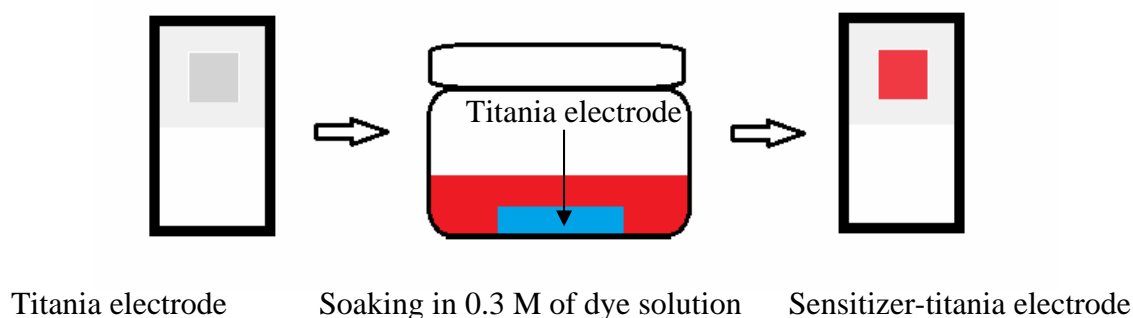

Titania electrode   Soaking in 0.3 M of dye solution   Sensitizer-titania electrode

Figure 3.19 Preparation of sensitizer-titania electrode

The sensitized titania electrode and the platinised counter electrode were assembled by using hot-melt ionomer film (Surlyn) as electrodes separator. The electrolyte containing 0.5 M of LiI, 0.05 M of I_2, and 0.4 M of pyridine in mixed γ-butyrolactone and 1-methyl-2-pyrrolidone with ratio of 3:7 was filled by vacuum back filling system. The hole for electrolyte injection was sealed using sealant and cover glass.
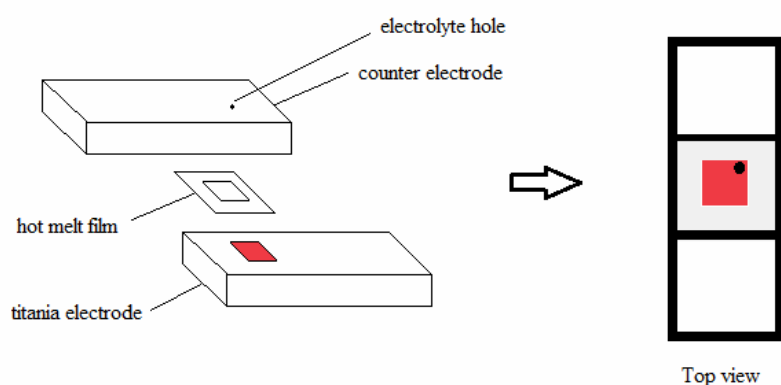

Figure 3.20 Cell assemble

For cell preparation, copper foils, silver paint, and silver wires were contacted directly at the rest area of glass electrode for electron collector. Till the end of the processes, the cells are ready for the photovoltaic test.
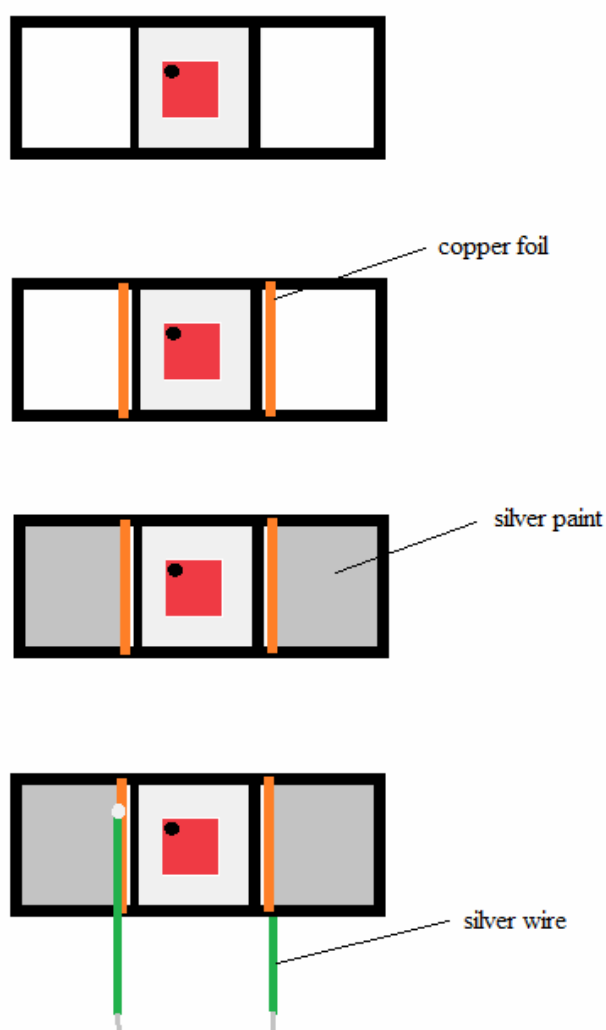

Figure 3.21 Preparation of device for the efficiency measurement

3.10   Photovoltaic performance

The photovoltaic performance of **SS01-05** and standard N719 dye were illustrated in a relationship between Current (mA.cm^{-2}) and voltage (V) as shown in **Figure 3.22**. The relationships indicate that the current obtained from cell with N719 provides the highest value. This means that N719 can inject electron most efficiently

when compare to the synthetic dyes (**SS01-05**). The all photovoltaic parameters: short-circuit current density (J_{sc}), open-circuit voltage (V_{oc}), fill factor (*ff*), and overall conversion efficiency (η), were illustrated in **Table 3.6**. The overall conversion efficiencies of all compounds indicated that N719 provides the most conversion efficiency. This may be the cause of the aggregation of dyes onto the TiO$_2$ surface. From the DFT calculation revealed that, although the phenyl moieties are twisted, but the arrangement of all molecules is quite planar. This might the cause of the low efficiency. Interestingly, **SS03** (NEt$_2$-substituted complex) containing the sufficiently electron-donating group provides the lower efficiency when compare to **SS02** (OMe-substituted complex). The result contrasts to the spectroscopic experiment which shows the broader absorption property of **SS03** when compare to the other even N719. This phenomenon was also observed in the study of Han *et al.*[a] mentioned that the interaction of amine with I$_2$ should be taken into consideration. This interaction might lead the local concentration of oxidized form of electrolyte is higher compared to the other compounds. This dominates the charge recombination process of sensitizer molecule by TiO$_2$ electrode which is the cause of lower conversion efficiency of **SS03** compared to **SS02**.
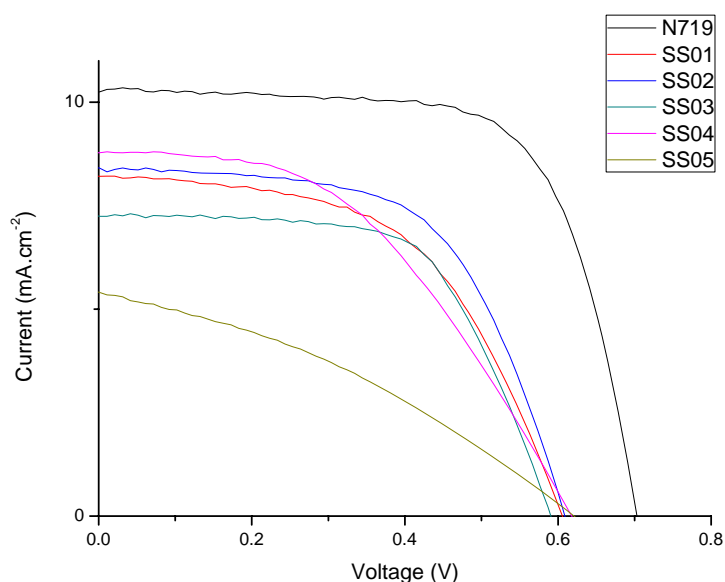

Figure 3.22 Current (mA.cm^{-2}) - voltage (V) characteristic curves for **SS01-05** and N719

Talble 3.6 Photovoltaic character of **SS01-05** and standard N719

Ru complexes	J_{sc}	V_{oc}	ff	$\eta(\%)$
SS01 (H)	8.05	0.61	0.53	2.60
SS02 (OMe)	8.41	0.61	0.59	3.04
SS03 (Net$_2$)	7.37	0.59	0.60	2.60
SS04 (Me)	8.80	0.62	0.46	2.50
SS05 (Br)	5.27	0.62	0.33	1.06
N719	10.55	0.69	0.69	5.07

For incident photo- to-current efficiency, all curves of **SS01-05** show plateau efficiency of 30-40% from 350 to 550 nm whereas the curve of N719 shows the higher efficiency with the maximum of about 80%. This is correlated with the conversion efficiency that standard N719 provides the best conversion efficiency because it can sufficiently harvest the light over the wide range of spectrum. Although the UV-Vis absorption spectra show that the synthetic dyes (**SS01-05**) provide the higher molar extinction coefficient when compared to N719, the electron injection of N719 is better indicated by J_{sc} value. This leads the higher IPCE efficiency of N719 sensitizer.
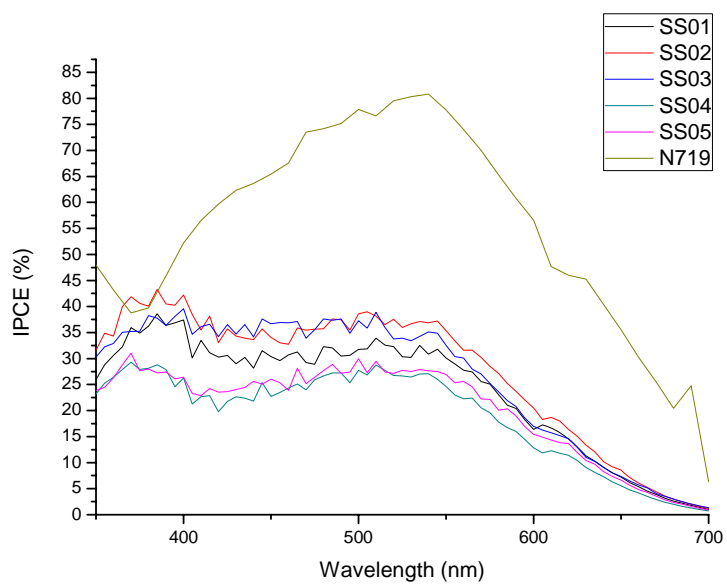
Figure 3.23 IPCE efficiencies of **SS01-05** and standard N719

CHAPTER IV

CONCLUSION

4.1   Conclusion

Five new heteroleptic ruthenium complexes **SS01**-**SS05** were synthesized for dye-sensitized solar cell application. The complexes consisted of a ruthenium (II) ion coordinated with two thiocyanate ligands and two different bipyridine ligands. One of bipyridine ligand containing carboxylic group, 4,4´-dicarboxy-2,2´-bipyridine, was used to anchor onto TiO_2 surface. The other containing quinoxaline moiety, 2,3-diphenylpyrazino[2,3-*f*][1,10]phenanthroline, was employed as a light-harvesting unit. ^{1}H NMR and ATR-IR spectroscopy were used to identify the structure of the **SS01**-**SS05** that the structures of all complexes belonged to C_l-point group of symmetry. The cyclic voltammogram was used together with absorption spectrum to determine the HOMO and LUMO electronic levels of each complex. The results indicated that **SS01**-**SS05** could be used as photosensitizer for dye-sensitized solar cell application, due to the fact that LUMO and HOMO levels of all complexes are higher than the conduction band of TiO_2 and lower than the HOMO level of the redox couple (I_2/I_3^-) in the electrolyte system. For theoretical study, DFT calculation with B3LYP/LanL2DZ model provided by *Gaussian03* was used to calculate the electronic structures and to confirm the results obtained from the experimental section. In studying of photovoltaic performance, the devices were prepared by using TiO_2 nanoparticle coated on transparent glass electrode as working electrode, platinised glass electrode as counter electrode, and I_2/I_3^- as electrolyte system. The cells were assembled after staining the working electrodes with **SS01**-**SS05**. The overall conversion efficiency of **SS01**-**SS05** complexes are 2.60, 3.04, 2.60, 2.50, and 1.06%, respectively. Even though **SS01**-**SS05** provided the lower conversion efficiency compared to the standard N719 complex, the distinct was observed that **SS03** could absorb the light at the wider range of spectrum. This is the promising properties which

make the device can absorb light with wider range and also convert to more electricity.

4.2 Suggestion for future work

The future work should relate to find bipyridine ligand conjugated with chromophore which can enhance the ability of the light absorption of the overall ligand molecule. Not only the ligand with high molar extinction coefficient is required for this application, but also the wide region of light absorption.

REFERENCES

[1]   Grätzel, M. Solar energy conversion by dye-sensitized photovoltaic cells, *Inorg. Chem.* **44** (2005): 6841-6851.

[2]   Grätzel, M. Photoelectrochemical cells. *Nature* **414** (2001): 338-344.

[3]   Choi, H., Lee, J.K., Song, H.K., Song, K., Kang, S.O. and Ko, J. Synthesis of new julolidine dyes having bithiophene derivatives for solar cell. *Tetrahedron* **63** (2007): 1553-1559.

[4]   Boschloo, G. and Hagfeldt, A. Characteristics of the iodide/triiodide redox mediator in dye-sensitized solar cells. *Acc. Chem. Res.* **42** (2009): 1819-1826.

[5]   Imahori, H., Umeyama, T. and Ito, S. Large π-aromatic molecules as potential sensitizers for highly efficient dye-sensitized solar cells. *Account. Chem. Res.* **42** (2009): 1809-1818.

[6]   O'regan, B. and Grätzel, M. A low-cost, high-efficiency solar cell based on dye sensitized colloidal TiO2 films. *Nature* **353** (1991): 737—740.

[7]   Bisquert, J., Cahen, D., Hodes, G., Rühle, S. and Zaban, A. Physical chemical principles of photovoltaic conversion with nanoparticulate, mesoporous dye-sensitized solar cells. *J. Phys. Chem. B.* **108** (2004): 8106-8118.

[8]   Zhoa, J., Wang, A. and Green, M. A. 24.5% Efficiency silicon PERT cells on MCZ substrates and 24.7% efficiency PERL cells on FZ substrates. *Prog. Photovolt.: Res. Appl.* **7** (1999): 471-474.

[9]   Bhimwal, M. K. and Gangotri, K. M. A comparative study on the performance of photogalvanic cells with different photosensitizers for solar energy conversion and storage: D-Xylose-NaLS systems. *Energy* **36** (2011): 1324-1331.

[10] Kitano, M., Matsuoka, M., Ueshima, M. and Anpo, M. Recent developments in titanium oxide-based photocatalysts. *Appl. Catal., A* **325** (2007): 1–14.

[11] Drechsel, J., Männig B., Gebeyehu, D., Pfeiffer, M., Leo, K. adn Hoppe, H. MIP-type organic solar cells incorporating phthalocyanine/fullerene mixed layers and doped wide-gap transport layers. *Org. Electron.* **5** (2004): 175–186.

[12] Hagfeldt, A., Boschloo, G., Sun, L., Kloo, L. and Pettersson, H. Dye-sensitized solar cells. *Chem. Rev.* **110** (2010): 6595-6663.

[13] Ferrere, S., Zaban, A. and Gregg, B. A. Dye sensitization of nanocrystalline tin oxide by perylene derivatives. *J. Phys. Chem. B.* **101** (1997): 4490-4493.

[14] Nazeeruddin, M. K., Kay, A., Rodicio, I., Humphry-Baker, R., Mueller, E., Liska, P., Vlachopoulos, N. and Grätzel, M. Conversion of light to electricity by cis-X2bis (2,2'-bipyridyl-4,4'-dicarboxylate) ruthenium (II) charge-transfer sensitizers (X = Cl-, Br-, I-, CN-, and SCN-) on nanocrystalline titanium dioxide electrodes. *J. Am. Chem. Soc.* **115** (1993): 6382-6390.

[15]   Nazeeruddin, M. K., Zakeeruddin, S. M., Humphry-Baker, R., Jirousek, M., Liska, P., Vlachopoulos, N., Shklover, V., Fischer, C. H. and Grätzel, M. Acid−base equilibria of (2,2´-bipyridyl-4,4´-dicarboxylic acid)ruthenium(II) complexes and the effect of protonation on charge-transfer sensitization of nanocrystalline titania. *Inorg. Chem.* **38** (1999): 6298-6305.

[16] Hara, K., Wang, Z. S., Sato, T., Furube, A., Katoh, R., Sugihara, H., Dan-Oh, Y., Kasada, C., Shinpo, A. and Suga, S. Oligothiophene-containing coumarin dyes for efficient dye-sensitized solar cells. *J. Phys. Chem. B* **109** (2005): 15476-15482.

[17] Koops, S.E., Barnes, P. R. F., O'Regan, B. C. and Durrant, J.R. Kinetic competition in a coumarin dye-sensitized solar cell: Injection and recombination limitations upon device performance. *J. Phys. Chem. C* **114** (2010): 8045-8061.

[18]   Hara, K., Sato, T., Katoh, R., Furube, A., Ohga, Y., Shinpo, A., Suga, S., Sayama, K., Sugihara, H. and Arakawa, H. Molecular design of coumarin dyes for efficient dye-sensitized solar cells. *J. Phys. Chem. B* **107** (2003): 597-606.

[19]   Horiuchi, T., Miura, H. and Uchida, S. Highly-efficient metal-free organic dyes for dye-sensitized solar cells. *Chem. Commun.* (2003): 3036-3037.

[20]   Chen, R., Yang, X., Tian, H. and Sun, L. Tetrahydroquinoline dyes with different spacers for organic dye-sensitized solar cells. *J. Photochem. Photobiol., A* **189** (2007): 295-300.

[21]   Kitamura, T., Ikeda, M., Shigaki, K., Inoue, T., Anderson, N. A., Ai, X., Lian, T. Q. and Yanagida, S. Phenyl-conjugated oligoene sensitizers for TiO_2 solar cells. *Chem. Mater.* **16** (2004): 1806-1812.

[22]   Zhou, G., Pschirer, N., Schoneboom, J. C., Eickemeyer, F., Baumgarten, M. and Mullen, K. Ladder-type pentaphenylene dyes for dye-sensitized solar cells. *Chem. Mater.* **20** (2008): 1808-1815.

[23]   Hara, K., Kurashige, M., Ito, S., Shinpo, A., Suga, S., Sayama, K. and Arakawa, H. Novel polyene dyes for highly efficient dye-sensitized solar cells. *Chem. Commun.* (2003): 252-253.

[24]   Garcia, C. G., Polo, A. S. and Iha, N. Y. M. Fruit extracts and ruthenium polypyridinic dyes for sensitization of TiO_2 in photoelectrochemical solar cells. *J. Photochem. Photobiol., A* **160** (2003): 87-91.

[25]   Hao, S. C., Wu, J. H., Huang, Y. F. and Lin, J. M. Natural dye as photosensitizer for dye-sensitized solar cells. *Sol. Energy* **80** (2006): 209-214.

[26]   Klein, C., Baranaoff, E., Nazeerudding, M. K. and Grätzel, M. Convenient synthesis of functionalized 4,4´-disubstituted-2,2´-bipyridine with extended π-system for dye-sensitized solar cell applications. *Tetrahedron Lett.* **51** (2010): 6161-6165.

[27] Chan, H.T., Mak, C. S. K., Djurišić, A. B. and Chan, W. K. Synthesis of ruthenium complex containing conjugated polymers and their applications in dye-sensitized solar cells. *Macromol. Chem. Phys.* **212** (2011): 774-784.

[28] Fan, S.H., Zhang, A.G., Ju, C.C., Gao, L.H. and Wang, K.Z. A triphenylamine-grafted imidazo[4,5-f][1,10]phenanthroline ruthenium(II) complex: acid-base and photoelectric properties. *Inorg. Chem.* **49** (2010) : 3752-3763.

[29] Islami, M. R. and Hassani, Z. One-pot and efficient protocol for synthesis of quinoxaline derivatives. *ARKIVOC*. **xv** (2008): 280-287.

[30] Wang, P., Zakeeruddin, S.M., Mose, J.E., Humphry-Baker, R., Comte, P., Aranyos, V., Hagfeldt, A., Nazeeruddin, M.K. and Grätzel, M. Stable new sensitizer with improve light harvesting for nanocrystalline dye sensitized solar cell. *Adv. Mater.* **16** (2004): 1806-1811.

[31] Wang, P., Klein, C., Mose, J.E., Humphry-Baker, R., Cevey-Ha, N.L., Charvet, R., Comte, P., Zakeeruddin, S. M. and Grätzel, M. Amphiphilic ruthenium sensitizer with 4,4'-diphosphonic acid-2,2'-bipyridine as anchoring ligand for nanocrystalline dye sensitized solar cells. *J. Phys. Chem. B*. **108** (2004): 17553-17559.

[32] Klein, C., Nazeeruddin, M. K., Liska, P., Di Censo, D., Hirata, N., Palomares, E., Durrant, J. R. and Grätzel, M. Engineering of a novel ruthenium sensitizer and its application in dye sensitized solar cell for conversion of sunlight into electricity. *Inorg. Chem.* **44** (2005): 178-180.

[33] Nazeeruddin, M. K., Bessho, T., Cevey, L., Ito, S., Klein, C., De Angelis, F., Fantacci, S., Comte, P., Liska, P., Imai, H. and Grätzel, M. A high molar extinction coefficient charge transfer sensitizer and its application in dye sensitized solar cell. *J. Photochem. Photobiol., A* **185** (2007): 331 -337.

[34] Kuang, D., Klein, C., Ito, S., Mose, J.E., Humphry-Baker, R., Evans, N., Duriaux, F., Grätzel, C., Zakeeruddin, S.M. and Grätzel, M. High-efficiency

and stable mesoscopic dye sensitized solar cells based on a high molar extinction coefficient ruthenium sensitizer and nonvolatile electrolyte. *Adv. Mater.* **19** (2007): 1133-1137.

[35]   Cao, Y., Bai, Y., Yu, Q., Cheng, Y., Liu, S., Shi, D., Gao, F. and Wang, P. Dye sensitized solar cells with a high absorbtivity ruthenium sensitizer featuring a 2-(hexylthio)thiophene conjugated bipyridine. *J. Phys. Chem C*. **113** (2009): 6290-6297.

[36]   Yamada, M., Tanaka, Y. and Yoshimoto, Y. Synthesis and properties of diamino-substituted dipyrido [3,2-a: 2´,3´-c]phenazine. *Bull. Chem. Soc. Jpn.* **65** (1992): 1006-1011.

[37]   Muccioli, G.G., Martin, D., Scriba, G.K.E., Poppitz, W., Poupaert, J. H., Wouters, J. and Lambert, D. M. Substituted 5,5´-diphenyl-2-thioxo-imidazolidin-4-one as CB_1 cannabinoid receptor ligands: synthesis and pharmacological evaluation. *J. Med. Chem.* **48** (2005): 2509−2517.

[38]   Bodige, S. and MacDonnell, F.M. Synthesis of free and ruthenium coordinated 5,6-diamino-1,10-phenanthroline. *Tetrahedron Lett.* **38** (1997): 8159-8160.

[39]   Jiwu, R., Zhongjing, H., Liwu, F., Lin, M. and Lianquan, G. Study on the nucleophilic substitutions of 4,4´-difluorobenzil with amines. *Chin. J. Org. Chem.* **23** (2003): 861-864.

[40]   Alphen, J.V. Anisil II. *Recl. Trav. Chim.* **48** (1929): 1199-1204.

[41]   Muldoon, J., Ashcroft, A.E. and Wilson, A.J. Selective protein-surface sensing using ruthenium(II) tris-(bipyridine) complexes. *Chem. Eur. J.* **16** (2010): 100-103**.**

[42]   Szydlo, F., Andrioletti, B. and Rose, E. Facile preparation of doubly dipyrrolylquinoxaline-bridged expanded porphyrins. Synthesis and structural characterization of an unprecedented[20]tetraphyrin-(2.1.2.1). *Org. Lett*. **8** (2006): 2345-2348.

[43]   Fan, S.H., Zhang, A.G., Ju, C.C., Gao, L.H. and Wang, K.Z. A triphenylamine-grafted imidazo[4,5-f][1,10]phenanthroline ruthenium(II) complex: acid-base and photoelectric properties. *Inorg. Chem.* **49** (2010): 3752-3763.

[44]   Hallett, A.J. and Jones, J.E. Purification-free synthesis of a highly efficient ruthenium complex for dye-sensitized solar cells (DSSCs). *Dalton. Trans.* **40** (2011): 3871-3876.

[45]   Han, W. S., Han, J. K., Kim, H. Y., Choi, M. J., Kang, Y. S., Pac, C. and Kang, S. O. Electronic optimization of heteroleptic Ru(II) bipyridine complexes by remote substituents: synthesis, characterization and application to dye-sensitized solar cells. *Inorg. Chem.* **50** (2011): 3271-3280.

[46]   Collin, J.P., Harriman, A., Heitz, V, Odobel, F. and Sauvage, J.P. Photoinduced electron- and energy-transfer processes occurring within porphyrin-metal-bisterpyridyl conjugates. *J. Am. Chem. Soc.* **116** (1994): 5679-5690.

[47]   Hagemann, O., Jørgensen, M. and Krebs, F.C. Synthesis of an all-in-one molecule (for organic solar cells). *J. Org. Chem.* **71** (2006): 5546-5559.

[48]   Isalami, M.R. and Hassani, Z. One-pot and efficient protocol for synthesis of quinoxaline derivatives. *ARKIVOC*. **xv** (2008): 280-287.

[49]   Fan, S.H., Zhang, A.G., Ju, C.C., Gao, L.H. and Wang, K.Z. A triphenylamine-grafted imidazo[4,5-f][1,10]phenanthroline ruthenium(II) complex: acid-base and photoelectric properties. *Inorg. Chem.* **49** (2010): 3752-3763.

[50]   Nazeeruddin, M.K., Zakeeruddin, S.M., Hamphry-Baker, R., Gorelsky, S.I., Lever, A.B.P. and Grätzel, M. Synthesis, spectroscopic and a ZINDO study of *cis*- and *trans*-(X2)bis(4,4´-dicarboxylic acid-2,2´-bipyridine)ruthenium(II) complexes (X = Cl$^-$, H$_2$O, NCS$^-$). *Coord. Chem. Rev.* **208** (2000): 213-225.

[51] Jiang, K.J., Masaki, N., Xia, J.B., Noda, S. and Yanagida, S. A novel ruthenium sensitizer with a hydrophobic 2- thiophen-2-yl-vinyl-conjugated bipyridyl ligand for effective dye sensitized TiO$_2$ solar cells. *Chem. Commun.* (2006): 2460-2462.

[52] Chen, C.Y., Lu, H.C., Wu, C.G., Chen, J.G. and Ho, K.C. New Ruthenium complexes containing oligoalkylthiophen-substituted 1,10-phenanthroline for nanocrystalline dye-sensitized solar cells. *Adv. Funct. Mater.* **17** (2003): 29-36.

[53] Chen, C.Y., Chen, J.G., Wu, S.J., Li, J.Y., Wu, C.G. and Ho, K.C. Multifunctionalized ruthenium-based supersensitizers for highly efficient dye-sensitized solar cells. *Angew. Chem. Int. Ed.* **47** (2008): 7342-7345.

[54] Zhu, R., Jiang, C.Y., Liu, B. and Ramakrishna, S. Highly efficient nanoporous TiO$_2$-polythiophene hybrid solar cells based on interfacial modification using a metal-free organic dye. *Adv. Matet.* **21** (2009): 994-1000.

[55] Jiao, Y., Zhang, F. and Meng, S. Dye sensitized solar cells principles and new design**.** Kosyachenko, L.A., Solar Cells – Dye-Sensitized Devices, 131-148. China: InTech, 2011.

[56] Preat, J., Michaux, C., Jacquemin, D. and Perpe`te, E.A. Enhanced efficiency of organic dye-sensitized solar cells: triphenylamine derivatives *J. Phy. Chem. C* **113** (2009): 16821-16833.

APPENDIX
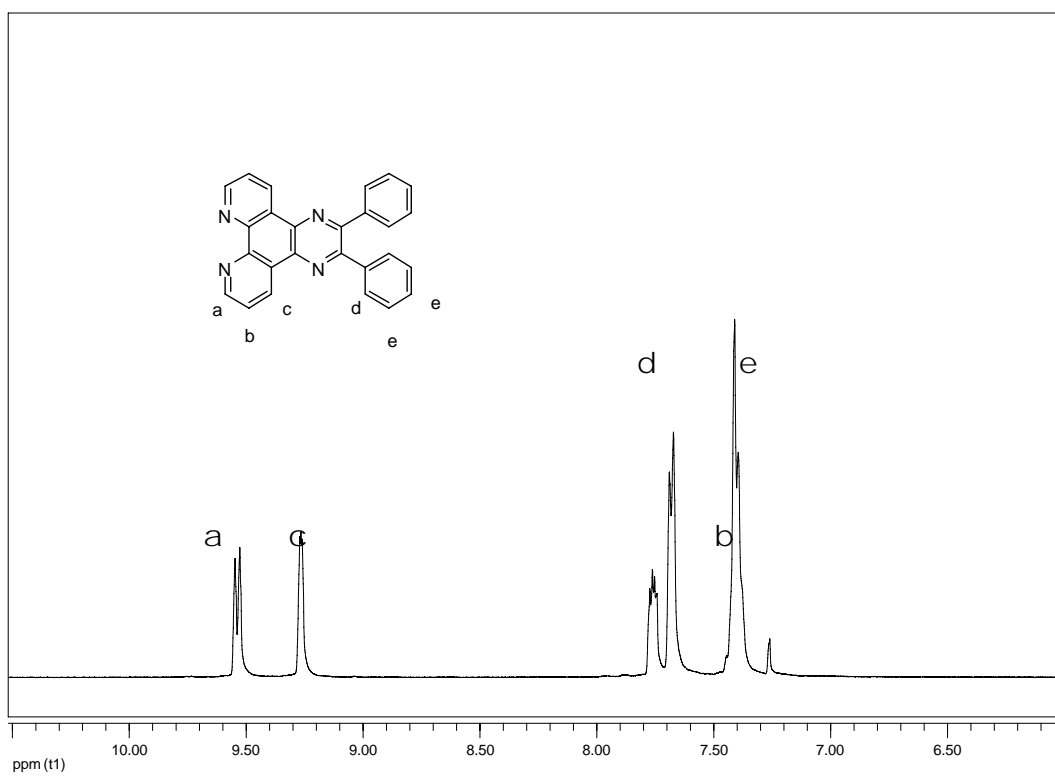
Figure A1. [^1]H NMR of 2,3-diphenylpyrazino[2,3-f][1,10]phenanthroline **6a**
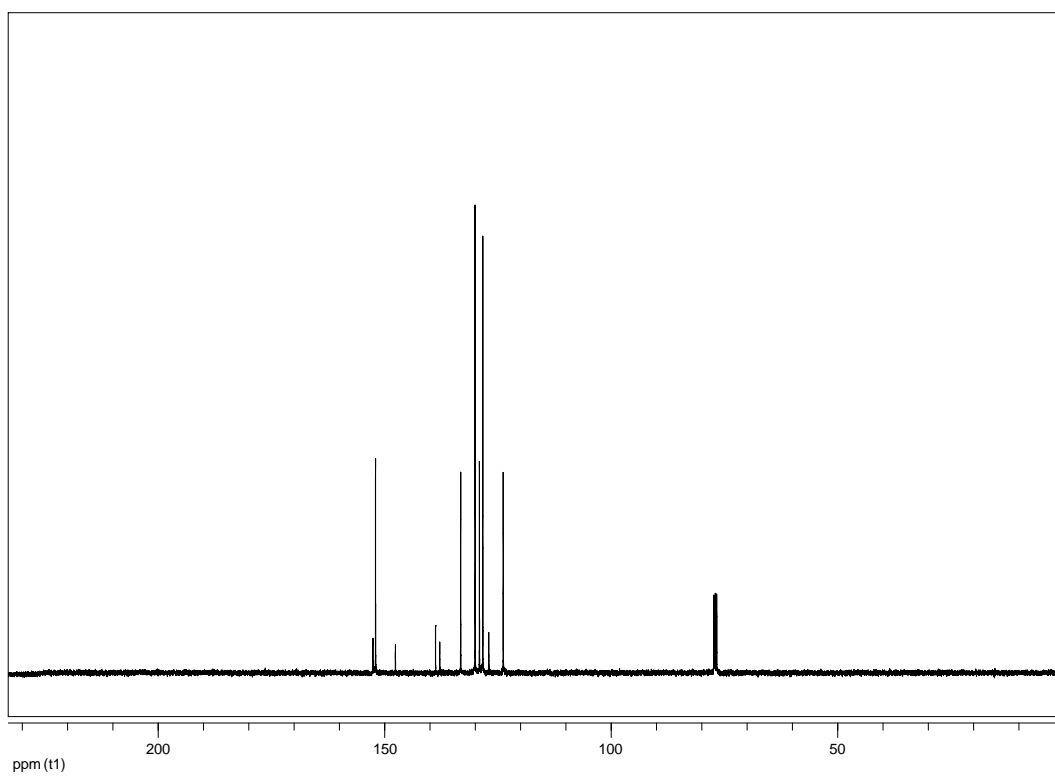
Figure A2. [^13]C NMR of 2,3-diphenylpyrazino[2,3-f][1,10]phenanthroline **6a**
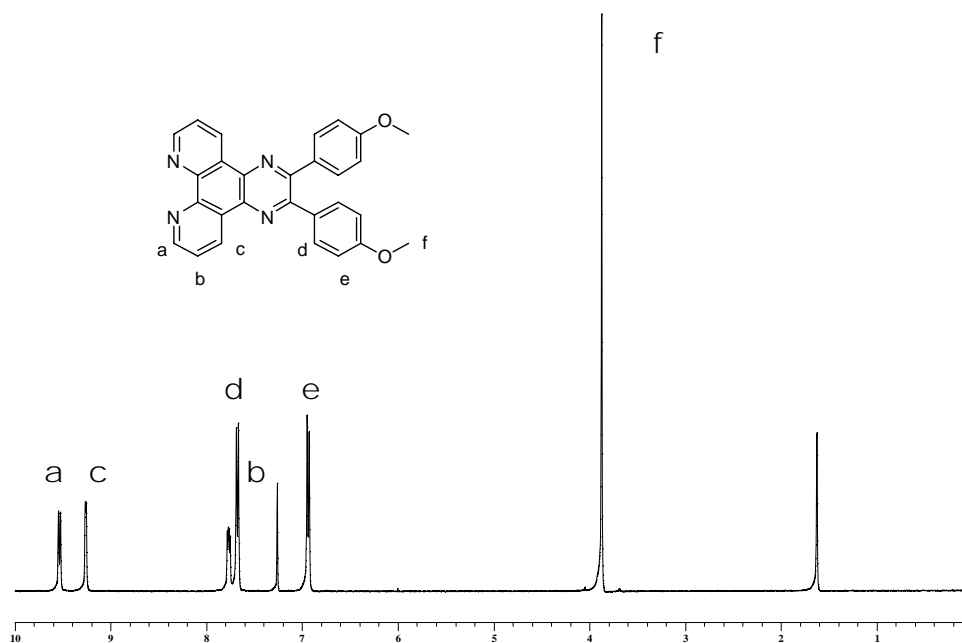
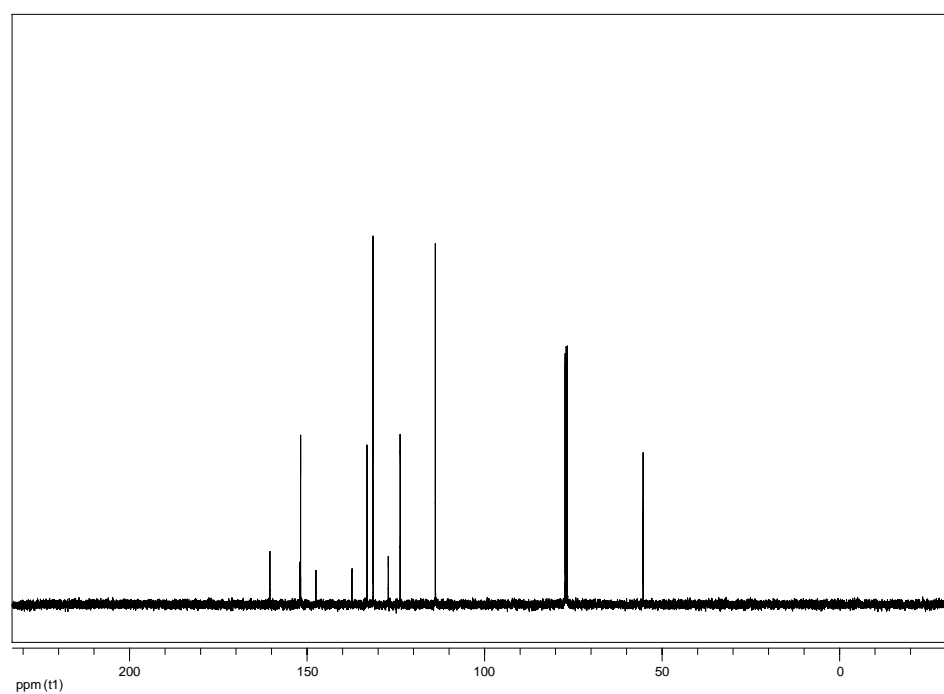**Figure A3**. ^{1}H NMR of 2,3-bis(4-methoxyphenyl)pyrazino[2,3-f][1,10]phenanthroline **6b**

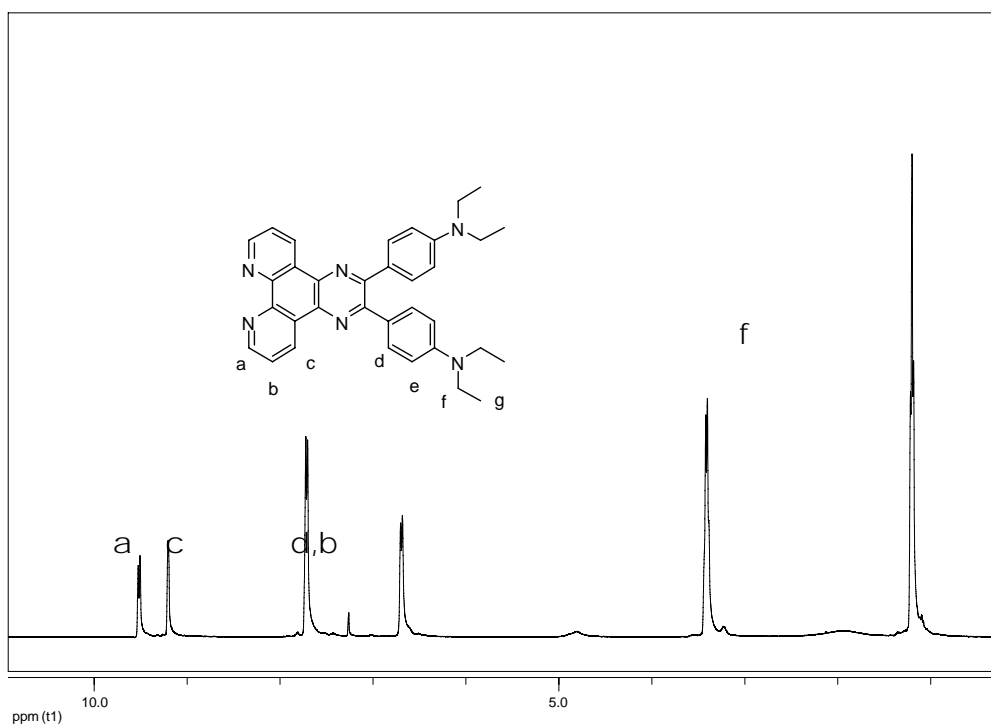**Figure A4**. ^{13}C NMR of 2,3-bis(4-methoxyphenyl)pyrazino[2,3-f][1,10]phenanthroline **6b**

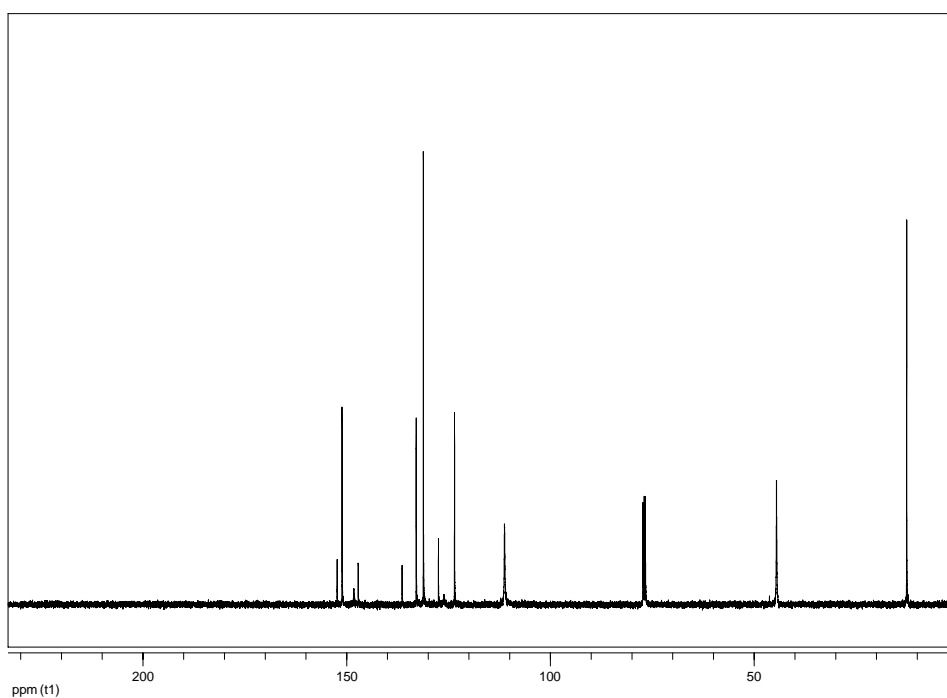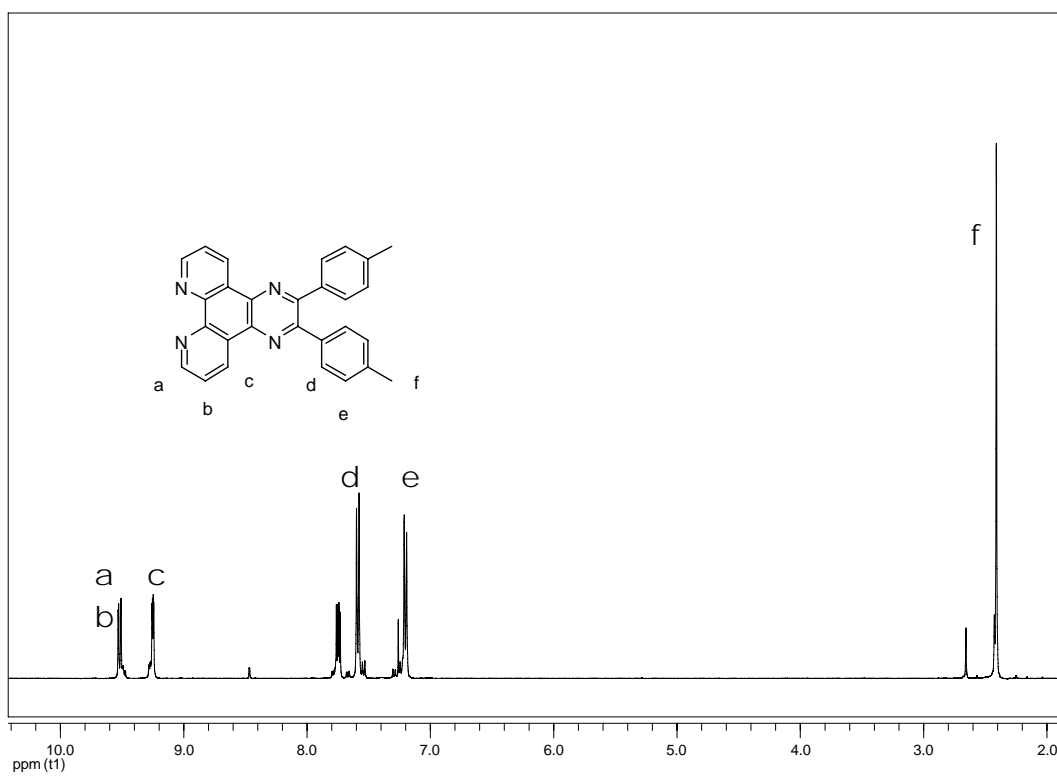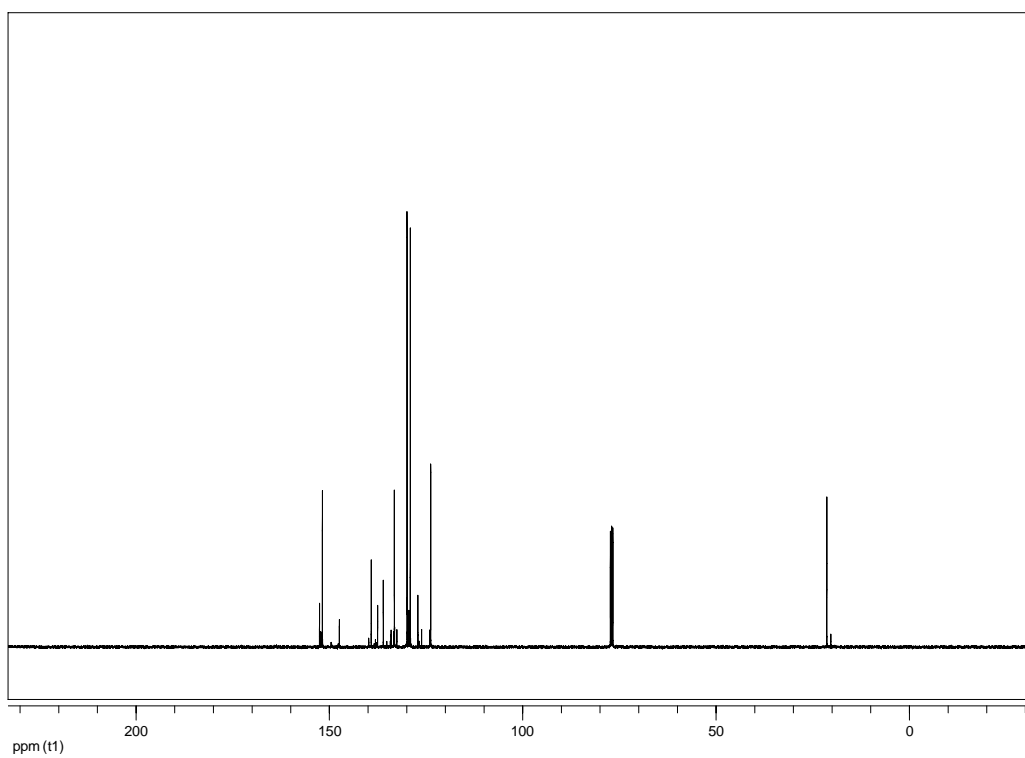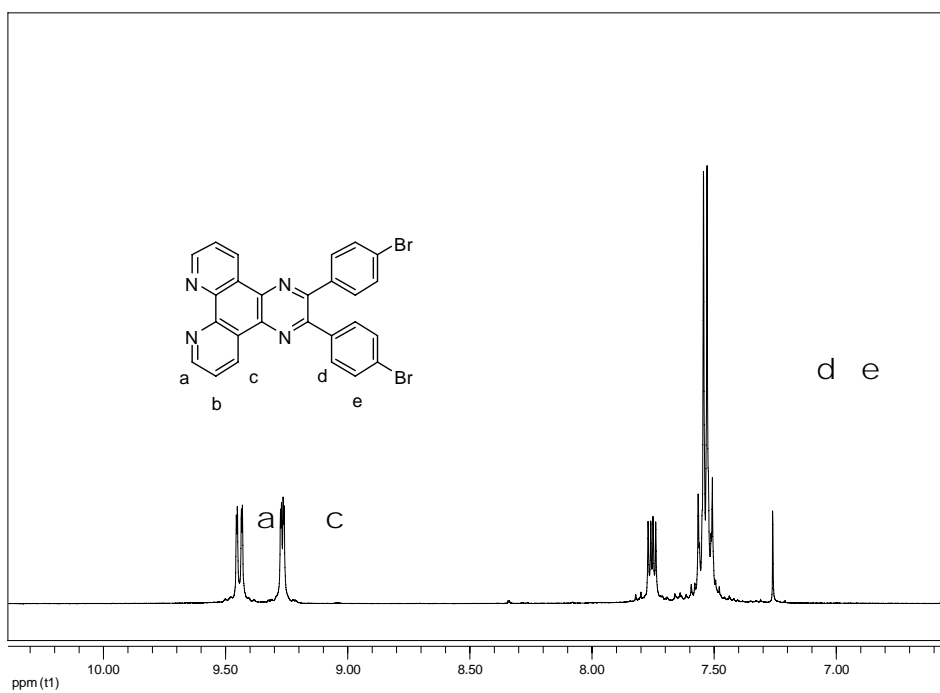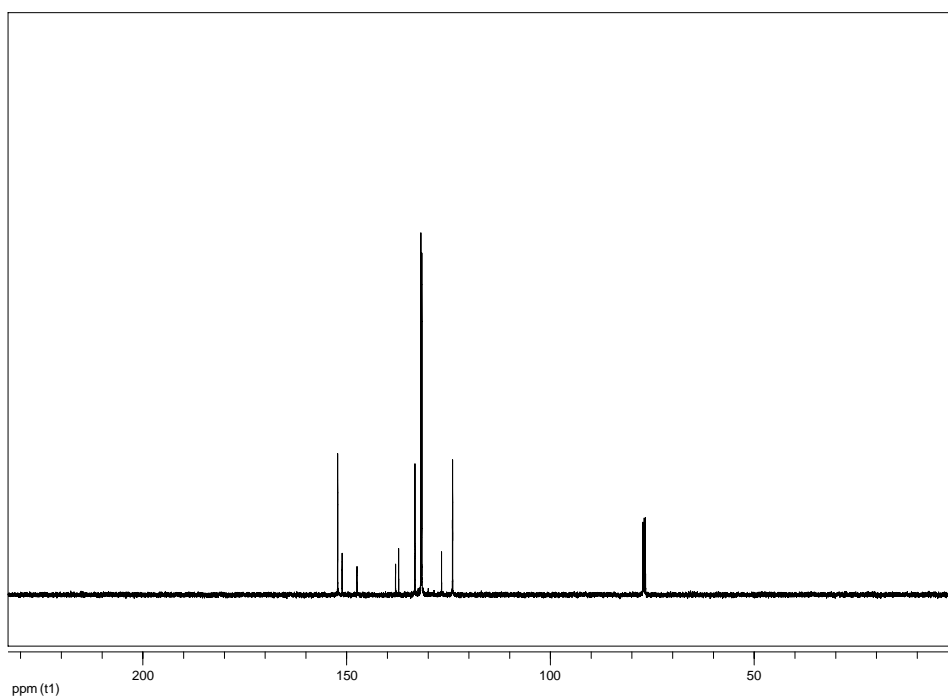**Figure A5**. ^{1}H NMR of 4,4'-(pyrazino[2,3-f][1,10]phenanthroline-2,3-diyl)bis(N,N-diethylaniline) **6c**

Figure A6. ^{13}C NMR of 4,4'-(pyrazino[2,3-f][1,10]phenanthroline-2,3-diyl)bis(N,N-diethylaniline) **6c**

Figure A7. ¹H NMR of 2,3-dip-tolylpyrazino[2,3-f][1,10]phenanthroline **6d**

Figure A8. ¹³C NMR of 2,3-dip-tolylpyrazino[2,3-f][1,10]phenanthroline **6d**

Figure A9. ^{1}H NMR of 2,3-bis(4-bromophenyl)pyrazino[2,3-f][1,10]phenanthroline **6e**

Figure A10. ^{13}C NMR of 2,3-bis(4-bromophenyl)pyrazino[2,3-f][1,10]phenanthroline **6e**
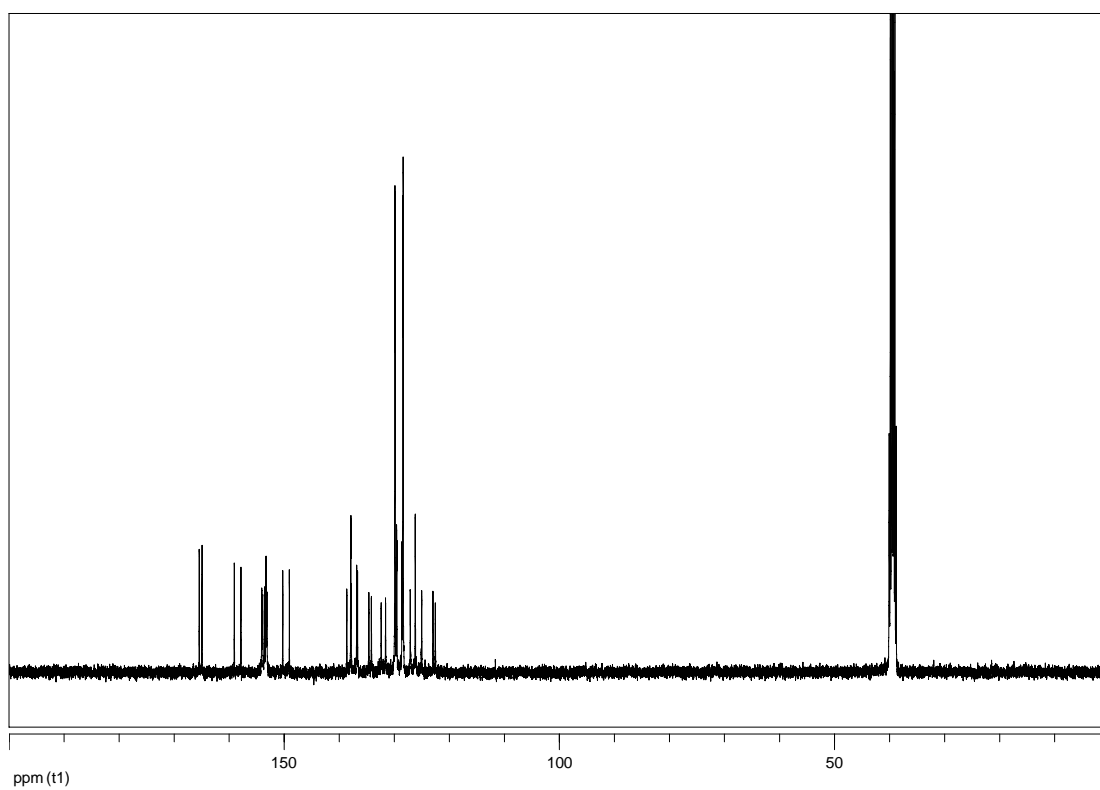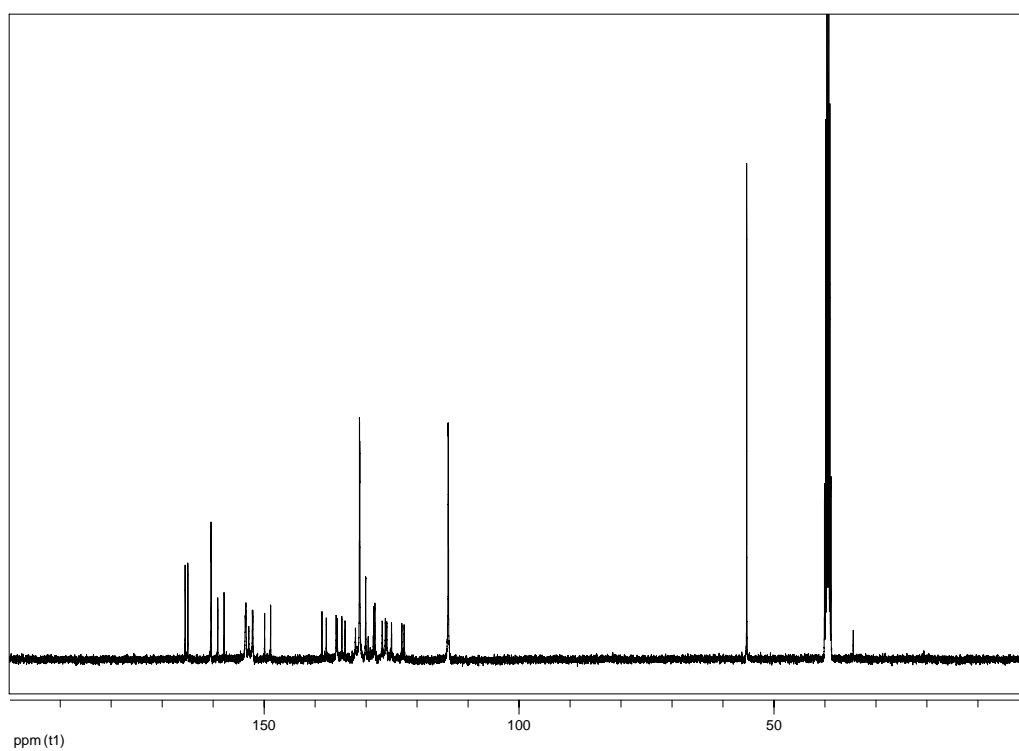
Figure 11. ^{13}C NMR of **SS01**
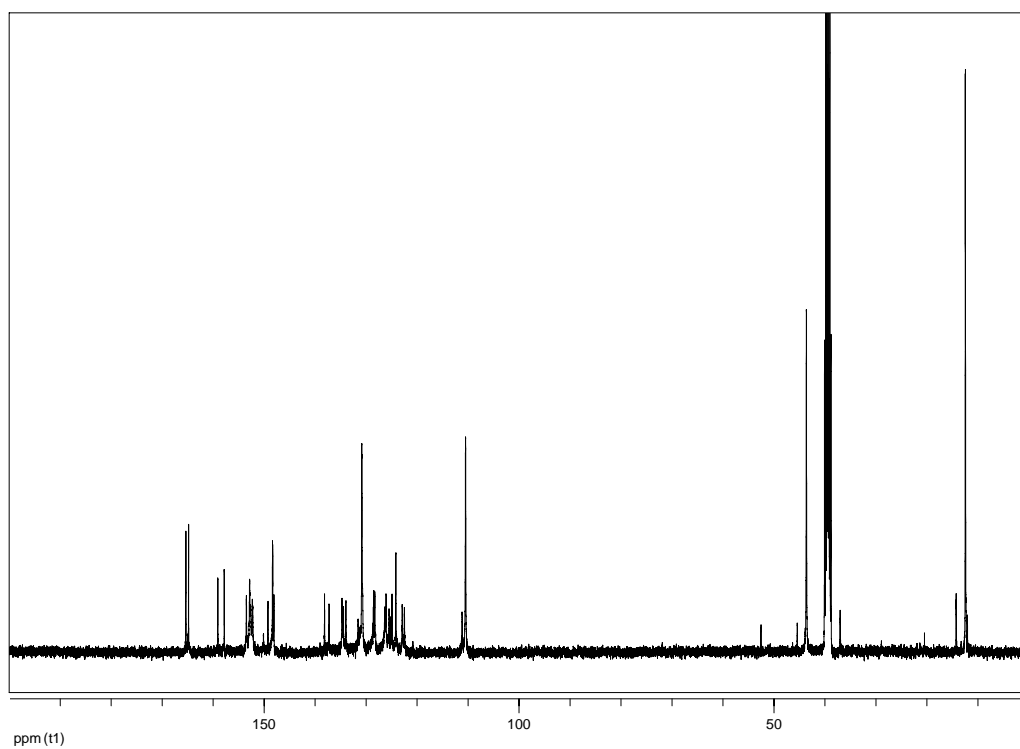

Figure 12. ^{13}C NMR of **SS02**

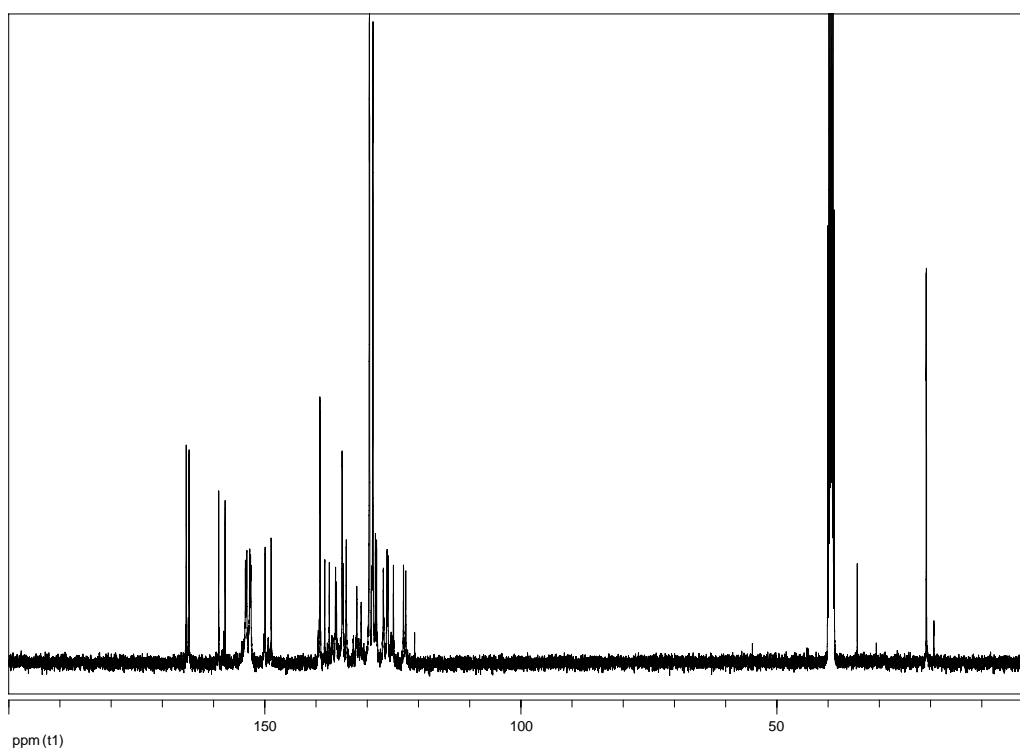**Figure 13**. ^{13}C NMR of **SS03**

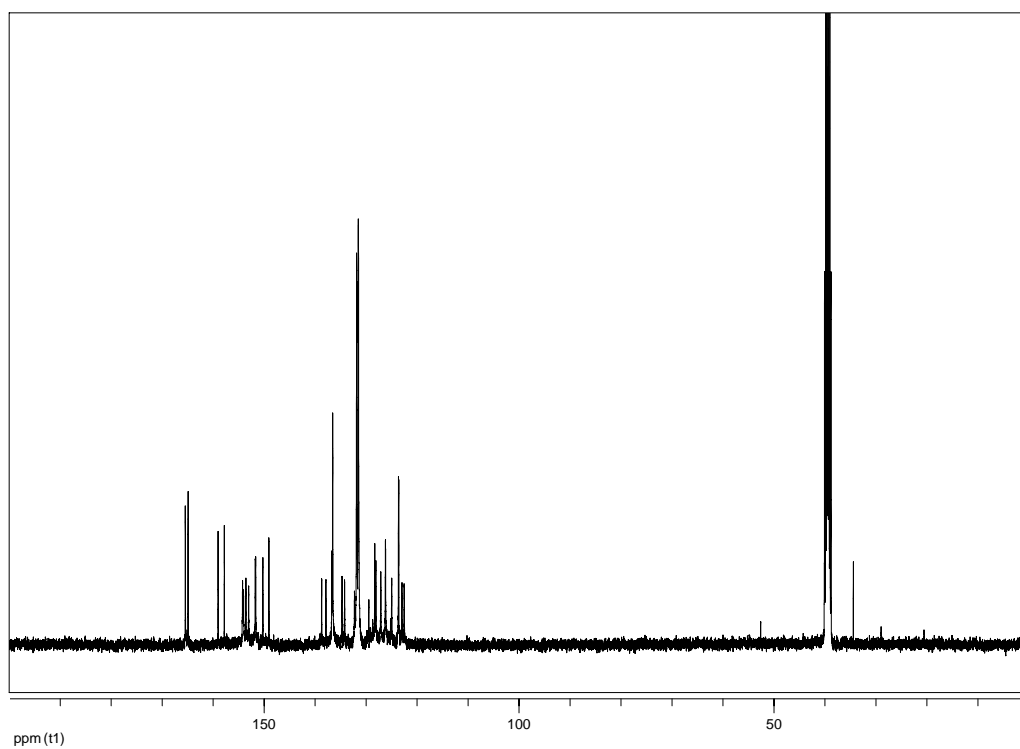**Figure 14**. ^{13}C NMR of **SS04**

Figure 15. ^{13}C NMR of **SS05**

VITAE

Mr.Supawiriya Saranarak was born on January 21st, 1987 in Khon Kaen, Thailand. He finished secondary School at Kaennakhonwithayalai School. He graduated and received a Bachelor's degree from Department of Chemistry, Faculty of Science, Chulalongkorn University in 2008. After that he continued his Master's Degree in major of Organic Chemistry at Department of Chemistry, Faculty of Science, Chulalongkorn University. His address is 124/24 Ratkanung Rd., Maung District, Khonkaen, Thailand 40000.